UNIVERSITY OF CALIFORNIA SAN DIEGO

Predicting, Measuring and Modulating Localization of Nuclear-Encoded Mitochondrial mRNAs

A Dissertation submitted in partial satisfaction of the requirements
for the degree Doctor of Philosophy

in

Biochemistry and Molecular Biophysics

by

Ximena Garcia Arceo

Committee in charge:

      Professor Brian M Zid, Chair
      Professor Suckjoon Jun
      Professor Elena Koslover
      Professor Tatiana Mishanina

2023

The Dissertation of Ximena Garcia Arceo is approved, and it is acceptable in quality and form for publication on microfilm and electronically.

University of California San Diego

2023

DEDICATION

Para mis papas Virginia y Manuel, que vinieron a este pais para que sus futuros hijos tuvieran una vida con mas oportunidades para la autodeterminacion; y para las personas que intentaron hacer lo mismo pero no sobrevivieron la venida.

TABLE OF CONTENTS

List of Figures

List of Tables

Acknowledgements

Vita

2018   Bachelor of Science in Physics, University of California Santa Barbara

2023   Doctor of Philosophy in Biochemistry and Molecular Biophysics, University of California San Diego

Publications

Phillip Kohl, Chaeyeon Song, Bretton Fletcher, Rebecca L. Best, Christine Tchounwou, Ximena Garcia Arceo, Peter J. Chung, Herbert P. Miller, Leslie Wilson, Myung Chul Choi, Youli Li, Stuart C. Feinstein, Cyrus R. Safinya. Complexes of tubulin oligomers and tau form an intervening network cross-bridging microtubules into bundles. bioRxiv (Uploaded 2022).

Ximena G. Arceo, Elena F. Koslover, Brian M. Zid, Aidan I. Brown. Mitochondrial mRNA localization is governed by translation kinetics and spatial transport. PLOS Comp Biol (2022).

Tatsuhisa Tsuboi, Matheus P Viana, Fan Xu, Jingwen Yu, Raghav Chanchani, Ximena G Arceo, Evelina Tutucci, Joonhyuk Choi, Yang S Chen, Robert H Singer, Susanne M Rafelski, Brian M Zid. Mitochondrial volume fraction and translation duration impact mitochondrial mRNA localization and protein synthesis. eLife (2020).

ABSTRACT OF THE DISSERTATION

Predicting, Measuring and Modulating Localization of Nuclear-Encoded Mitochondrial mRNAs

by

Ximena Garcia Arceo

Doctor of Philosophy in Biochemistry and Molecular Biophysics

University of California San Diego, 2023

Professor Brian M Zid, Chair

Mitochondria are organelles whose function, protein composition, size, and morphology are highly variable and regulated in response to nutrient availability and other environmental conditions. Their crucial role in metabolism involves the production of adenosine triphosphate (ATP), the energy currency of the cell, by the oxidative phosphorylation pathway. TEM studies observed ribosomes enriched at the mitochondrial

surface, suggesting that mRNAs localize co-translationally. mRNA localization is a post transcriptional method for regulating gene expression in parallel with transcriptional methods. While mRNA localization is a way to control protein production or limit translation activity to specific cellular locations, the potential of mRNA localization as a strategy for altering the composition of mitochondrial proteins in different environmental conditions has not been explored. For brewer's yeast, 99% of mitochondrial proteins are encoded in the nuclear genome. To ensure mitochondrial function, nuclear-encoded proteins are imported into the mitochondria through mitochondrial translocases on the outer mitochondrial membrane. mRNA localization is implicated in mitochondrial protein homeostasis along two axes: it helps synchronize the nuclear and mitochondrial genome translation programs to ensure proper stoichiometry of nuclear- and mitochondrial-encoded proteins and it is required for initiating the co-translational import of highly hydrophobic nascent peptides that are vulnerable to aggregation and misfolding in the cytosol. While it is clear that mRNA localization is important for mitochondrial biogenesis and homeostasis, the mechanism of localization has not been fully elucidated for mRNAs that do not have known RNA-binding proteins partners that regulate their localization. More than 200 genes associate to the mitochondria after translating a 5' amphiphilic mitochondria targeting sequence (MTS) that can interact with translocation machinery only after the mRNA-ribosome complex has found the mitochondria through diffusive search. Additionally, the nascent peptides produced by co-translationally localized mRNAs bind to the chaperones Hsp70 (in brewer's yeast) and Hsp90 (in mammalian cells) that are implicated in the proper recognition of the preprotein by other components of translocation machinery.

Based on our understanding of the MTS-driven mechanism of mRNA localization, I developed a mathematical model and stochastic simulation of translation, peptide signal maturation, and mRNA diffusion in cells of varying mitochondrial volume. After reproducing experimental observations of mRNA localization in diverse cellular states, including in fermentative versus respiratory metabolic conditions, we predicted that increasing translation duration would drive mRNA localization *in vivo*. However, quantitative microscopy in brewer's yeast reveals that ribosome stalls downstream of the MTS drive localization regardless of translation duration. This has given us new insights into the peptide signal maturation component of MTS-driven localization mechanism, and has been incorporated into the stochastic simulation as well as experimental design. The mechanism of mRNA localization is based on fundamental processes like translation and diffusion instead of relying on gene-specific or condition-specific regulatory factors. Therefore, we postulate that it is conserved to mammalian systems given the high degree of conservation of mammalian genes and peptide-binding chaperones. We find that our stochastic simulation of translation, peptide signal maturation, and mRNA diffusion can reproduce experimental observations of mRNA localization behaviors in brewer's yeast and mammalian cells, indicating that the biophysical mechanism of MTS-driven localization is conserved between eukaryotes. The combination of translation and diffusion kinetics is a novel mechanism for regulating mitochondrial gene expression post-transcriptionally across eukaryotes and adds to our understanding of mitochondrial homeostasis and mitochondrial biogenesis in shifting environmental conditions.

Chapter 1

Introduction

1.0.1   Mitochondrial diseases and dysfunction

Damage to mitochondria leads to cell-wide dysfunction and eventually to disease at the organismal level. Cell types with large energetic demands, like motor neurons and muscle cells, typically contain more mitochondria and are thus particularly vulnerable to the effects of mitochondrial dysregulation. Numerous pathologies are directly linked to mitochondria's role as a regulator of cellular calcium levels because calcium signaling, pH regulation, and ionic gradients are important for the functions of specific cells [2]. For example, excitable neurons must maintain ionic gradients in order to propagate a signal when stimulated. Many others are linked to mitochondria's more well known role as the generator of energy molecules (ATP) through the respiratory chain, which is coupled to cytosolic calcium levels but has outsized effects for muscle tissue. Skeletal muscle, cardiac muscle, and smooth muscle in the gut rely on ATP production from oxidative phosphorylation in the mitochondria to contract and pick up an object, or keep the heart beating, or push food through the entire digestive system. Many vascular cell types, e.g. system microvessels, endothelial cells, and smooth muscle cells, primarily utilize the oxygen-independent glycolysis pathway to meet their energy needs [3]. However, they still upregulate mitochondrial-dependent oxidative phosphorylation during periods of higher metabolic loads or when glycolysis is inhibited [3]. Their ability to control oxidative phosphorylation activity helps maintain an oxygen gradient that ensures sufficient oxygen diffuses into deeper tissues that rely heavily or exclusively on the more efficient process of oxidative phosphorylation [3].

Currently, in the study of muscle-related diseases, experimentation on mitochondrial function primarily uses mitochondria isolated from mammalian tissues and permeabilized [4]. However, harvesting typically results in spherical organelles that retain many of their biochemical properties, like membrane potential and oxidative phosphorylation activity, but lose their natural morphology of branched and highly connected networks of tubes. Turning to *in vivo* experimentation would elucidate the role of morphology and size in all aspects of mitochondrial regulation, including

biogenesis, protein homeostasis, and motility. Disrupted mitochondrial morphology has been implicated in apoptosis (programmed cell death) and senescence (age-related loss of function). Mitochondria are constantly undergoing fission and fusion, resulting in ever-changing networks of branched tubes that nonetheless carry out all of their biochemical functions in conjunction with physical reorganization. The effects of fission and fusion have resulted in seemingly contradictory findings such that upregulating fusion or downregulating fission can result in either promote or reduce pro-apoptotic cell signalling. More *in vivo* studies would elucidate the role of mitochondria network structure in apoptosis as well as healthy function.

Interestingly, mitochondrial volume was found to remain at a constant 10-11% of cytosolic volume throughout the life cycle of HeLa cells [5]. The Zid lab has made interesting findings regarding how mitochondrial volume fraction controls the localization of a class of nuclear-encoded mitochondrial mRNAs thereby correlating its own size with localized protein production through the fundamental process of diffusion [6, 7]. Additionally, the ability to quantify or track mitochondria over time in living cells has also led to a greater appreciation for the importance of inter-organelle contacts [8] and how mitochondria are trafficked along the challenging length of the axon in energy-hungry neurons [9]. Mitochondrial motility is thought to help regulate the mitochondrial genome itself because fusion and fission events lead to exchanges of mitochondrial DNA (mtDNA). With age, mtDNA accumulates many random mutations and exchanging genomic information diminishes the risk of loss of function mutations in mitochondria-encoded proteins at any one mitochondrial tubule. Fusion, fission, and motility are also important for contacts with the endoplasmic reticulum (ER), another very large organelle, and others, ensuring consistent intracellular communication [8]. While this has direct implications in apoptosis and age-related dysfunction, it begs the more fundamental question of how gene expression strategies can keep up with the highly dynamic mitochondrial structure and rapidly responsive mitochondrial functions. I propose that translation kinetics and mRNA diffusive search times for mitochondria combine to determine mRNA localization dynamics and thus gene expression during rapidly shifting demands and environmental conditions.

1.0.2   mRNA localization to the mitochondria

mRNA localization is a post transcriptional method for regulating gene expression in parallel with transcriptional methods. The regulation of subcellular mRNA localization has been studied in Drosophila melanogaster embryos [10], neurons [11], Xenopus laevis oocytes [12], and other eukaryotes [13] with a particular focus on the mechanisms of recognition and transport by cytoskeleton-associated motor proteins. The current view of mRNA sequences as subcellular "zipcodes" or localization elements (LEs) [13, 14, 15] that function as recognition sites for RNA-binding proteins positions the RNA-protein complex, or RNA granule, as the foundation of mRNA localization regulation more generally. While the mechanisms of mRNA localization to the mitochondria are not entirely understood, TEM studies observed ribosomes enriched at the mitochondrial surface, suggesting that mitochondrial localization can occur

co-translationally. While mRNA localization is a way to control protein production overall or localize translation activity, the potential of mRNA localization as a strategy for altering the composition of mitochondrial proteins in different environmental conditions has not been explored.

Mitochondria are organelles whose function, protein composition, size, and morphology are highly variable and regulated in response to nutrient availability and other environmental conditions. Their crucial role in metabolism involves the production of adenosine triphosphate (ATP), the energy currency of the cell, by the oxidative phosphorylation pathway. In the brewer's yeast, *Saccharomyces cerevisiae*, cells can switch their source of ATP towards or away from oxidative phosphorylation, and thus towards and away from mitochondria, depending on the environment. In addition to many other non-metabolic functions, its role as a key player in ATP generation is important for understanding how cells regulate mitochondrial function broadly. Furthermore, understanding the regulation of mitochondrial protein levels in the context of metabolic switching switching may provide insight into the loss of mitochondrial function and the disruption of healthy mitochondrial morphology, hallmarks of many age-related and metabolic diseases. The volume, protein composition, and protein content show drastic changes in response to cellular metabolic need and nutrient availability. When a fermentable carbon source is highly available, brewer's yeast and many cancer cell types will rely on glycolysis–even in the presence of oxygen–to meet its energy needs, a metabolic mode that is less biomass-efficient but produces ATP more quickly. Mitochondria are small in volume and mitochondrial protein levels are lower overall. By contrast, when brewer's yeast is grown without a fermentable carbon source and in plenty of oxygen, it switches to oxidative phosphorylation, spurring mitochondrial biogenesis with 10 to 20 fold increases of transcript and protein levels [16]. In addition to the increase in size, metabolic mitochondrial proteins, such as those involved in oxidative phosphorylation, are specifically upregulated to support mitochondria in their larger role as the cell's primary generator of ATP.

For *S. cerevesiae*, 99% of mitochondrial proteins are encoded in the nuclear genome. To ensure mitochondrial function, nuclear-encoded proteins are imported into the mitochondria through mitochondrial translocases on the outer mitochondrial membrane. Therefore, many mRNAs that encode mitochondrial proteins are synthesized in the nucleus and localize to mitochondria through a variety of mechanisms. Additionally, the cell can modulate the localization of certain mRNAs in response to shifting conditions. While some mRNAs always localize asymmetrically to the mitochondria, others only do so during deprivation of fermentable carbon sources [17], after translation elongation inhibition [18], or when mitochondria are large in size [6]. mRNA localization assists with co-translational import of mitochondrial proteins, particularly for proteins destined for the inner mitochondrial membrane, which are typically more structured, larger, and more hydrophobic. In addition to protecting membrane proteins from the relatively hydrophilic cytosol, mRNA localization has also been proposed as a post-transcriptional method of coordinating the expression of the nuclear and mitochondrial genomes. The complex ATP synthase, among others, contains subunits of dual genomic origin, and its stoichiometry is tightly regulated to ensure function. For some nuclear-encoded

mitochondrial genes, it is known that mRNAs associate to the translocation machinery using the mRNA-binding protein Puf3. Loss of Puf3 or Puf3 function impairs mitochondrial biogenesis and the ability of brewer's yeast to survive in a non-fermentable carbon source. While Puf3p-binding domains are located at the 3' untranslated region (UTR) of 256 nuclear-encoded mitochondrial genes, 224 genes have no Puf3p-binding site and their localization is not controlled by Puf3 [19]. While it is clear that mRNA localization is important for mitochondrial biogenesis and homeostasis, the mechanism of localization has not been fully elucidated for mRNAs that do not have known RNA-binding proteins partners that regulate their localization.

Eukaryotic cells coordinate the mitochondrial and nuclear genomes to ensure proper stoichiometry of large key complexes. For example, human ATP synthase comprises 25 subunits of nuclear origin and 2 subunits of mitochondrial origin [20]. Similarly, *S. cerevisiae* ATP synthase comprises 17 subunits and requires the coordination of nuclear and mitochondrial gene expression [21]. Given the degree of conservation between *S. cerevisiae* and mammalian mitochondrial proteins, brewer's yeast has long been a model organism for elucidating the key molecular players in metabolic switching, mitochondrial biogenesis, and the coordination of the nuclear and mitochondrial genomes. In addition to a subunit of ATP synthase (in OXPHOS complex V), the *S. cerevisiae* mitochondrial genome encodes 7 more proteins that form part of 3 other major dual-origin protein complexes: the mitoribosome and OXPHOS complexes III and IV [22]. Mitochondrial transcription (i.e. transcription of the mitochondrial genome) of OXPHOS genes is induced more slowly than nuclear transcription of OXPHOS genes after a switch from fermentable to non-fermentable media [22], yet translational regulation of all dual-origin OXPHOS subunits is quickly synchronized, i.e. less than 15 minutes after the change in media [22]. Synchronization was found to be unidirectional such that changes in cytosolic mRNAs, and possibly mRNA localization, spur rapid changes to mitochndrial translational activity [22], and translational programs in the mitochondria and cytosol quickly synchronize to produce more metabolic proteins with proper subunit stoichiometry.

Cells regulate mitochondrial biogenesis in relation to the metabolic needs of the cell, and it is largely thought that this gene expression program is centralized in the transcriptional step. However, it is still unclear how mRNA localization may be impacted by changing mitochondrial dynamics or by perturbations to translation efficiency in ageing or stress [23]. Furthermore, it is unknown how cells regulate the asymmetrical localization to the mitochondria for these mRNAs in both a gene-specific manner and in response to shifting nutrient conditions. The Zid lab recently showed for the first time that mRNA localization to the mitochondria can be dynamically regulated during different environmental conditions[6]. Whereas specific RNA-binding protein partners have not been identified, the nascent peptides produced by co-translationally localized mRNAs do bind to the chaperones Hsp70 and Hsp90 [24, 25]. The cytosolic chaperones Hsp70 and Hsp90 have been implicated in the proper recognition of nascent peptides, and thus the import of proteins, at the outer mitochondrial membrane. In brewer's yeast, Hsp70 binds to the nascent peptide and helps deliver the mRNA-ribosome complex to the outer membrane. Translocation machinery at the outer mitochondrial

membrane, Tom20 and Tom22, interact with MTSs in the nascent peptide while Tom70 interacts with Hsp70 chaperones [25, 26]. We need to understand how these two binding events work together in the MTS-driven mechanism of mRNA localization. Hundreds of mitochondrial genes use this mechanism yet it is unknown why this MTS-driven system gives rise to both constitutively high localization and condition- or environment-sensitive localization. MTS-swapping experiments indicate that the MTS is required but not sufficient for asymmetric localization, pointing to the downstream coding sequence (CDS) as the likely factor in quantitatively determining localization and, for conditionally localized mRNAs, in responding to environmental changes [27, 6].

Bioinformatic studies [28], experimental research on chimeric sequences [6], and structural studies of mitochondrial import machinery [29] have shed light on the biochemical mechanism of nascent peptide-mediated association of a mRNA-ribosome complex to the mitochondrial surface. There are many key features found across the hundreds of so-called Class II mRNAs. Mitochondrial targeting sequences (MTSs) are located at the 5' of the mRNA's open reading frame (ORF), i.e. the N-terminus of the preprotein [25, 26], and form an amphiphilic helix adept at interacting with phospholipids [30] and the larger Tom20 complex. While computer programs predict that MTSs can be of various lengths, depending on the gene [28], the amphiphilic structure and location at the 5' end are general characteristics found across Class II and are essential for association with mitochondrial import machinery. For some genes, internal "MTS-like" sequences have been found downstream of the primary 5' MTS, but their deletion had a small effect on mitochondrial association [26]. I posit that internal "MTS-like" sequences and other significant motifs, like ribosome stalls, are implicated in Hsp70 or Hsp90 binding, the other component of MTS-driven recogntion and import at the outer mitochondrial membrane.

The existent literature is largely in consensus about the essential biochemical components of the system, which is conducive to building theoretical, mathematical, and computational models for predicting mRNA localization in various environments and in response to perturbations. These models should be quantitative in their predictions, generate testable hypotheses at the bench, and elaborated on with the resulting experimental findings. Our model is based on the fundamental biophysics of mRNA diffusion, translation, and chaperone-binding, and not in condition-specific chaperones or other regulatory factors. I investigated how much translation elongation kinetics can tune mRNA localization and whether this is implicated in Hsp70 chaperone recruitment, the other half of this puzzle. As the model continues being tested experimentally and expanded in brewer's yeast, it has also opened an avenue into understanding mRNA localization in mammalian cells. Given the high degree of conservation of mitochondrial genes, functions, and morphology between yeast and mammalian cells, we investigated whether our generic mechanism of mRNA localization was conserved to human cells. I was able to calculate the necessary translation parameters in human cells [31] and compare simulation results to enrichment data in human cells from [1]. Our findings suggest that human cells may also be using this mechanism to set localization ratios for mitochondrial genes, resulting in both constitutively localized and environment-sensitive mRNAs. By iteratively integrating experiments and computational modeling, we

can identify and control novel mechanisms of mRNA-mitochondrial association.

Chapter 2

Two-state model of mRNA association to the outer mitochondrial surface

Excerpt from [6]: "As yeast cells shift to respiratory conditions, mitochondrial biogenesis increases the mitochondrial volume while the cell cytoplasmic volume decreases, thus leading to an increase in the mitochondrial volume fraction in respiratory conditions. While ATP3 mRNA showed a strong condition-dependent localization, TIM50 and TOM22 mRNAs also showed modestly increased mitochondrial association during respiratory conditions. We wondered what impact the reduction in the availability of free cytoplasmic space due to mitochondrial expansion had on mRNA co-localization, especially for TOM22, which is not known to bind to the mitochondria. To test this, we quantified both the mitochondrial localization of each mRNA and changes in mitochondrial volume fraction at a single-cell level Fig. 2.1." ... To further test our hypothesis that mRNA localization is regulated by mitochondrial volume fraction, I designed *in silico* experiments based on the primary investigator's experimentally measured cell and mitochondrial boundaries. I created a two-state model wherein a particle with an affinity for the mitochondria can be found at the mitochondria ("local") or away from the mitochondria ("diffuse"). The biochemical basis for the affinity is the interaction between mitochondrial import machinery and a nascent peptide that is part of the mRNA-ribosome complex during active translation. Experimental measurements of localization were based on confocal microscopy of fluorescently-labelled mRNAs. Although it is likely that some mRNAs are not part of an mRNA-ribosome complex at the timepoint of observation, the two-state model particle represents an mRNA molecule with an intrinsic and time-invariable affinity for the mitochondria. Therefore, the probability of localization can be written simply as Eq(2.1)

$$p_{local} = \frac{N_{local}}{N_{local} + N_{diffuse}} \tag{2.1}$$
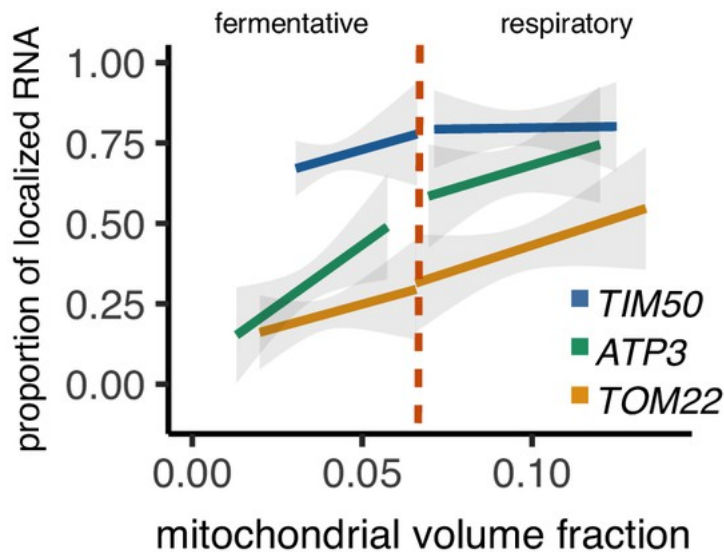
Figure 2.1: mRNA localization increases with respect to mitochondrial volume fraction

The probability of being found at the mitochondria p_{local} depends, in part, on the strength of the affinity ΔG in Eq(2.2). Consistent with the application of the two state model, we define the number of "local" mRNAs and "diffuse" mRNAs of a given gene according to the multiplicity of the "local" microstate Ω_{local} and "diffuse" microstate $\Omega_{diffuse}$, and the energy difference between the two states ΔG. These theoretical mRNAs have no affinity for other cellular compartments are thus free to diffuse around the volume of the cytosol whenever they are not at the mitochondrial surface.

$$p_{local} = \frac{\Omega_{local}e^{-\Delta G/k_BT}}{\Omega_{diffuse} + \Omega_{local}e^{-\Delta G/k_BT}} \tag{2.2}$$

Mitochondrial import machinery are distributed along the surface of mitochondrial tubules. Therefore, the multiplicity of the "local" state depends explicitly on the surface area of the mitochondrion, which is cylindrical.

$$\Omega_{local} = A_{mito} = 2\pi r l_{mito} \tag{2.3}$$

The volume of the mitochondria, $V_{mito} = \pi r^2 l_{mito}$ allows us to substitute l_{mito} and re-write Ω_{local} in terms of r_{mito}, which is a constant 350 nm, and the observable V_{mito}.

$$\Omega_{local} = \frac{2V_{mito}}{r} \tag{2.4}$$

In the "diffuse" state, particles explore the volume of the cytosol without any affinity for other cellular compartments. $\Omega_{diffuse}$ can be written simply as, V_{cyto}. For this system, define the cytosol as the volume of the cell without mitochondria,
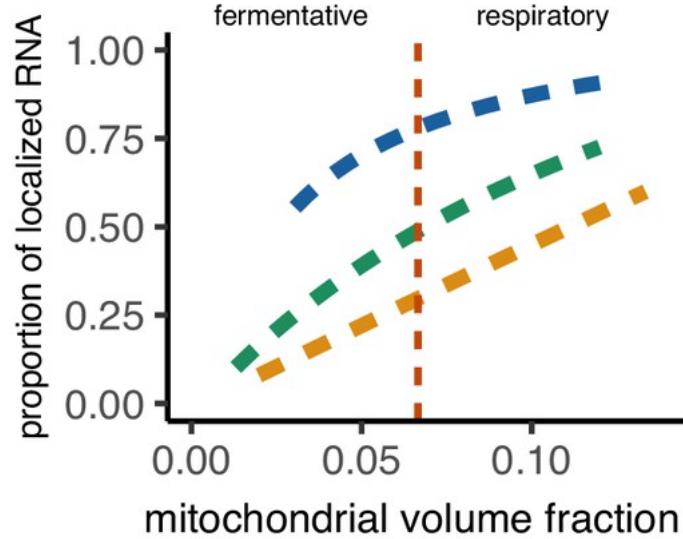
Figure 2.2: From Tsuboi et al. (2020). A two-state model of mRNA localization p_{local} recapitulates experimental measurements of localization with respect to mitochondrial volume fraction.
TOM22 (yellow) has $\Delta G = 0$. TIM50 (blue) has $\Delta G = 8.8\ k_B T$. ATP3 (green) has $\Delta G = 2.4\ k_B T$.

and we define V_{cyto} in terms of the experimentally observable V_{cell} and V_{mito}.

$$\Omega_{\text{diffuse}} = V_{cell} - V_{mito} \tag{2.5}$$

I re-write p_{local} with our new expressions for Ω_{local} and Ω_{diffuse} in Eq(2.6).

$$p_{local} = \frac{V_{mito}e^{-\Delta G/k_B T}}{(V_{cell} - V_{mito}) + (2/r)V_{mito}e^{-\Delta G/k_B T}} \tag{2.6}$$

Rewriting V_{mito} and V_{cell} in terms of mitochondrial volume fraction v (Eq(2.7)) renders p_{local} in terms of the empirical parameter v and the gene-specific free parameter ΔG in Eq(2.8).

$$v \equiv V_{mito}/V_{cell} \tag{2.7}$$

$$p_{local} = \frac{ve^{-\Delta G/k_B T}}{1 - v + ve^{-\Delta G/k_B T}} \tag{2.8}$$

I plotted the localization curves for the mRNAs of all three available genes and determined the value of the free parameter ΔG for ATP3 and TIM50 in Fig 2.2. TOM22 is known to not have an MTS and therefore no affinity for the mitochondria. Its $\Delta G = 0$ by definition. In this case, $p_{local} = v$. Empirical data reveals that the localization curve of TOM22 has a non-zero y-intercept that does not appear in the simple p_{local} and a slope slightly greater than 1. Nonetheless, p_{local} qualitatively captures the dependence of TOM22's localization on mitochondrial volume fraction.

ATP3 and TIM50 are known to have an MTS and demonstrate an affinity for the mitochondria given that their localization ratios are higher than TOM22's across the range of mitochondrial volume fractions. The strength of their affinity ΔG must be fit to the localization curve of each gene. Intuitively, TIM50 is expected to have a greater affinity for the mitochondria than ATP3 given that TIM50 localization is consistently high and displays less dependence on v. p_{local} with $\Delta G = 8.8\ k_B T$ closely matches the empirical localization curve of TIM50 whereas p_{local} with $\Delta G = 2.4\ k_B T$ closely matches the empirical localization curve of ATP3.

Modeling the localization of mRNAs with an affinity for mitochondria as a two-state model presumes that mRNAs exist in one of two states rather than in a variety of molecular states. Molecular states could be generated by tiered recruitment of binding factors, subsequent translation of mitochondrial targeting sequences, or distinct interactions with the mitochondrial versus cytosolic milieu. Using a two-state model implies that all these processes and phenomena do not lead to conditional or incremental affinity. Conditional affinity in a biochemical context would be the recruitment of an essential chaperone that is only present under certain conditions, like respiratory metabolism. Incremental affinity would arise if the affinity of the nascent peptide increased with the recruitment of subsequent chaperones, or if the affinity of the mRNA-ribosome complex increased with respect to the number of bound ribosomes and thus the number of translated MTSs. Capturing the increase in mRNA localization with respect to mitochondrial volume with a mathematically simple mathematical model implies that we can treat affinity as an inherent characteristic that does not turn on and off, and does not increase or decrease, across the range of mitochondrial volumes despite the difference in metabolic mode and the associated reorganizations of the proteome and transcriptome.

Mitochondria grow in volume but do not change any other characteristic despite the aforementioned changes in metabolism. I assumed that interaction sites on the mitochondrial surface remain constant across mitochondrial volumes and that every mRNA-ribosome complex with affinity is equally capable of finding and interacting with the mitochondrial surface. Any mRNA-ribosome complex with affinity has a probability curve of binding to the surface whose shape and maximum are determined by the inherent, gene-specific binding affinity and the probability of being in the proximity of a mitochondrial surface, which we measure as mitochondrial volume. This two-state model necessarily treats kinetic effects as negligible: mRNA-ribosome complexes can switch between localized and non-localized based solely on their proximity to a generic mitochondrial surface but the characteristic time scale cannot be parsed in this model.

Altogether, the two-state model points to the paramount roles of mitochondrial volume and an inherent gene-specific parameter that, crucially, are independent variables that combine to set the localization behavior of mRNAs with MTSs. While a two-state model has the benefit of conferring numerous phenomenological insights, such as the lack of conditional affinity in this system, it is limited to description and cannot be used to make predictions about biochemical mechanisms or kinetic properties. Therefore, we built on these insights and created a minimal kinetic model with parameters that are more connected to quantitatively measurable or modifiable rates, such as diffusivity in cytosols of

varying volume.

Chapter 2, in part, is a reprint of the material as it appears in Mitochondrial volume fraction and translation duration impact mitochondrial mRNA localization and protein synthesis. Tsuboi, Tatsuhisa; Viana, Matheus P.; Xu, Fan; Yu, Jingwen; Chanchani, Raghav; Arceo, Ximena G.; Tutucci, Evelina; Choi, Joonhyuk; Chen, Yang S.; Singer, Robert H.; Rafelski, Susanne M; Zid Brian M. The dissertation author was not the primary investigator nor the author of this paper.

Chapter 3

Translation and diffusion kinetics combine to regulate Class II mRNA localization in brewer's yeast

Chapter 3, in full, is a reprint of the material as it appears in Mitochondrial mRNA localization is governed by translation kinetics and spatial transport in PLoS Computational Biology 2022. Arceo, Ximena G.; Koslover, Elena F.; Zid, Brian M.; Brown, Aidan I. The dissertation author was the primary investigator and author of this paper.

PLOS COMPUTATIONAL BIOLOGY

RESEARCH ARTICLE

Mitochondrial mRNA localization is governed by translation kinetics and spatial transport

Ximena G. Arceo[1], Elena F. Koslover[2], Brian M. Zid[1]*, Aidan I. Brown[3]*

1 Department of Chemistry & Biochemistry, University of California, San Diego, La Jolla, California, United States of America, **2** Department of Physics, University of California, San Diego, La Jolla, California, United States of America, **3** Department of Physics, Ryerson University, Toronto, Canada

* zid@ucsd.edu (BMZ); aidan.brown@ryerson.ca (AIB)
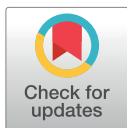
Abstract

For many nuclear-encoded mitochondrial genes, mRNA localizes to the mitochondrial surface co-translationally, aided by the association of a mitochondrial targeting sequence (MTS) on the nascent peptide with the mitochondrial import complex. For a subset of these co-translationally localized mRNAs, their localization is dependent on the metabolic state of the cell, while others are constitutively localized. To explore the differences between these two mRNA types we developed a stochastic, quantitative model for MTS-mediated mRNA localization to mitochondria in yeast cells. This model includes translation, applying gene-specific kinetics derived from experimental data; and diffusion in the cytosol. Even though both mRNA types are co-translationally localized we found that the steady state number, or density, of ribosomes along an mRNA was insufficient to differentiate the two mRNA types. Instead, conditionally-localized mRNAs have faster translation kinetics which modulate localization in combination with changes to diffusive search kinetics across metabolic states. Our model also suggests that the MTS requires a maturation time to become competent to bind mitochondria. Our work indicates that yeast cells can regulate mRNA localization to mitochondria by controlling mitochondrial volume fraction (influencing diffusive search times) and gene translation kinetics (adjusting mRNA binding competence) without the need for mRNA-specific binding proteins. These results shed light on both global and gene-specific mechanisms that enable cells to alter mRNA localization in response to changing metabolic conditions.

Author summary

Mitochondria are important generators of adenosine triphosphate (ATP), the energy currency of the cell. In the brewer's yeast, Saccharomyces cerevisiae, cells can switch ATP generation towards or away from mitochondria depending on the environment. Understanding how cells carry out this switch of mitochondrial function may provide insight into the loss of mitochondrial function, a hallmark of many age-related diseases. Many mRNAs that encode mitochondrial proteins are synthesized in the nucleus, but become localized to the mitochondrial surface during protein production. While some of these

Mitochondrial mRNA localization is governed by translation kinetics and spatial transport

mRNAs always localize to the mitochondria, others do so only in response to certain food sources driving energy production. In this study we created a mathematical model of mRNA localization to the mitochondria to understand what factors differentiate these two mRNA classes. Our analysis implicates protein translation kinetics as well as the mitochondrial volume as the key factors that control whether mRNA localize to mitochondria. This work provides insight into how global alteration in mitochondrial content and gene-specific modulation of protein synthesis kinetics can couple together to adjust mRNA localization and potentially mitochondrial function.

Introduction

To sustain life and function, cells maintain a homeostatic internal state while retaining the capacity to respond to variable environments and challenges. For eukaryotic cells, homeostasis requires not only regulation of gene expression, but also maintainance of internal organization through the sorting of proteins among organelles and subcellular compartments. Spatial targeting of proteins to specific cellular destinations can occur through a variety of transport and retention mechanisms, sometimes acting in combination [1–7].

Protein localization is often controlled by first transporting the mRNA to a specific region [8], and then translating proteins locally. mRNA localization serves as a key mechanism for delivering proteins to far-flung cell regions in neurons [9], expediting protein synthesis when locally required [10], and ensuring proteins are provided a suitable environment for folding [11]. Failure to localize mRNA can result in developmental defects [12] and cognitive disorders [13].

Canonical descriptions of protein localization through mRNA transport include translational suppression en route [8, 14], with protein synthesis beginning only after the mRNA reaches its target destination. By contrast, some mRNA are known to begin translation while in transit [15, 16]. For such cases, we explore how translational dynamics themselves can control mRNA localization, focusing on nuclear-encoded mitochondrial genes in yeast.

While some mitochondrial genes are encoded by mitochondrial DNA, the vast majority of mitochondrial proteins are translated from nuclear-encoded mRNA [17] and a subset of those mRNAs have been observed to localize to the mitochondrial surface. In *Saccharomyces cerevisiae* these mitochondrially localized mRNAs have been subclassified based on their mechanism of localization. Class I mRNAs are primarily targeted to the mitochondria by the RNA binding protein Puf3, while Class II mRNAs localize independently of Puf3 [18, 19]. Class II mRNAs are proposed to localize through translation of the amino-terminal mitochondrial targeting sequence (MTS) that can associate with import complexes on the cytosolic side of the outer mitochondrial membrane [20].

S. cerevisiae yeast rely heavily on glucose fermentation even in aerobic conditions. With non-fermentable carbon sources, the shift to a respiratory metabolism involves dramatic changes to the mitochondrial proteome [21, 22]. This shift also leads to an increase in the fraction of the cytosol occupied by mitochondria (mitochondrial volume fraction, or MVF) [23], which form dynamic tubular networks distributed throughout the cell [24]. While Class II mRNAs were initially found to be mitochondrially localized under respiratory conditions, many exhibit condition-dependent localization, as almost 70% do not robustly localize to mitochondria under fermentative conditions [23, 25, 26]. This may be due at least in part to changes in MVF, which can quantitatively predict the conditional localization behavior of mRNAs *ATP2* and *ATP3* [23]. Additionally, many Class II mRNAs that do not robustly

localize under fermentative conditions, including *ATP2* and *ATP3*, become mitochondrially localized upon application of the translation elongation inhibitor cycloheximide (CHX) [23, 25]. By contrast, other Class II mRNAs such as *TIM50* have high, constitutive localization to mitochondria even in fermentative conditions [23], and respond little to increased MVF [23] or CHX application [25]. Given that all Class II mRNAs contain an MTS but only some are localized under fermentative conditions, these observations suggest that the presence of the MTS is required but not sufficient for preferential localization to mitochondria. This idea has been further supported through MTS swapping experiments [20].

Localization of a Class II mRNA to a mitochondrion requires exposure of an MTS peptide sequence while the mRNA is very near to the mitochondrial membrane, implying that such localization can be modulated through the relative kinetics of MTS exposure and spatial movement throughout the cell. By arresting translation, CHX leaves nascent peptides and any of their translated MTS motifs exposed indefinitely. The increase in mRNA localization upon CHX application thus substantiates the importance of gene-specific translation dynamics for mitochondrial localization. Similarly, the dependence of mitochondrial localization on the MVF suggests that the geometry encountered by a diffusing mRNA can meaningfully control the frequency of mitochondrial proximity and opportunities for an MTS to interact with a mitochondrial surface.

The physical process of localization requires a transport mechanism enabling an mRNA to encounter its target region and a retention mechanism to limit mRNA escape. In the relatively small volume of a yeast cell, diffusion is sufficient to distribute mRNA, with diffusive arrival rates to cellular targets modulated by intracellular geometry [7, 27–32]. Once an mRNA has diffusively reached a destination, binding interactions then determine the time period of mRNA localization. Equilibrium mRNA localization would be determined by the probability of occupying a binding-competent state and the volume of the localization region, i.e. the MVF. However, the energy-consuming process of translation pushes mRNA localization out of equilibrium, similar to other driven processes necessary to maintain cellular organization, including protein targeting [6, 7, 33–36].

To address how translational dynamics could control the localization of mRNA for mitochondrial genes, we developed a stochastic, quantitative model for mitochondrial mRNA localization that incorporates translation and diffusion within a yeast cell. The model is parameterized against published genome-wide measurements of both constitutively and conditionally localized Class II mRNAs [22, 37, 38]. We find that the kinetics of translation, as well as the diffusive search time-scales, determine the level of mRNA localization to mitochondria, enabling both low and high localization within the physiological range of key parameters. Crucial to our description of mitochondrial mRNA localization is a proposal for an MTS maturation time following translation of the MTS peptide sequence. Our work suggests a distinct mode of spatial protein regulation and a mechanism for yeast and other cells to control protein localization using gene-specific translation dynamics combined with global adjustments of organelle size.

Results

Localization depends on both equilibrium and kinetic contributions

To help guide our investigation of the translational control of mRNA localization, we begin by analyzing a general minimal model (Fig 1A). We assume that mRNA is capable of switching between a binding-competent ("sticky") state and a binding-incompetent ("non-sticky") state. For mitochondrial targeting, a binding-competent state corresponds to an mRNA with at least one partially-translated peptide with an exposed MTS sequence. We define two rate constants:
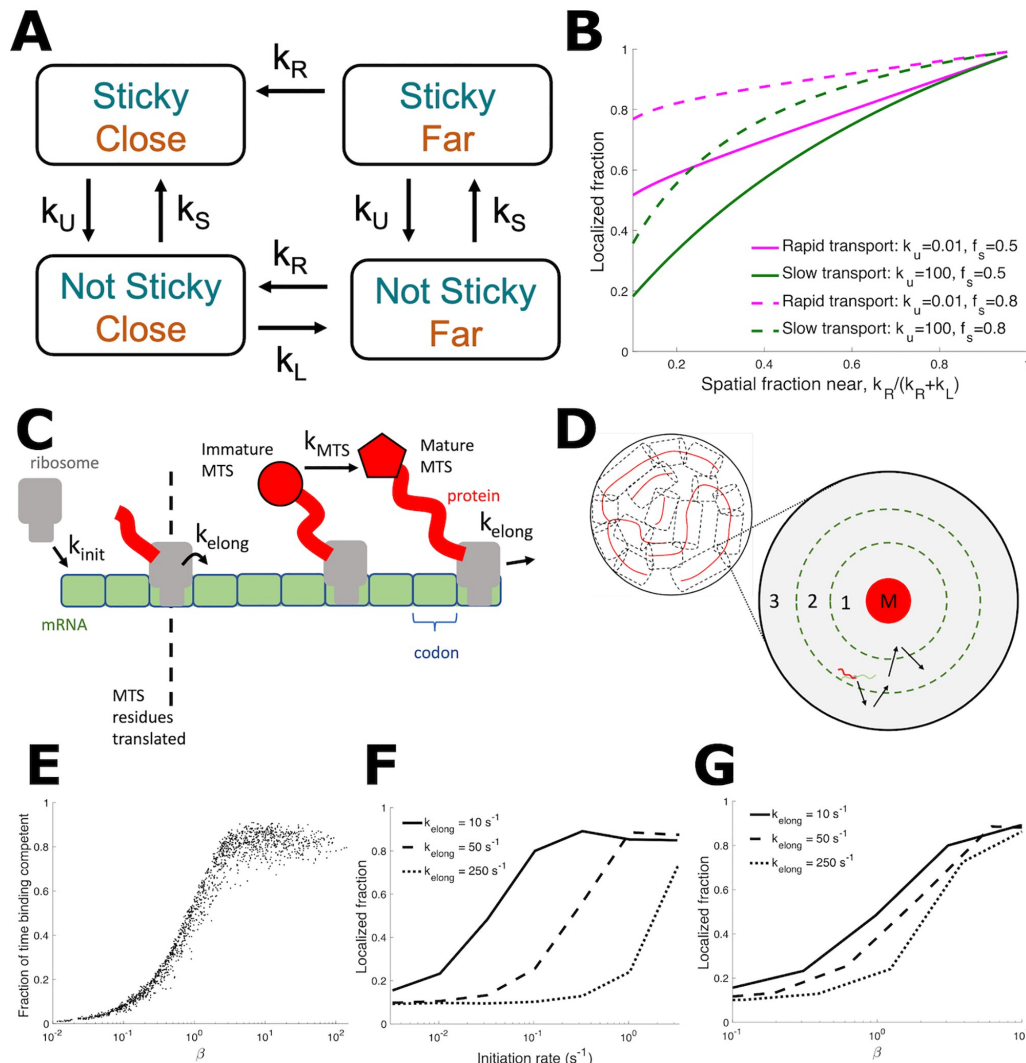
Fig 1. Quantitative models show equilibrium and kinetic contributions to mitochondrial mRNA localization. (A) Simplified discrete-state model of mRNA mitochondrial localization. mRNA can be either binding competent ('sticky') or not binding competent ('not sticky'), and either within binding range of mitochondria ('close') or not within binding range ('far'). mRNA transition between these states with rates described in the text. (B) Localized fraction [defined as 'close' in (A)] as the spatial fraction of the cell near mitochondria (Eq 2) is varied. Rapid transport curves indicate rapid switching from close to far relative to switching between sticky and not sticky, while for slow transport the relative switching speeds are reversed. (C) Stochastic model of mRNA translation. Ribosomes initiate translation at rate k_{init} and progress to the next codon at rate k_{elong}. MTS is translated after the first 100 amino acids. Once MTS is translated, MTS becomes binding-competent at rate k_{MTS}. (D) Schematic of mRNA diffusion in spatial model, shown in cross-section. The cytoplasmic space is treated as a cylinder centered on a mitochondrial cylinder (red): the three dimensional volume extends along the cylinder axis. mRNA in region 1 are sufficiently close for binding-competent mRNA to bind to the mitochondria, mRNA in region 2 are considered mitochondrially localized in diffraction-limited imaging data, and region 3 represents the remainder of the cell volume. mRNA not bound to mitochondria will freely diffuse between these regions. (E) For the stochastic translation model shown in (C), the fraction of mRNA lifetime that an mRNA is binding-competent vs. $\beta = k_{init}(L - L_{MTS})/k_{elong}$, the mean number of translated MTSs per mRNA. For each data point, mRNA translation parameters k_{init}, L, and k_{elong} were randomly selected from the ranges $k_{init} \in [10^{-3}\ s^{-1}, 0.5\ s^{-1}]$, $L \in [150\ aa, 600\ aa]$, and $k_{elong} \in [1\ s^{-1}, 10\ s^{-1}]$. (F) Mitochondrial localization from the stochastic model illustrated in C and D, as k_{init} is varied. $L = 400$ aa, 4% mitochondrial volume fraction, and k_{elong} as indicated in legend. (G) is the same data as F, but plotted against β.

Figure 3.1: Quantitative models shows equilibrium and kinetic contributions to mitochondrial mRNA localization

16

k_S and k_U for switching into and out of the competent state, respectively, assumed to be independent of the mRNA location. At equilibrium the fraction

$$f_s = \frac{k_S}{k_S + k_U} \tag{1}$$

is in the competent state. For a binding-competent mRNA to bind to a mitochondrion, it must be sufficiently proximal to a mitochondrial surface. Binding-incompetent molecules can move from the bulk into binding range of a mitochondrion with rate k_R and can leave the near-surface region with rate k_L. These rates are expected to depend on the diffusivity of the mRNA and the geometry (size and shape) of mitochondria within the cell. At equilibrium,

$$f_d = \frac{k_R}{k_R + k_L} \tag{2}$$

is the fraction of the mRNA-accessible cell volume that is within binding range of the mitochondrial surface. As the cytosolic volume fraction that is near mitochondria, f_d is distinct from but related to the MVF, the cell volume fraction occupied by mitochondria. The binding-competent mRNA reach the mitochondrial region with the same rate k_R but are assumed to bind irreversibly and cannot leave until they switch into the incompetent state.

The resulting four-state model (binding-competent vs not, proximal to mitochondria vs not) is illustrated in Fig 1A. Given the assumed irreversible binding of competent mRNAs, the model is inherently out of thermal equilibrium. The kinetic equations can be solved to find the steady-state fraction of mRNA localized to the proximal region, as a function of the kinetic rates (see Methods).

The solutions exhibit two limiting regimes of interest. In the rapid-transport regime where mRNA transport is much faster than the competence switching rate ($k_U, k_S \ll k_R, k_L$), incompetent mRNA can equilibrate throughout the entire cell prior to a switching event. Similarly, competent mRNA can rapidly reach the proximal region and bind to mitochondria. The fraction of mRNA that are mitochondrially localized is then given by the two equilibrium fractions,

$$f_{loc} = f_s + (1 - f_s)f_d \ . \tag{3}$$

In this spatially equilibrated situation, changing the mitochondrial volume fraction would affect only f_d. If binding dynamics are held fixed (fixed f_s), the mitochondrially localized fraction f_{loc} will depend linearly on the proximal volume fraction f_d, with the slope determined by the equilibrium binding competence f_s.

In the opposite slow-transport regime, mRNA transport is much slower than the switching rate ($k_R, k_L \ll k_U, k_S$) and the fraction localized is given by:

$$f_{loc} = \frac{1}{1 + (1 - f_s)(1 - f_d)/f_d} \ . \tag{4}$$

This regime exhibits nonequilibrium behavior. In the limit of low mitochondrial volume fraction ($f_d \ll 1$), the localization probability goes to zero. This is a fundamental difference from the rapid-transport regime, where even at low volume fractions, binding-competent mRNA localize to mitochondria. As a result, the regime with slow transport and fast switching is expected to exhibit a steeper, more non-linear increase in localization with increasing mitochondrial volume fraction (green lines in Fig 1B) compared to the rapid-transport regime (magenta lines in Fig 1B).

This highly simplified, analytically tractable, four-state model is agnostic to the mechanistic details for how the switching between binding-competent and incompetent states occurs, as well as the geometric details of diffusive transport to and from the mitochondria-proximal region. Specifically, it highlights some important non-intuitive features of localization for any molecule that can switch between competent and incompetent states. Namely, the localization behavior is expected to depend not just on the equilibrated binding-competent fraction f_s (Eq 1) and proximal fraction f_d (Eq 2) but also on the relative kinetics of spatial transport and competence switching. In the nonequilibrium regime of fast switching and slow transport, localization becomes non-linearly sensitive to the volume fraction of the target region.

For the mitochondrial localization of mRNA, the switching times between competent and incompetent states are determined by translation kinetics that control exposure duration for attached MTS peptide sequences. The transport kinetics are determined by diffusion time-scales towards and away from the mitochondrial surface. We next proceed to develop a more mechanistically detailed model for mitochondrial localization that directly incorporates translation and diffusion.

Stochastic simulation incorporates translation and diffusive kinetics

The translation kinetics model (Fig 1C) tracks ribosome number and position. Ribosomes initiate translation on an mRNA with rate k_{init}, and then proceed along the mRNA codons at elongation rate k_{elong}. The mRNA is L codons in length. The number of codons that must be translated to complete the MTS is set to $l_{MTS} = 100$ to account for an MTS length of up to 70 amino acids and a ribosome exit tunnel length of ~ 30 amino acids [39, 40]. We begin with an 'instantaneous' model, where once translation moves past l_{MTS}, the mRNA-ribosome complex is assumed to be binding competent until translation completes ($k_{MTS} \rightarrow \infty$ in Fig 1C). In subsequent sections we will consider alternative binding-competence models with finite k_{MTS}.

An mRNA can have multiple MTS-containing nascent peptides if a subsequent ribosome initiates and translates another MTS before the prior translation event is complete. The average number of such binding-competent peptides on a given mRNA is given by

$$\beta = \frac{k_{init}(L - l_{MTS})}{k_{elong}} \quad . \tag{5}$$

To describe the diffusive encounter of an mRNA with the mitochondrial network, we use a simplified geometric model appropriate for diffusive search towards a narrow tubular target. Specifically, we treat the geometry as a sequence of concentric cylinders, each representing an effective region surrounding a tubule of the mitochondrial network (Fig 1D). Fig 1D shows a two-dimensional cross-sectional view of this three-dimensional geometry. The innermost cylinder represents a mitochondrial tubule and serves as a reflective boundary for the mRNA. A slightly larger cylinder represents the region where a binding-competent mRNA is sufficiently close to bind to the mitochondrial surface. If one or more binding-competent MTSs are exposed on an mRNA when it reaches the vicinity of the innermost cylinder, the mRNA will remain associated to the mitochondrial surface until the mRNA returns to zero binding-competent MTSs after peptide translation is completed. A still wider cylindrical region represents locations where the transcript would appear close to the mitochondrial tube in diffraction-limited imaging data, but may not be sufficiently close to bind the mitochondrial surface. Finally, the outermost reflecting cylinder represents the cytoplasmic space available to the diffusing mRNA. The radius of this external cylinder is set such that the innermost mitochondrial cylinder encloses the correct volume fraction of mitochondria to correspond to experimental measurements (which can range from 1%–15%).

This simplified geometry gives an approximate description of the search process for the mitochondrial surface, based on the idea that whenever the mRNA wanders far from any given mitochondrial tubule it will approach another tubule in the network (Fig 1D), so that its movement can be treated as confinement within an effective reflecting cylinder. Such an approach has previously been used successfully to approximate the diffusive process of proteins searching for binding sites on long coils of DNA [31]. More detailed geometrical features, such as the specific junction distribution and confinement of the yeast mitochondrial network to the cell surface are neglected in favor of a maximally simple model that nevertheless incorporates the key parameters of mitochondrial volume fraction and approximate diffusive encounter time-scale.

Simulations of our stochastic model for simultaneous translation and diffusion can be carried out with any given set of gene-specific translation parameters (k_{init}, k_{elong}, L). The simulated mRNA trajectories are then analyzed to identify the fraction of mRNA found within the region proximal to the mitochondrial surface (see Methods for details). By exploring the physiological range of translation parameters, many orders of magnitude of the mean number of translated MTSs per mRNA (β, see Eq 5) are covered, which also covers the full range of mRNA binding competence (Fig 1E). We find that, for any set of physiological translation parameters, the number of binding-competent MTS sequences (β) is predictive of the fraction of time (f_s) that each mRNA spends in the binding competent state (Fig 1E). The greatest variation is near $\beta \approx 1$, where different parameter combinations with the same average number of exposed MTSs can give competency fractions ranging from $30 - 50\%$.

Our analytically tractable 4-state model (Fig 1B) indicates that localization fraction should depend not only on the binding competent fraction f_s (related to β) but also on the kinetics of switching between competent and incompetent states. We explore the effect of translation kinetics on localization in the stochastic model by varying the initiation and elongation rates of a fixed-length mRNA (Fig 1F). This approach samples the scope of localization behaviors by simulating multiple combinations of translation parameters. We include unphysiologically high elongation rates to compare to the expected behavior from the 4-state model. As expected, faster elongation rates (which decrease the period an MTS is exposed on an mRNA and decrease β) result in lower localization, and higher initiation rates (which increase β while leaving MTS exposure time unaffected) result in higher localization (Fig 1F). While the number of exposed MTSs, β, can explain much of the effect of changing elongation and initiation rates (Fig 1G), there is substantial variability in localization around $\beta \approx 1$, with faster elongation decreasing localization. This result is consistent with the prediction of the 4-state model that rapid switching of binding competence can lead to lower localization even for equal binding competent fractions f_s.

Physiological translation parameters lead to high mitochondrial binding competence and localization

Because translation kinetics and length vary between genes, we expect the kinetics of binding-competence switching and thus the mitochondrial localization to be gene-specific. To explore the relationship between translation kinetics and mitochondrial localization, we define two categories of Class II mRNAs that were all found to be localized in respiratory conditions [19] by their localization sensitivity to translation elongation inhibition by cycloheximide (CHX) in fermentative conditions [25]. "Constitutive" mRNAs preferentially localize to mitochondria both in the absence and presence of CHX. "Conditional" mRNAs do not preferentially localize to mitochondria in the absence of CHX, but do so following CHX application.

Fig 2. Instantaneous model is insufficient to explain differential mitochondrial localization of different gene groups. (A) Cumulative distributions of conditional and constitutive mRNA genes vs number of binding-competent ribosomes β (lines indicate fraction of genes with given β or less). β for each mRNA gene is calculated from gene-specific k_{init} and k_{elong} that are estimated from experimental data (see Methods). Inset is cumulative distribution of ribosome occupancy [38], showing ribosome occupancy and β have similar distributions. (B) Violin plot [41] showing mRNA localization fraction of individual genes with instantaneous model (no maturation delay), with translation kinetics for each gene estimated from experimental data (see Methods). 4% MVF. For direct comparison to experimental data, mRNA in region 1 (see Fig 1D) recorded as mitochondrially localized. (C) Mitochondrial localization vs mitochondrial volume fraction for *TIM50* and *ATP3* with instantaneous model (solid lines), with translation kinetics for both genes estimated from experimental data (see Methods). For direct comparison to experimental data (dotted lines with circles), mRNA in regions 1 and 2 (see Fig 1D) recorded as mitochondrially localized. (D) Cumulative distributions of MTS exposure time $t_{expo} = (L - l_{MTS})/k_{elong}$. The steeper rise of conditional genes indicates more conditional gene mRNAs have low exposure times. Translation kinetics for each gene estimated from experimental data (see Methods). Inset shows the cumulative distribution of elongation rate, for which constitutive genes have a steeper rise, indicating slower typical elongation, which contributes to the longer exposure times in the main plot.

https://doi.org/10.1371/journal.pcbi.1010413.g002

Using protein per mRNA and ribosome occupancy data [22, 37, 38, 42], we estimated the gene specific initiation rate k_{init} and elongation rate k_{elong} for 52 conditional and 70 constitutive genes (see Methods). Along with the known mRNA lengths L, these parameters quantitatively describe translation of each gene in the yeast transcriptome. These measurements [38] indicate that conditional and constitutive genes have similar distributions of ribosome occupancy (Fig 2A, inset; see S1 Fig for similar distributions of conditional and constitutive gene

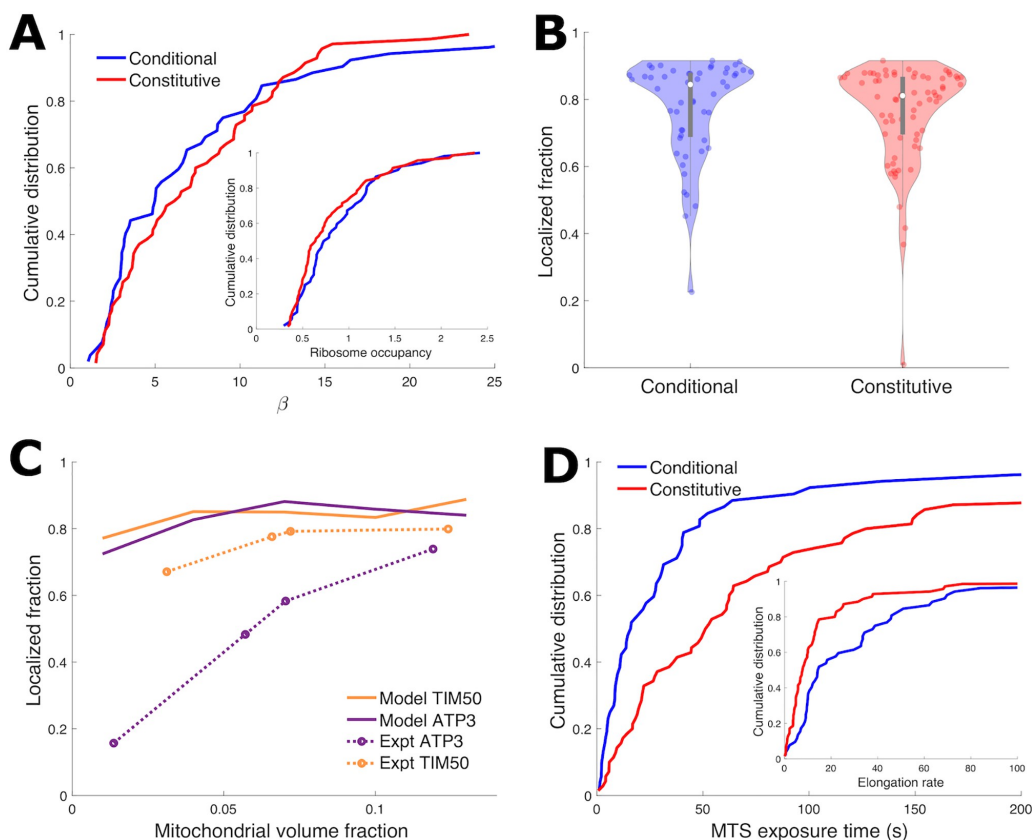Figure 3.2: Instantaneous model is insufficient to explain differential mitochondrial localization of different gene groups

20

ribosome occupancy derived from [43]). Conditional and constitutive genes also have similar distributions of the number of exposed MTSs, β, as calculated from estimated translation parameters (Fig 2A). Notably, the predicted β values were relatively large, with 90% of both constitutive and conditional mRNA estimated to have $\beta > 2$. Consequently, the stochastic simulation predicts median localization fractions above 80% for both the conditional and constitutive gene groups, with no significant difference between the two groups (Fig 2B). Comparison of two specific genes (*ATP3* and *TIM50*) known to have mitochondrial localizations with distinct dependence on mitochondrial volume fraction [23] also yielded similarly high localization fractions in stochastic simulations, across all mitochondrial volume fractions (Fig 2C).

These simulation results using gene-specific estimates of the translation parameters k_{init}, k_{elong}, and L (Fig 2B and 2C) run directly counter to experimental measurements. Specifically, they over-predict mitochondrial localization for transcripts, such as *ATP3*, that are known to exhibit low localization values at low mitochondrial volume fractions. Given the high calculated values of β, and the importance of MTS exposure kinetics in predicting localization at intermediate β values, we more closely examined the quantities underlying this parameter, which describes the number of exposed complete MTSs. We find that the distributions of both the elongation rate and the MTS exposure time $t_{\text{expo}} = (L - l_{\text{MTS}})/k_{\text{elong}}$ substantially differ between the two gene groups, with conditionally localized genes exhibiting more rapid elongation and shorter MTS exposure times (Fig 2D; see S2 Fig for similar distributions of conditional and constitutive gene elongation rates derived from [42]). These differences in MTS exposure kinetics between the two gene groups point towards a mechanism, thus far not part of our quantitative model, that would reduce the number of exposed MTSs (β), allowing for more variability in localization between the two groups. At the same time, this mechanism should have a greater effect in reducing MTS exposure time in conditionally localized genes, enabling reduced localization of this group at low mitochondrial volume fractions.

Mitochondrial binding competence requires a maturation period

To reduce β and MTS exposure time, we introduce into our quantitative model a time delay between complete translation of the MTS and maturation of the MTS signal to become binding competent (Fig 1C, $k_{\text{MTS}} < \infty$). This additional parameter is consistent with evidence that mitochondrially imported proteins require the recruitment of cytosolic chaperones to target them for recognition [44] and import by receptors on the mitochondrial surface [45–47]. During MTS maturation, which could include autonomous folding or interaction with additional chaperone proteins [48], the MTS becomes capable of binding the mitochondrial surface.

In the model, MTS maturation is treated as a stochastic process with constant rate k_{MTS} corresponding to an average maturation time $\tau_{\text{MTS}} = 1/k_{\text{MTS}}$. This maturation period decreases the binding-competent exposure time uniformly across all mRNA, and decreases the number of binding-competent MTS signals (i.e. lowers β) for all mRNA. The maturation period has the largest effect on short mRNAs with fast elongation, reducing their already short exposure times. Consequently, it is expected to have a larger effect on conditional versus constitutive genes.

The additional MTS maturation time does not alter the total time to translate an mRNA ($T_{\text{total}} = L/k_{\text{elong}}$). The ribosome continues elongating during maturation, and is located at a downstream codon when the MTS becomes binding competent. The mean steady-state

number of binding-competent MTSs per mRNA is

$$\beta_{\text{mature}} = \frac{k_{\text{init}}}{k_{\text{elong}}} \left\{ L - l_{\text{MTS}} - \frac{k_{\text{elong}}}{k_{\text{MTS}}} \left[1 - \exp\left(-\frac{k_{\text{MTS}}}{k_{\text{elong}}} [L - l_{\text{MTS}}] \right) \right] \right\} \; . \tag{6}$$

The mean time that each MTS is binding competent is

$$t_{\text{expo,mature}} = (1 - e^{-k_{\text{MTS}} t}) \left[\frac{1}{k_{\text{MTS}}} \frac{1 - e^{-k_{\text{MTS}} T_{\text{total}}} (k_{\text{MTS}} T_{\text{total}} + 1)}{1 - e^{-k_{\text{MTS}} T_{\text{total}}}} \right] \; . \tag{7}$$

For mRNA localization to be sensitive to mitochondrial volume fraction, we expect the
MTS exposure time to be shorter than the diffusive search times at low MVF (slow search,
long search time) and longer than diffusive search times at high MVF (fast search, short search
time). Such an intermediate exposure time will allow for high mitochondrial localization
exclusively at high MVF.

The mean search time for a particle of diffusivity D to find a smaller absorbing cylinder of
radius r_1 when confined within a larger reflecting cylinder of radius $r_2 > r_1$ is [28]

$$t_{\text{search}} = \frac{1}{2D} \left[\frac{r_2^4}{r_2^2 - r_1^2} \log\left(\frac{r_2}{r_1} \right) - \frac{3r_2^2 - r_1^2}{4} \right] \; . \tag{8}$$

The smaller, absorbing radius r_1 represents the cylinder sufficiently close to bind the mito-
chondrial surface, while r_2 is the cylinder representing a typical distance that the diffusing par-
ticle must move through the cytoplasm to approach a different region of the mitochondrial
network. As the mitochondrial volume fraction decreases, the radius r_2 and the diffusive search
time to find the mitochondrial surface t_{search} both increase.

To understand the impact of MTS maturation, we consider a typical conditional and consti-
tutive mRNA from each group, using median translation rates and gene length. Fig 3A shows
the exposure time $t_{\text{expo,mature}}$ as the maturation time is varied. We find exposure times for a
typical conditional gene to be intermediate between the high and low MVF diffusive search
times when the maturation time is in the range $\tau_{\text{MTS}} = 10$—100 seconds (Fig 3A). By contrast,
the typical constitutive gene maintains an exposure time that is higher than the diffusive search
time for this parameter range.

In addition to modulating the kinetics of binding competency, the maturation period
decreases the expected number of functional MTS signals per mRNA, β (Fig 3B). For the typi-
cal conditional gene, β decreases to approximately 1 for maturation times of 40—50 seconds,
while $\beta \approx 2.5$ for the typical constitutive gene in this range. The introduction of the MTS matu-
ration time can thus selectively shift the expected number of functional MTS signals on condi-
tional mRNA to the intermediate range ($\beta \approx 1$) necessary to allow for MVF sensitivity in the
localization behavior. Under the same conditions, the constitutive mRNA would maintain a
high number of functional MTSs and thus should remain localized even at low MVF.

Fig 3C shows how the localization for the prototypical conditional and constitutive mRNA
varies with the maturation time. For very rapid MTS maturation ($\tau_{MTS} \rightarrow 0$), the MTS matura-
tion model shows consistently high localization, as expected from the earlier model wherein
the MTS became binding competent immediately upon translation. As the MTS maturation
time increases and binding competency drops, both typical conditional and constitutive
mRNA decrease their mitochondrial localization. However, the localization of the typical con-
ditional mRNA begins to fall at approximately 10 seconds of maturation, while constitutive
mRNA localization remains high until approximately 40 seconds of maturation. To provide a
specific estimate of the maturation time, we determine the maturation times for which the
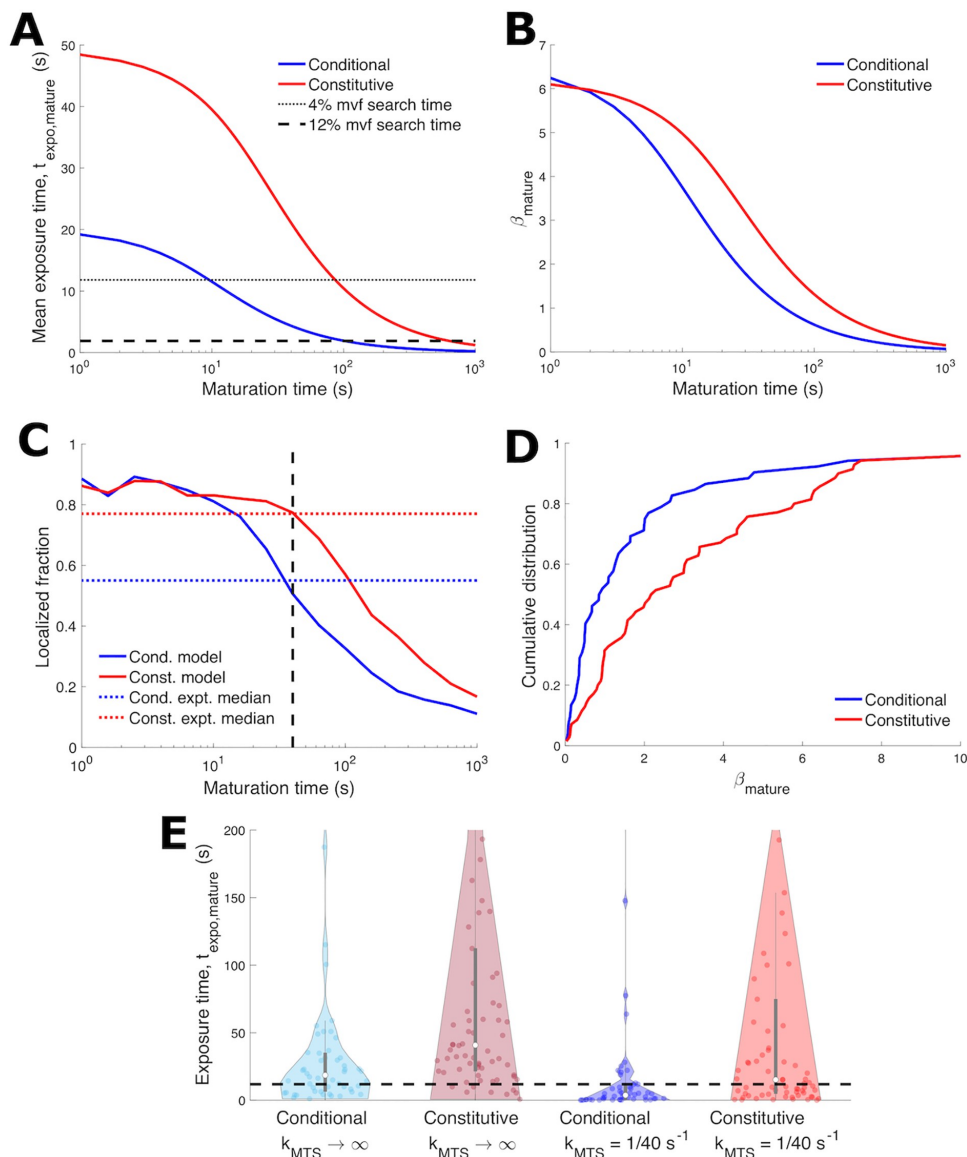
Fig 3. MTS binding-competence maturation time underlies distinct mitochondrial localization behavior of conditional and constitutive genes. (A) Mean exposure time of a binding-competent MTS before completing translation (Eq 7) vs binding-competence maturation time. Data for median conditional ($L = 393$ aa, $k_{init} = 0.3253$ s^{-1}, $k_{elong} = 14.5086$ s^{-1}) and constitutive genes ($L = 483$ aa, $k_{init} = 0.1259$ s^{-1}, $k_{elong} = 7.7468$ s^{-1}) is shown. Horizontal dashed lines are the mean diffusive search times (Eq 8) to reach binding range of mitochondria (region 1 in Fig 1D). (B) β_{mature} (mean number of mature binding-competent MTS signals, Eq 6) vs maturation time for median conditional and constitutive genes. (C) Mitochondrial localization (to region 1) vs maturation time for median conditional and constitutive genes with 4% MVF. Horizontal dotted lines indicate experimental localization medians. 40 second maturation time (vertical dashed line) allows model to match experimental localization for both conditional and constitutive genes. (D) Cumulative distribution of β_{mature} (mean mature MTS signals per mRNA) for conditional and constitutive genes. Steeper rise of conditional genes indicates more conditional genes have low β than

Figure 3.3: MTS maturation time underlies distinct mitochondrial localization behavior of conditional and constitutive genes

23

constitutive genes; compare to Fig 2A, which lacked MTS maturation time. (E) Violin plot showing model exposure times with 40-second MTS maturation and the instantaneous model without MTS maturation ($k_{MTS} \to \infty$). 4% MVF. Median conditional exposure time with maturation is below the diffusive search time to find the binding region (horizontal dashed line, Eq 8 for 4% MVF) while the other three medians are above this search time. For (C)—(E), the translation kinetics for each gene are estimated from experimental data (see Methods).

https://doi.org/10.1371/journal.pcbi.1010413.g003

model predicts the median experimental localization for conditional and constitutive genes (Fig 3C, intersection of dotted lines and solid lines). A single value of $\tau_{MTS} \approx 40$ seconds yields a simultaneous accurate prediction for the localization of both groups (Fig 3C, dashed).

Overall, the experimental data is consistent with a single gene-independent time-scale for MTS maturation. The stochastic model with a 40-second MTS maturation period was next applied to each of the conditional and constitutive mRNAs, for which translation parameters were calculated individually. With this maturation time, β_{mature} is substantially lower for conditional mRNA in comparison to constitutive mRNA (Fig 3D).

For conditional mRNAs without the maturation period ($k_{MTS} \to \infty$), the median MTS exposure time is greater than the diffusive search time (Fig 3E, dashed black line). With a maturation time of $\tau_{MTS} = 40$ s, the median conditional MTS exposure time decreases to be faster than diffusive search (Fig 3E). In contrast, constitutive mRNAs retained a median MTS exposure time longer than the diffusive search time, both with and without the 40-second maturation period.

Mitochondrial localization of conditional mRNAs is sensitive to inhibition of translational elongation and to mitochondrial volume fraction

Using the stochastic model with a 40-second MTS maturation period, we compute the localization of individual mRNAs in the constitutive and conditional groups, at a low mitochondrial volume fraction of 4%. Unlike the instantaneous model (with no MTS maturation delay), the localization of conditional genes is predicted to be significantly lower than that of constitutive genes (Fig 4A). While introduction of this maturation time distinguishes the mitochondrial localization of conditional and constitutive gene groups (Figs 4A vs 2B), changes to diffusivity are unable to separate the two gene groups (S3 Fig).

Furthermore, we use our model to predict localization in the presence of cycloheximide (CHX), which halts translation [49]. The localization difference in response to CHX application was used originally to define the constitutive and conditional groups [25]. The effect of CHX is incorporated in the model by assuming that all mRNAs with an exposed MTS at the time of CHX application will be able to localize to the mitochondrial surface, since further translation will be halted by CHX. We therefore compute from our simulations the fraction of mRNAs that have at least one fully translated (but not necessarily mature) MTS, defining this as the localization fraction in the presence of CHX. The model predicts that conditional genes will have a substantial difference in localization upon application of CHX, while the difference for localization of constitutive genes will typically be much smaller (Fig 4B). Qualitatively, this effect is similar to the observed difference in localization for experimental measurements with and without CHX (Fig 4C).

The predicted mitochondrial localization of the two example mRNAs, *ATP3* and *TIM50*, is shown in Fig 4D as a function of mitochondrial volume fraction. The model predicts *ATP3* localization is strongly sensitive to MVF, switching from below 30% at low MVF to above 70% localization at high MVF. By contrast, high localization of *TIM50* is predicted regardless of the MVF. The sensitivity of *ATP3* and insensitivity of *TIM50* localization to the MVF is consistent with experimental measurements indicating that *ATP3* exhibits switch-like localization under different metabolic conditions, while *TIM50* remains constitutively localized [23] (Fig 4D,
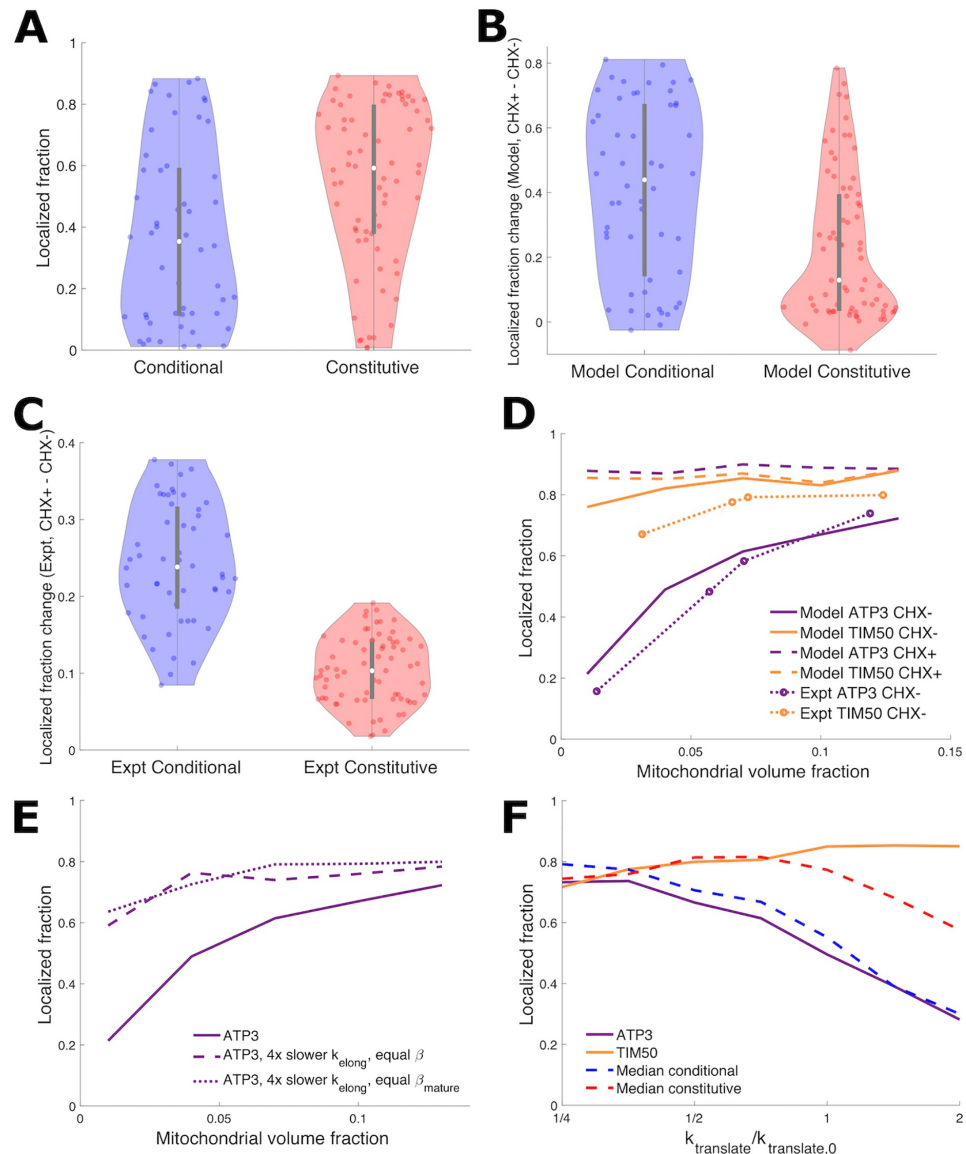
Fig 4. MTS maturation time distinguishes mRNA localization of conditional and constitutive genes. (A) Violin plots of mitochondrial localization of conditional and constitutive genes for model with 40-second maturation time; compare to Fig 2B, which lacked MTS maturation time. p-value = 0.5% for two-sample Kolmogorov-Smirnov test for a difference between conditional and constitutive localization distributions. (B,C) Violin plots of localization increase upon cycloheximide application for model with 40-second MTS maturation time (B) and from experiment (C). (D) Mitochondrial localization for *ATP3* and *TIM50* vs MVF for model with 40-second MTS maturation time. Solid lines are CHX-, which closely corresponds to experimental data [23] shown with dotted lines with circles. Dashed lines are CHX + model predictions, exhibiting large increase upon CHX application for *ATP3* and limited increase for *TIM50*. (E) Comparing model mitochondrial localization results for *ATP3* to similar hypothetical construct gene with decreased elongation rate and initial rate selected to maintain either MTS number β or mature MTS number β_{mature}. (F) Comparing model mitochondrial localization results for median

Figure 3.4: MTS maturation time distinguishes mRNA localization of conditional and constitutive genes

25

conditional and constitutive genes, *ATP3*, and *TIM50* as both elongation and initiation rates ($k_{translate}$) are varied. $k_{translate,0}$ is the elongation or initiation rate for each of *ATP3*, *TIM50*, and median conditional and constitutive genes. For all panels, the translation kinetics for each gene are estimated from experimental data (see Methods). For (F), see Fig 3 for median conditional and constitutive translation kinetics. (A), (B), and (F) use 4% MVF.

dotted lines with circles). Dashed lines in Fig 4D show the predicted localization after CHX application, highlighting the difference in response to CHX between *ATP3* and *TIM50*.

The introduction of a delay period for MTS maturation both reduces the average number of binding-competent MTSs on each mRNA (lower β) and decreases the exposure time of each MTS. The latter effect results in faster switching between binding-competent and incompetent states for an mRNA. In the basic 4-state model, we saw that a steep sensitivity to the spatial region available for binding depends on having relatively rapid binding-state switching kinetics compared to the diffusion timescale (Fig 1B). As shown in Fig 3, the exposure time for conditional mRNAs is intermediate between the diffusive search times at high and low mitochondrial volume fractions. We therefore expect that the high rate of losing binding competence associated with the limited MTS exposure time to be critical for the switch-like response to mitochondrial volume fraction by *ATP3*.

As initiation rate can compensate for slowing translation elongation rates to maintain ribosome density [50, 51], we consider hypothetical constructs which have the same average ribosome density (equal β) or mature MTS number (β_{mature}) as *ATP3*, but 4-fold slower translational elongation rates. This results in slower switching kinetics, causing high localization and a loss of sensitivity to mitochondrial volume fraction (Fig 4E). We also consider how translation rate adjustment could control mRNA localization while remaining at a fermentative mitochondrial volume fraction (4%). Localization substantially decreases with increasing elongation and initiation rates for the median conditional gene and *ATP3*, while localization is less responsive to increased translation rates for the median constitutive gene and *TIM50* (Fig 4F). For responsive genes, translation rate modulation can adjust localization in a similar manner to mitochondrial volume fraction, with the potential for targeting of specific genes.

Overall, these results highlight the importance of translation kinetics, including both elongation rates and the maturation time of the MTS, in determining the ability of transcripts to localize to the mitochondrial surface. These kinetic parameters determine not only the equilibrated fraction of mRNAs that host a mature MTS but also the rate at which each mRNA switches between binding-competent and incompetent states. In order to achieve switch-like localization that varies with the mitochondrial volume fraction or CHX application, a transcript must exhibit an average of approximately one binding-competent MTS, with an exposure time that is intermediate between diffusive search times at low and high MVFs.

Discussion

We have investigated, using quantitative physical modeling and analysis of yeast transcriptome data, the role of translation kinetics in controlling MTS-mediated localization of nuclear-encoded mRNA to mitochondria. Specifically, we explored how mRNA binding competence and association with the mitochondrial surface, across a range of cellular conditions, is governed by the interplay of timescales for translation and cytoplasmic diffusion. We compared two sets of mRNA: one that is localized conditionally, when mitochondrial volume is expanded or when translational elongation is halted by cycloheximide, and another that localizes constitutively regardless of these conditions. For these 52 conditional and 70 constutitive mRNA we estimated gene-specific translation kinetics to apply in the model. Our analysis indicates that these two sets of transcripts exhibit global differences in translation kinetics, and

that these differences control mRNA localization to mitochondria by adjusting the number and duration of exposure for mitochondrial targeting sequences (MTSs) that are competent to bind to the mitochondrial surface.

It has previously been noticed when comparing mitochondrially localized versus non-localized yeast mRNAs, that localized mRNAs have features that reduce translation initiation and lower ribosome occupancy [52]. This observation seemed counterintuitive as MTS exposure was thought to be important for the localization of many of these mRNAs and hence higher ribosome occupancy would be expected to enhance localization by increasing the number of exposed MTSs [25, 53]. Lower occupancy was proposed to drive mRNA localization through increased mRNA mobility of a poorly loaded mRNA [52], as more mobile mRNA could more quickly find mitochondria when binding competent, increasing the localization of these mRNA. By contrast, our results imply an alternate prediction—that translational kinetics lead to enhanced localization of longer mRNAs, due to the increased number of loaded ribosomes bearing a binding-competent MTS. Indeed, constitutively localized mRNAs are on average longer than conditionally localized mRNAs. We show that translational parameters which yield a moderate number of approximately 1—2 binding competent ribosomes (via associated MTSs) per mRNA nevertheless allow robust localization under physiological conditions. Furthermore, this model occupancy allows for localization levels to be steeply sensitive to mitochondrial volume fraction, enabling transcript localization to be modulated by the MVF during changes to nutrient conditions and the metabolic mode. By contrast, transcripts with a high occupancy are expected to remain constitutively localized to mitochondria, regardless of the metabolic state of the cell. Thus, tuning of translational kinetics allows for differential response of transcript localization under varying nutrient conditions without the need for additional signaling pathways.

Translation kinetics can widely vary between genes, with greater than 100-fold variation in mRNA translation initiation rates and approximately 20-fold variation of elongation rates in yeast [42]. Translation duration can be further impacted by the length of the coding sequence. Constitutively localized mRNAs are on average longer and have slower translation elongation than conditionally localized mRNAs. Experimentally testing our proposal for translation-controlled localization would involve using combined mRNA and live translational imaging (as yet undeveloped in yeast), to directly measure translation and correlate localization with a time delay, presenting a fruitful pathway for future study. Cis regulators of translation elongation rates include mRNA features such as codon usage, codon context, and secondary structures [54, 55]. For the constitutively localized mRNA *TIM50* it was previously found that a stretch of proline residues, which are known to slow ribosome elongation, were necessary to maximize mRNA localization of this mRNA to the mitochondria [23].

To investigate the role of these varied parameters, we first explore an abstracted four-state model, wherein each transcript can be near or far from the mitochondrial surface and competent or not for binding to the mitochondria. This model shows that increasing the equilibrium fraction of time in the binding-competent state is indeed expected to enhance mitochondrial localization. Furthermore, the simplified model demonstrates that in order for transcript localization to be sensitive to the fraction of space where binding is possible (i.e., the mitochondrial volume fraction), the kinetics of switching in and out of the binding-compentent state must be relatively rapid compared to the kinetics for spatial movement.

We then proceed to develop a more detailed model that explicitly incorporates translational initiation and elongation, the formation of an MTS that enables mitochondrial binding, and diffusive search for the mitochondrial surface. This model confirms that tuning of the translation parameters can substantially alter mitochondrial localization, but only in a regime where the ribosome occupancy of the transcripts is relatively low. Surprisingly, plugging

physiological parameters into this instantaneous model resulted in the prediction that all mRNA transcripts studied would be highly localized to mitochondria in all conditions. In other words, the physiological parameters appeared to be in a regime where most transcripts had multiple binding-competent MTS sequences with long exposure time, resulting in global localization.

Motivated by differences in transcript length and elongation rate between constitutive and conditional gene groups, we incorporated an MTS maturation period into the model, driving the system into a parameter regime with lower numbers of binding-competent MTSs and shorter MTS exposure times, particularly for the more rapidly elongating and shorter conditional transcripts. Although we are unable to directly attribute this maturation period to a particular process, it aligns with other observations related to mitochondrial protein import. It is known that mitochondria targeting sequences mediate interactions with mitochondrial recognition machinery, namely TOM22 and TOM20 subunits of the translocase of the outer membrane (TOM) complex, and are necessary for efficient protein import into the mitochondria [56]. The folding process for some proteins that must be recognized and imported into mitochondria occurs on a timescale that competes with translocation [57, 58]. Furthermore, the formation of a secondary structure has been shown to be required for import of MTS-bearing proteins into mitochondria [59]. Together, these observations suggest the MTS is likely to require time to mature prior to becoming fully competent. Slowed translation has been suggested as providing an opportunity for proteins to fold, implying the MTS maturation time may also be regulated by translation kinetics [60].

In addition, molecular chaperones such as Hsp70 and Hsp90 are important for the delivery and recognition of the mitochondrial preproteins to the Tom70 receptor [46, 61]. Hsp70 expression levels have been found to have a direct effect on mRNA localization to the mitochondria [62]. STI1 is another cochaperone of Hsp70 and Hsp90 chaperones that plays a role in recognizing mitochondrial preproteins and mediates targeting to the mitochondria [47]. While the diffusive search for a newly-synthesized MTS by chaperones is expected be very fast ($\ll 40$ s), chaperone- and co-chaperone-mediated folding can occur on timescales comparable to 40 seconds, including approximately tens of seconds in bacterial homologs [63, 64] and > 100 seconds for human chaperone-mediated folding [65]. All of these data point to the need for a delay time between MTS translation and its maturation into a binding-competent state, via either autonomous folding or association with a chaperone, before it can be optimally recognized by the surface of the mitochondria.

Upon incorporation of a uniform (gene-independent) 40-second MTS maturation time into the model, we found that many genes fell into a parameter regime with only a few mature, binding-competent MTS sequences per transcript, and with intermediate exposure times for those sequences. This single choice of the maturation time made it possible to simultaneously match the expected localization of prototypical constructs representing both the constitutive and conditional gene groups. This choice of parameter yielded a mature MTS exposure time in the conditional gene that was longer than the diffusive search time at high mitochondrial volume fraction, yet shorter than the search time at low volume fraction. Consequently, the model with an MTS maturation time could adequately predict the decreased localization of conditional genes under metabolic conditions with low MVF, while genes in the constitutive group were localized regardless of the MVF. Previous experimental work suggested that changing mitochondrial volume fraction could control mitochondrial mRNA localization [23]—our quantitative modeling work provides further support for this mechanism of regulating mRNA localization.

Notably, conditional localization in our model required not only a modest number of mature MTS per transcript ($\beta_{\mathrm{mature}} \approx 1$) but also relatively fast translational initiation and

elongation kinetics (short exposure times compared to diffusive search). This result demonstrates the out-of-equilibrium nature of the localization process, wherein localization is dictated by the kinetic rates themselves rather than their ratios or the equilibrated fraction of transcripts in different states. This feature arises due to broken detailed balance [66] in the kinetic scheme illustrated in Fig 1A, wherein binding-competent transcripts bind irreversibly to the mitochondrial surface and can be dislodged only by the completion of the energy-consuming translation process. Subcellular localization of mRNA can thus be added to the extensive list of biomolecular processes wherein the tools of non-equilibrium statistical mechanics elucidate the relevant physical parameters governing system behavior [6, 7, 33–36].

While we have focused on how variation in translational kinetics between genes can impact mitochondrial mRNA localization, there is also significant variation in mRNA decay timescales [67, 68]. Our model suggests (see S4 Fig) that the mRNA decay timescale has a limited effect on mitochondrial mRNA localization, unless the decay time is sufficiently short to compete with the timescale for a newly-synthesized mRNA to first gain binding competence. We leave specific factors thought to modulate mRNA decay, such as ribosome stalling [69], as a topic of future study.

In this work our quantitative model assumed uniform ribosome elongation rates along mRNA transcripts. In the presence of ribosome interactions, such dynamics can lead to both uniform and non-uniform ribosome densities and effective elongation rates along the transcript [70, 71]. With these uniform ribosome elongation rates, previous theoretical results suggest that collisions will be rare [70, 71]. However, elongation may not be homogeneous along an mRNA transcript, due to factors such as tRNA availability [72], boundaries between protein regions [73], amino acid charge [74], and short peptide sequences related to ribosome stalling [75]. We have found that slow (homogeneous) elongation facilitates mitochondrial mRNA localization, by providing time for MTS maturation, diffusive search, and to maintain binding-competent MTS-mediated mRNA binding to mitochondria. We expect that inhomogeneities in elongation rate along mRNA could either enhance or reduce mitochondrial mRNA localization, controlled by whether slower elongation is in regions that favor longer MTS exposure. For example, a ribosome stall site following full MTS translation could provide more time for MTS maturation and facilitate mitochondrial localization. Future experimental work could identify such stalling sequences and point towards how modeling can improve understanding of sequence impact on localization.

From the perspective of biological function, it remains unclear why some mitochondrial mRNAs localize conditionally under different metabolic conditions, while others remain constitutively localized. Both types contain an MTS [25, 76] and code for proteins rich in hydrophobic residues that are susceptible to misfolding and aggregation in the cytosolic space [44]. One reason for the differential localization may center on the altered function of mitochondria from fermentative to respiratory conditions. ATP synthase, the linchpin of the mitochondrial OXPHOS metabolic process, is comprised of subunits of both prokaryotic and eukaryotic origin [77]. Interestingly, all but one of the prokaryotic-origin subunits are conditionally localized to the mitochondria [23]. As mitochondrial mRNA localization has been found to be sufficient to upregulate protein synthesis [23, 78] we posit that conditional or switch-like localization behavior is a post-transcriptional regulation mechanism of protein synthesis that is sensitive to mitochondrial growth and metabolic state. In particular, this mechanism can act globally, altering expression levels for a large set of transcripts, even without the involvement for specific signaling pathways to adjust protein synthesis in response to metabolic state.

Furthermore, we propose that the effects of a respiratory metabolic state, which increases mitochondrial volume fraction and decreases the mRNA diffusion search time, can be mimicked through global translation elongation inhibition by pushing MTS signal dynamics into a

much slower regime than mRNA diffusive search, potentially altering mitochondrial composition. This hints at translation elongation inhibition as an avenue or tool for toggling metabolic modes within the cell. Similar means of post-transcriptional regulation may take place in mammalian cells as genome-wide mRNA localization measurements to the mitochondria have found a class of mRNAs that are constitutively localized while others are found to become localized after CHX administration [79].

Our results link the nonequlibrium physics governing localization of transiently binding-competent mRNA and the observed differential response of transcript groups that localize to mitochondria under varying metabolic conditions. The general principles established here, including the importance of translation kinetics and transport timescales to the organelle surface, apply broadly to cellular systems that rely on a peptide targeting sequence for co-translational localization of proteins. For example the localization of mRNAs encoding secretory proteins to the surface of the endoplasmic reticulum (ER) through interactions between the signal recognition sequence on the nascent peptide, the signal recognition particle that binds it, and receptors on the ER surface, may well be governed by analogous principles [80, 81]. By coupling together quantitative physical models and analysis of measured translational parameters for the yeast transcriptome, this work provides general insight on the mechanisms by which a cell regulates co-translational localization of proteins to their target organelles.

Methods

Simplified discrete-state model

Fig 1A describes a minimal model for mRNA localization with four discrete states: sticky and close (S_N), sticky and far (S_F), not sticky and close (U_N), and not sticky and far (U_F). mRNA can transition between these states with rates k_R, k_L, k_U, and k_S, as shown in Fig 1A. These transitions are mathematically described by

$$\frac{dS_N}{dt} = k_S U_N + k_R S_F - k_U S_N \ , \tag{9a}$$

$$\frac{dS_F}{dt} = k_S U_F - (k_U + k_R)S_F \ , \tag{9b}$$

$$\frac{dU_N}{dt} = k_U S_N + k_R U_F - (k_S + k_L)U_N \ , \tag{9c}$$

$$\frac{dU_F}{dt} = k_U S_F + k_L U_N - (k_S + k_R)U_F \ . \tag{9d}$$

Note that there is no direct transition from S_N to S_F because if an mRNA is bound to the mitochondria it cannot leave the mitochondrial vicinity. Setting all derivatives in Eq 9 to zero, the

steady-state solution is

$$\hat{S}_{\mathrm{N}} = \frac{1}{Z} \frac{k_{\mathrm{R}} k_{\mathrm{S}} (k_{\mathrm{L}} + k_{\mathrm{R}} + k_{\mathrm{S}} + k_{\mathrm{U}})}{k_{\mathrm{L}} k_{\mathrm{U}} (k_{\mathrm{R}} + k_{\mathrm{U}})} \quad , \tag{10a}$$

$$\hat{S}_{\mathrm{F}} = \frac{1}{Z} \frac{k_{\mathrm{S}}}{k_{\mathrm{R}} + k_{\mathrm{U}}} \quad , \tag{10b}$$

$$\hat{U}_{\mathrm{N}} = \frac{1}{Z} \frac{k_{\mathrm{R}} (k_{\mathrm{R}} + k_{\mathrm{S}} + k_{\mathrm{U}})}{k_{\mathrm{L}} (k_{\mathrm{R}} + k_{\mathrm{U}})} \quad , \tag{10c}$$

$$\hat{U}_{\mathrm{F}} = \frac{1}{Z} \quad , \tag{10d}$$

with

$$Z = \frac{(k_{\mathrm{S}} + k_{\mathrm{U}})[k_{\mathrm{L}}(k_{\mathrm{R}} + k_{\mathrm{U}}) + k_{\mathrm{R}}(k_{\mathrm{R}} + k_{\mathrm{S}} + k_{\mathrm{U}})]}{k_{\mathrm{U}} k_{\mathrm{L}} (k_{\mathrm{U}} + k_{\mathrm{R}})} \quad , \tag{11}$$

for state probabilities $\hat{S}_{\mathrm{N}} + \hat{S}_{\mathrm{F}} + \hat{U}_{\mathrm{N}} + \hat{U}_{\mathrm{F}} = 1$.

In the regime where mRNA transport is much faster than the binding-competence switching rate ($k_{\mathrm{R}}, k_{\mathrm{L}} \gg k_{\mathrm{U}}, k_{\mathrm{S}}$), the near fraction is

$$P_{\mathrm{N}} = \hat{S}_{\mathrm{N}} + \hat{U}_{\mathrm{N}} \simeq f_{\mathrm{s}} + (1 - f_{\mathrm{s}}) f_{\mathrm{d}} \quad , \tag{12}$$

where $f_{\mathrm{s}} = k_{\mathrm{S}}/(k_{\mathrm{S}} + k_{\mathrm{U}})$ and $f_{\mathrm{d}} = k_{\mathrm{R}}/(k_{\mathrm{R}} + k_{\mathrm{L}})$. In the opposite regime, where mRNA transport is much slower than the binding-competence switching rate ($k_{\mathrm{R}}, k_{\mathrm{L}} \ll k_{\mathrm{U}}, k_{\mathrm{S}}$), the near fraction is

$$P_{\mathrm{N}} \simeq \frac{1}{1 + (1 - f_{\mathrm{s}})(1 - f_{\mathrm{d}})/f_{\mathrm{d}}} \quad . \tag{13}$$

Stochastic simulation with translation and diffusion

We use stochastic simulations to determine mitochondrial mRNA localization and fraction of time spent in the binding-competent state. Individual (non-interacting) mRNA molecules are simulated from synthesis in the nucleus to decay in the cytosol.

mRNA synthesis, translation, and MTS binding competence.   The mRNA simulation begins after exit from the nucleus, as experiments can fluorescently label and track mRNA once synthesized in the nucleus. The time spent by mRNA in the nucleus is a normally-distributed time period with mean 60 s and standard deviation of 30 seconds (if a negative time is selected, the distribution is resampled until a positive time is yielded). After nuclear exit, the mRNA begins simulated translation and diffusion through the cytosol.

Each mRNA has L codons. Ribosomes arrive and initiate translation with rate k_{init} if the first codon is not occupied. Each ribosome on an mRNA moves forward to the next codon at rate k_{elong} if the next codon is not occupied. A ribosome on the L'th (final) codon completes translation at rate k_{elong}, leaving the final codon unoccupied. mRNA decay at a rate k_{decay} once in the cytosol. The parameters k_{init}, k_{elong}, and L are varied to represent different genes (see below for the calculation of k_{init} and k_{elong} for particular genes). The mRNA decay rate is set to $k_{\mathrm{decay}} = 0.0017$ s^{-1} per mRNA molecule, such that the typical decay time for an mRNA molecule is 600 s. This decay time is consistent with measured average yeast mRNA decay times

ranging from 4.8 minutes [68] to 22 minutes [67]. Stochastic translation trajectories are generated using the Gillespie algorithm [82, 83].

We applied two models of mRNA gaining mitochondrial binding competence through mitochondrial targeting sequence (MTS) translation. For the instantaneous model, mRNA are competent to bind mitochondria if there is a least one ribosome at or past codon $l_{\mathrm{MTS}} = 100$. For the maturation model, once a ribosome reaches $l_{\mathrm{MTS}} = 100$, the ribosome will gain competence to bind the mRNA to a mitochodrion at a rate k_{MTS}. This rate k_{MTS} is included in the Gillespie algorithm, to select when a ribosome will confer binding competence.

Diffusion. The cell volume is defined as concentric cylinders. Fig 1D shows a two-dimensional cross-sectional view of this three-dimensional geometry: the volume extends along the cylinder axis. The central cylinder is the mitochondria, which is maintained at a radius $r_{\mathrm{m}} = 350$ nm. The radius R of the outer cylinder is selected to establish a desired mitochondrial volume fraction. A typical yeast cell volume is $V = 42\ \mu\mathrm{m}^3$. We assume that 80% of this volume is not occupied by the nucleus and vacuole, and thus available to mitochondria, the cytosol, and other cell components. Thus, the mitochondrial volume fraction in the simulation (r_{m}^2/R^2) is set equal to $f_m/0.8$ where f_m is the reported volume fraction. Specifically, we set $R = r_{\mathrm{m}}/\sqrt{f_{\mathrm{m}}/0.8}$. We note that this outer radius represents not the size of the cell as a whole, but rather the typical separation between non-proximal tubes within the mitochondrial network. A particle that hits the boundary of this outer cylinder would then begin to approach either the same or another mitochondrial network tube (see Fig 1D). We thus treat the outer cylinder as a reflecting boundary.

The simulation uses a propagator approach to sample the transitions of the mRNA between concentric regions around the mitochondrion, analogous to previous approaches used to simulate the dynamics of DNA-binding proteins [31] and diffusing organelles [84]. The closest region (region 1), for radial distances $r_{\mathrm{m}} < r < r_a = r_{\mathrm{m}} + 25$ nm, is sufficiently close for a binding-competent mRNA to bind a mitochondrion. mRNA within the intermediate cylindrical shell (region 2), with $r_a < r < r_b = r_{\mathrm{m}} + 250$ nm, are sufficiently close to the mitochondrion that they appear close in diffraction-limited imaging but are not sufficiently close to be able to bind. The last cylindrical shell (region 3), for $r_b < r < R$, represents the cell region where an mRNA would not be near any mitochondria.

We estimate the 25-nm binding distance by combining several contributions. The yeast ribosome has a radius of 13—14 nm [85]. The MTS region, up to 70 amino acids long, forms an amphipathic helix [39], a form of alpha helix. With an alpha helical pitch of 0.54 nm and 3.6 amino acids per turn, a 31 amino acid MTS (the mean of 20 yeast MTS lengths [86]) is approximately 5 nm in length. An additional few nanometers of other peptide regions bridging the MTS to the ribosome provides an estimate of 25 nm for the range of an MTS-bearing mRNA to bind mitochondria. The 250-nm imaging distance is based on the Abbe limit to resolution with visible light [87].

In the simulations, region 1 is treated as a cylinder with an absorbing boundary at $r_a + \epsilon$. A particle that first enters the region is placed at initial position $r_a - \epsilon$ and the first passage time to the absorbing boundary is sampled from the appropriate Green's function for radially symmetric diffusion in a cylindrical domain [88]. Region 2 is treated as a hollow cylinder with absorbing boundaries at $r_a - \epsilon$ and $r_b + \epsilon$. Particles that enter region 2 from region 1 start at position $r_a + \epsilon$ and those that enter from region 3 start at $r_b - \epsilon$. Region 3 is a hollow cylinder with absorbing boundary at $r_b - \epsilon$ and reflecting boundary at R. Particles that enter region 3 from region 2 start at position $r_b + \epsilon$. The buffer width to prevent very short time-steps at the region boundaries is set to $\epsilon = 10$ nm. If the sampled transition time for leaving a region occurs before the next translation process selected by the Gillespie algorithm, the mRNA changes

regions and the translation state transition times are then resampled. mRNAs that first exit the nucleus are placed at position $r = R$.

Binding-competent mRNA in region 1 are unable to leave this region, because they are bound to the mitochondrion. When a binding-competent mRNA in this region loses binding competence, the mRNA is given a random radial position within $r_m < r < r_a$, with the probability of the radial position proportional to r.

Simulated mRNA have a diffusivity of 0.1 μm^2/s. This diffusivity remains constant across genes and mRNA states, consistent with experimental measurements showing little dependence of mRNA diffusivity on mRNA length [89] or number of translating ribosomes [15].

Localization measures.   We use two types of localization measures, corresponding to different experimental measurements. One measure considers an mRNA localized to mitochondria if the mRNA is close enough to bind ($r_m < r < r_m + 25$ nm). This measure corresponds to experiments that chemically bind nearby mRNA to mitochondria to determine the fraction localized. The other measure considers an mRNA localized if the mRNA is close enough that with diffraction-limited imaging the mRNA appears next to the mitochondria ($r_m < r < r_m + 250$ nm). While quantitatively distinct, these measures do not lead to qualitatively different results.

Ensemble averaging.   For each localization measurement shown in our results, we simulate 50 mRNA trajectories from synthesis to decay, with each trajectory having a lifetime (including time spent in the nucleus) and a fraction of that lifetime spent mitochondrially localized. The ensemble average is calculated by weighting the fraction localized of each trajectory by the trajectory lifetime,

$$f_{\text{loc}} = \frac{\sum_i f_{\text{loc},i} T_{\text{lifetime},i}}{\sum_i T_{\text{lifetime},i}} \quad, \tag{14}$$

where $f_{\text{loc},i}$ is the fraction of trajectory i spent mitochondrially localized and $T_{\text{lifetime},i}$ is the mRNA lifetime for trajectory i. The probability that an mRNA will be included in a localization measurement, through either experimental localization measurement technique, is proportional to the lifetime of the mRNA.

Calculation of translation rates

We assume that each mRNA produces proteins at a rate k_{init}, so that the cell produces a particular protein at a rate $N_{\text{mRNA}} k_{\text{init}}$, where N_{mRNA} is the number of mRNA for a gene. For a steady state number of proteins, protein production must be balanced by protein decay. We assume that the primary mode of effective protein decay is cell division, such that each protein has an effective lifetime equal to a typical yeast division time of $T_{\text{lifetime}} = 90$ minutes. The steady-state translation initiation rate is then taken as

$$k_{\text{init}} = \frac{N_{\text{prot}}/N_{\text{mRNA}}}{T_{\text{lifetime}}} \quad. \tag{15}$$

Protein per mRNA data [22, 37] provides relative, rather than absolute, numbers for the number of proteins in a cell per mRNA of the same gene. Accordingly, we can rewrite our expression for k_{init} as,

$$k_{\text{init}} = \frac{\alpha P}{T_{\text{lifetime}}} \quad, \tag{16}$$

where P is the protein per mRNA measurement [22, 37], and α is the proportionality constant. To calibrate, we use the gene *TIM50* as a standard, as there are available measurements of N_{prot}

33

= 4095 [22] and $N_{\text{mRNA,TIM50}}$ = 6 [23]. From Eq 15, $k_{\text{init,TIM50}}$ = 0.1264 s^{-1}, and with P_{TIM50} = 15.12 and from Eq 16 gives α = 45.14. With α and P, we estimate k_{init} across genes.

The steady-state number of ribosomes N_{ribo} on an mRNA balances ribosome addition to the mRNA at rate k_{init} and removal at rate $k_{\text{elong}}N_{\text{ribo}}/L$, such that $k_{\text{elong}} = k_{\text{init}}L/N_{\text{ribo}}$. Ribosome occupancy R [38] is proportional to the ribosome density N_{ribo}/L. We can thus write,

$$\frac{k_{\text{elong}}}{k_{\text{elong,TIM50}}} = \frac{k_{\text{init}}}{k_{\text{init,TIM50}}}\frac{R_{\text{TIM50}}}{R} \, , \tag{17}$$

and apply $k_{\text{elong,TIM50}}$ = 4 aa/s [42] to estimate k_{elong} across genes.

Calculating MTS exposure time and mature MTS numbers per mRNA

In this section Eqs 6 and 7 are derived.

We assume MTS maturation is a Poisson process, i.e. with constant rate k_{MTS}. The probability that an MTS has not yet matured at time t after its translation is $I(t) = e^{-k_{MTS}t}$. After the MTS has been translated, the ribosome completes translation after a mean time $t_{max} = (L - l_{\text{MTS}})/k_{\text{elong}}$. For an MTS that matures before the ribosome terminates translation, the mean waiting time t_{wait} from MTS translation to maturity is

$$
\begin{aligned}
\langle t_{wait} \rangle &= \frac{\int_0^{t_{\max}} t\ P_{\text{mature}}(t)\,\mathrm{d}t}{\int_0^{t_{\max}} P_{\text{mature}}(t)\,\mathrm{d}t} \\
&= \frac{1}{k_{\text{MTS}}}\frac{1 - e^{-k_{\text{MTS}}t_{\max}}(k_{\text{MTS}}t_{\max} + 1)}{1 - e^{-k_{\text{MTS}}t_{\max}}} \, ,
\end{aligned}
\tag{18}
$$

where $P_{\text{mature}} = k_{\text{MTS}}I(t)$.

A fraction $I(t_{\max})$ of translated MTS regions do not mature before translation termination, so the mean time that a mature MTS is exposed on the mRNA is

$$
\begin{aligned}
\langle t_{\text{expo,mature}} \rangle &= [1 - I(t_{\max})]\langle t_{\text{wait}} \rangle \\
&= \frac{1}{k_{\text{MTS}}}\left[1 - e^{-k_{\text{MTS}}t_{\max}}(k_{\text{MTS}}t_{\max} + 1)\right] \, .
\end{aligned}
\tag{19}
$$

The number of mature MTSs per mRNA, β_{mature}, is related to the mean number of ribosomes per mRNA codon, $\rho_{\text{ribo}} = k_{\text{init}}/k_{\text{elong}}$. The probability that an MTS is mature at time t after ribosome initiation is $1 - I(t)$. The ribosome reaches codon x beyond its initiation point at time $t(x) = x/k_{\text{elong}}$. Integrating over the codons beyond the MTS region,

$$
\begin{aligned}
\beta_{\text{mature}} &= \int_0^{L - l_{\text{MTS}}} \rho_{\text{ribo}}\{1 - I[t(x)]\}\ \mathrm{d}x \\
&= \frac{k_{\text{init}}}{k_{\text{elong}}}\int_0^{L - l_{\text{MTS}}}\left[1 - \exp\left(-\frac{k_{\text{MTS}}}{k_{\text{elong}}}x\right)\right]\ \mathrm{d}x \\
&= \frac{k_{\text{init}}}{k_{\text{elong}}}\left\{L - l_{\text{MTS}} - \frac{k_{\text{elong}}}{k_{\text{MTS}}}\left[1 - \exp\left(-\frac{k_{\text{MTS}}}{k_{\text{elong}}}[L - l_{\text{MTS}}]\right)\right]\right\} \, .
\end{aligned}
\tag{20}
$$

Supporting information

S1 Fig. Cumulative distribution of conditional and constitutive mRNA genes vs ribosome occupancy (lines indicate fraction of genes with given ribosome occupancy or less). Ribosome occupancy from Arava et al [43]. $n_{conditional} = 54$ and $n_{constitutive} = 160$. These ribosome occupancy values cover a distinct range, in comparison to those of Fig 2A, due to distinct experimental measurement techniques.
(PDF)

S2 Fig. Cumulative distribution of conditional and constitutive genes vs elongation rates (lines indicate fraction of genes with given elongation rate or less). Elongation rates calculated with data from and as described in Riba et al [42], with elongation rate equal to protein synthesis rate divided by ribosome density. $n_{conditional} = 9$ and $n_{constitutive} = 30$.
(PDF)

S3 Fig. Violin plot showing mRNA localization fraction of individual genes with instantaneous model (no maturation delay) with translation kinetics for each gene estimated from experimental data (see Methods) and 4% MVF. (A) is with mRNA diffusivity $D = 0.001 \ \mu m^2/s$, (B) with $D = 0.01 \ \mu m^2/s$, (C) with $D = 0.1 \ \mu m^2/s$, (D) with $D = 0.2 \ \mu m^2/s$, (E) with $D = 0.5 \ \mu m^2/s$, and (F) with $D = 1 \ \mu m^2/s$.
(PDF)

S4 Fig. Mitochondrial localization vs mitochondrial volume fraction for ATP3 for model with 40-second maturation time and with translation kinetics estimated from experimental data (see Methods). ATP3 mRNA decay time is varied, with the 600 s decay timescale used in other figures. Decay timescale has limited impact unless it is sufficiently short to compete with the timescale for a newly-synthesized mRNA to first gain binding competence.
(PDF)

S1 File. Supporting data. Data files and accompanying text files, as well as Matlab programs to create each plot.
(ZIP)

Acknowledgments

Author Contributions

Conceptualization: Elena F. Koslover, Brian M. Zid, Aidan I. Brown.

Funding acquisition: Elena F. Koslover.

Investigation: Ximena G. Arceo, Aidan I. Brown.

Methodology: Ximena G. Arceo, Elena F. Koslover, Brian M. Zid, Aidan I. Brown.

Supervision: Brian M. Zid, Aidan I. Brown.

Writing – original draft: Ximena G. Arceo, Brian M. Zid, Aidan I. Brown.

Writing – review & editing: Ximena G. Arceo, Elena F. Koslover, Brian M. Zid, Aidan I. Brown.

References

1. Bauer NC, Doetsch PW, Corbett AH. Mechanisms regulating protein localization. Traffic. 2015; 16(10):1039–1061. https://doi.org/10.1111/tra.12310 PMID: 26172624

2. Aviram N, Schuldiner M. Targeting and translocation of proteins to the endoplasmic reticulum at a glance. Journal of cell science. 2017; 130(24):4079–4085. https://doi.org/10.1242/jcs.204396 PMID: 29246967

3. Chio US, Cho H, Shan So. Mechanisms of tail-anchored membrane protein targeting and insertion. Annual review of cell and developmental biology. 2017; 33:417–438. https://doi.org/10.1146/annurev-cellbio-100616-060839 PMID: 28992441

4. Guardia CM, De Pace R, Mattera R, Bonifacino JS. Neuronal functions of adaptor complexes involved in protein sorting. Current opinion in neurobiology. 2018; 51:103–110. https://doi.org/10.1016/j.conb.2018.02.021 PMID: 29558740

5. Wheeler RJ, Hyman AA. Controlling compartmentalization by non-membrane-bound organelles. Philosophical Transactions of the Royal Society B: Biological Sciences. 2018; 373(1747):20170193. https://doi.org/10.1098/rstb.2017.0193 PMID: 29632271

6. Maza NA, Schiesser WE, Calvert PD. An intrinsic compartmentalization code for peripheral membrane proteins in photoreceptor neurons. Journal of Cell Biology. 2019; 218(11):3753–3772. https://doi.org/10.1083/jcb.201906024 PMID: 31594805

7. Mogre SS, Brown AI, Koslover EF. Getting around the cell: physical transport in the intracellular world. Physical Biology. 2020; 17(6):061003. https://doi.org/10.1088/1478-3975/aba5e5

8. Das S, Vera M, Gandin V, Singer RH, Tutucci E. Intracellular mRNA transport and localized translation. Nature Reviews Molecular Cell Biology. 2021; 22(7):483–504. https://doi.org/10.1038/s41580-021-00356-8 PMID: 33837370

9. Biever A, Donlin-Asp PG, Schuman EM. Local translation in neuronal processes. Current Opinion in Neurobiology. 2019; 57:141–148. https://doi.org/10.1016/j.conb.2019.02.008 PMID: 30861464

10. Bramham CR. Local protein synthesis, actin dynamics, and LTP consolidation. Current opinion in neurobiology. 2008; 18(5):524–531. https://doi.org/10.1016/j.conb.2008.09.013 PMID: 18834940

11. Stephens SB, Dodd RD, Brewer JW, Lager PJ, Keene JD, Nicchitta CV. Stable ribosome binding to the endoplasmic reticulum enables compartment-specific regulation of mRNA translation. Molecular biology of the cell. 2005; 16(12):5819–5831. https://doi.org/10.1091/mbc.E05-07-0685 PMID: 16221886

12. Trcek T, Lehmann R. Germ granules in Drosophila. Traffic. 2019; 20(9):650–660. https://doi.org/10.1111/tra.12674 PMID: 31218815

13. Das S, Singer RH, Yoon YJ. The travels of mRNAs in neurons: do they know where they are going? Current opinion in neurobiology. 2019; 57:110–116. https://doi.org/10.1016/j.conb.2019.01.016 PMID: 30784978

14. Besse F, Ephrussi A. Translational control of localized mRNAs: restricting protein synthesis in space and time. Nature reviews Molecular cell biology. 2008; 9(12):971–980. https://doi.org/10.1038/nrm2548 PMID: 19023284

15. Wang C, Han B, Zhou R, Zhuang X. Real-time imaging of translation on single mRNA transcripts in live cells. Cell. 2016; 165(4):990–1001. https://doi.org/10.1016/j.cell.2016.04.040 PMID: 27153499

16. Cioni JM, Lin JQ, Holtermann AV, Koppers M, Jakobs MA, Azizi A, et al. Late endosomes act as mRNA translation platforms and sustain mitochondria in axons. Cell. 2019; 176(1-2):56–72. https://doi.org/10.1016/j.cell.2018.11.030 PMID: 30612743

17. Boengler K, Heusch G, Schulz R. Nuclear-encoded mitochondrial proteins and their role in cardioprotection. Biochimica et Biophysica Acta (BBA)-Molecular Cell Research. 2011; 1813(7):1286–1294. https://doi.org/10.1016/j.bbamcr.2011.01.009 PMID: 21255616

18. Devaux F, Lelandais G, Garcia M, Goussard S, Jacq C. Posttranscriptional control of mitochondrial biogenesis: spatio-temporal regulation of the protein import process. FEBS letters. 2010; 584(20):4273–4279. https://doi.org/10.1016/j.febslet.2010.09.030 PMID: 20875412

19. Saint-Georges Y, Garcia M, Delaveau T, Jourdren L, Le Crom S, Lemoine S, et al. Yeast mitochondrial biogenesis: a role for the PUF RNA-binding protein Puf3p in mRNA localization. PLoS One. 2008; 3(6): e2293. https://doi.org/10.1371/journal.pone.0002293 PMID: 18523582

20. Garcia M, Delaveau T, Goussard S, Jacq C. Mitochondrial presequence and open reading frame mediate asymmetric localization of messenger RNA. European Molecular Biology Organization Reports. 2010; 11(4):285–291. https://doi.org/10.1038/embor.2010.17 PMID: 20224577

21. Di Bartolomeo F, Malina C, Campbell K, Mormino M, Fuchs J, Vorontsov E, et al. Absolute yeast mitochondrial proteome quantification reveals trade-off between biosynthesis and energy generation during

diauxic shift. Proceedings of the National Academy of Sciences. 2020; 117(13):7524–7535. https://doi.org/10.1073/pnas.1918216117 PMID: 32184324

22. Morgenstern M, Stiller SB, Lübbert P, Peikert CD, Dannenmaier S, Drepper F, et al. Definition of a High-Confidence Mitochondrial Proteome at Quantitative Scale. Cell Reports. 2017; 19(13):2836–2852. https://doi.org/10.1016/j.celrep.2017.06.014 PMID: 28658629

23. Tsuboi T, Viana MP, Xu F, Yu J, Chanchani R, Arceo XG, et al. Mitochondrial volume fraction and translation duration impact mitochondrial mRNA localization and protein synthesis. eLife. 2020; 9:e57814. https://doi.org/10.7554/eLife.57814 PMID: 32762840

24. Viana MP, Brown AI, Mueller IA, Goul C, Koslover EF, Rafelski SM. Mitochondrial fission and fusion dynamics generate efficient, robust, and evenly distributed network topologies in budding yeast cells. Cell systems. 2020; 10(3):287–297. https://doi.org/10.1016/j.cels.2020.02.002 PMID: 32105618

25. Williams CC, Jan CH, Weissman JS. Targeting and plasticity of mitochondrial proteins revealed by proximity-specific ribosome profiling. Science. 2014; 346(6210):748–751. https://doi.org/10.1126/science.1257522 PMID: 25378625

26. Tsuboi T, Leff J, Zid BM. Post-transcriptional control of mitochondrial protein composition in changing environmental conditions. Biochemical Society Transactions. 2020; 48(6):2565–2578. https://doi.org/10.1042/BST20200250 PMID: 33245320

27. Saffman P, Delbrück M. Brownian motion in biological membranes. Proceedings of the National Academy of Sciences. 1975; 72(8):3111–3113. https://doi.org/10.1073/pnas.72.8.3111 PMID: 1059096

28. Berg HC, Purcell EM. Physics of chemoreception. Biophysical journal. 1977; 20(2):193–219. https://doi.org/10.1016/S0006-3495(77)85544-6 PMID: 911982

29. Reguera D, Rubi J. Kinetic equations for diffusion in the presence of entropic barriers. Physical Review E. 2001; 64(6):061106. https://doi.org/10.1103/PhysRevE.64.061106 PMID: 11736170

30. Condamin S, Bénichou O, Tejedor V, Voituriez R, Klafter J. First-passage times in complex scale-invariant media. Nature. 2007; 450(7166):77–80. https://doi.org/10.1038/nature06201 PMID: 17972880

31. Koslover EF, de la Rosa MAD, Spakowitz AJ. Theoretical and computational modeling of target-site search kinetics in vitro and in vivo. Biophysical journal. 2011; 101(4):856–865. https://doi.org/10.1016/j.bpj.2011.06.066 PMID: 21843476

32. Brown AI, Westrate LM, Koslover EF. Impact of global structure on diffusive exploration of organelle networks. Scientific reports. 2020; 10(1):1–13. https://doi.org/10.1038/s41598-020-61598-8 PMID: 32188905

33. Murugan A, Huse DA, Leibler S. Speed, dissipation, and error in kinetic proofreading. Proceedings of the National Academy of Sciences. 2012; 109(30):12034–12039. https://doi.org/10.1073/pnas.1119911109 PMID: 22786930

34. Gladrow J, Fakhri N, MacKintosh FC, Schmidt C, Broedersz C. Broken detailed balance of filament dynamics in active networks. Physical review letters. 2016; 116(24):248301. https://doi.org/10.1103/PhysRevLett.116.248301 PMID: 27367410

35. Brown AI, Sivak DA. Theory of nonequilibrium free energy transduction by molecular machines. Chemical reviews. 2019; 120(1):434–459. https://doi.org/10.1021/acs.chemrev.9b00254 PMID: 31411455

36. Fang X, Wang J. Nonequilibrium thermodynamics in cell biology: Extending equilibrium formalism to cover living systems. Annual review of biophysics. 2020; 49:227–246. https://doi.org/10.1146/annurev-biophys-121219-081656 PMID: 32375020

37. Couvillion MT, Soto IC, Shipkovenska LS Gergana & Churchman. Synchronized mitochondrial and cytosolic translation programs. Nature. 2016; 533:499–503. https://doi.org/10.1038/nature18015 PMID: 27225121

38. Zid BM, O'Shea EK. Promoter sequences direct cytoplasmic localization and translation of mRNAs during starvation in yeast. Nature. 2014; 514(7520):117–121. https://doi.org/10.1038/nature13578 PMID: 25119046

39. Bacman SR, Gammage PA, M M, Moraes CT. Manipulation of mitochondrial genes and mtDNA heteroplasmy. Methods Cell Biol. 2020; 155:441–487. https://doi.org/10.1016/bs.mcb.2019.12.004 PMID: 32183972

40. Liutkute M, Samatova E, Rodnina MV. Cotranslational folding of proteins on the ribosome. Biomolecules. 2020; 10(1):97. https://doi.org/10.3390/biom10010097

41. Bechtold B. Violin Plots for Matlab, Github Project; 2016. https://github.com/bastibe/Violinplot-Matlab.

42. Riba A, Di Nanni N, Mittal N, Arhné E, Schmidt A, Zavolan M. Protein synthesis rates and ribosome occupancies reveal determinants of translation elongation rates. Proceedings of the National Academy of Sciences. 2019; 116(30):15023–15032. https://doi.org/10.1073/pnas.1817299116 PMID: 31292258

37

PLOS COMPUTATIONAL BIOLOGY   Mitochondrial mRNA localization is governed by translation kinetics and spatial transport

43. Arava Y, Wang Y, Storey JD, Liu CL, Brown PO, Herschlag D. Genome-wide analysis of mRNA translation profiles in Saccharomyces cerevisiae. Proceedings of the National Academy of Sciences. 2003; 100(7):3889–3894. https://doi.org/10.1073/pnas.0635171100 PMID: 12660367

44. von Heijne G. Mitochondrial targeting sequences may form amphiphilic helices. The EMBO Journal. 1986; 5(6):1335–1342. https://doi.org/10.1002/j.1460-2075.1986.tb04364.x PMID: 3015599

45. Bykov YS, Rapaport D, Herrmann JM, Schuldiner M. Cytosolic events in the biogenesis of mitochondrial proteins. Trends in Biochemical Sciences. 2020; 45(8):650–657. https://doi.org/10.1016/j.tibs.2020.04.001 PMID: 32409196

46. Young JC, Hoogenraad NJ, Hartl FU. Molecular Chaperones Hsp90 and Hsp70 Deliver Preproteins to the Mitochondrial Import Receptor Tom70. Cell. 2003; 112(1):41–50. https://doi.org/10.1016/0092-8674(87)90660-X PMID: 12526792

47. Hoseini H, Pandey S, Jores T, Schmitt A, Franz-Wachtel M, Macek B, et al. The cytosolic cochaperone Sti1 is relevant for mitochondrial biogenesis and morphology. The FEBS Journal. 2016; 283(18):3338–3352. https://doi.org/10.1111/febs.13813 PMID: 27412066

48. Stein KC, Kriel A, Frydman J. Nascent Polypeptide Domain Topology and Elongation Rate Direct the Cotranslational Hierarchy of Hsp70 and TRiC/CCT. Molecular Cell. 2019; 75(6):1117–1130.e5. https://doi.org/10.1016/j.molcel.2019.06.036 PMID: 31400849

49. Schneider-Poetsch T, Ju J, Eyler DE, Dang Y, Bhat S, Merrick WC, et al. Inhibition of eukaryotic translation elongation by cycloheximide and lactimidomycin. Nature Chemical Biology. 2010; 6:209–217. https://doi.org/10.1038/nchembio.304 PMID: 20118940

50. Chu D, Kazana E, Bellanger N, Singh T, Tuite MF, von der Haar T. Translation elongation can control translation initiation on eukaryotic mRNAs. The EMBO Journal. 2014; 33(1):21–34. https://doi.org/10.1002/embj.201385651 PMID: 24357599

51. Kasari V, Margus T, Atkinson GC, Johansson MJ, Hauryliuk V. Ribosome profiling analysis of eEF3-depleted Saccharomyces cerevisiae. Scinetific Reports. 2019; 9 (3037). https://doi.org/10.1038/s41598-019-39403-y PMID: 30816176

52. Poulsen TM, Imai K, Frith MC, Horton P. Hallmarks of slow translation initiation revealed in mitochondrially localizing mRNA sequences. bioRxiv. 2019; p. 614255.

53. Sylvestre J, Vialette S, Corral Debrinski M, Jacq C. Long mRNAs coding for yeast mitochondrial proteins of prokaryotic origin preferentially localize to the vicinity of mitochondria. Genome Biology. 2003; 4(7):R44. https://doi.org/10.1186/gb-2003-4-7-r44 PMID: 12844360

54. Gebauer F, Hentze MW. Molecular mechanisms of translational control. Nature reviews Molecular cell biology. 2004; 5(10):827–835. https://doi.org/10.1038/nrm1488 PMID: 15459663

55. Espah Borujeni A, Salis HM. Translation initiation is controlled by RNA folding kinetics via a ribosome drafting mechanism. Journal of the American Chemical Society. 2016; 138(22):7016–7023. https://doi.org/10.1021/jacs.6b01453 PMID: 27199273

56. Backes S, Hess S, Boos F, Woellhaf MW, Gödel S, Jung M, et al. Tom70 enhances mitochondrial preprotein import efficiency by binding to internal targeting sequences. Journal of Cell Biology. 2018; 217(4):1369–1382. https://doi.org/10.1083/jcb.201708044 PMID: 29382700

57. Mukhopadhyay A, Ni L, Weiner H. A co-translational model to explain the in vivo import of proteins into HeLa cell mitochondria. Biochemical Journal. 2004; 382(1):385–392. https://doi.org/10.1042/BJ20040065 PMID: 15153070

58. Regev-Rudzki N, Yogev O, Pines O. The mitochondrial targeting sequence tilts the balance between mitochondrial and cytosolic dual localization. Journal of Cell Science. 2008; 121(14):2423–2431. https://doi.org/10.1242/jcs.029207 PMID: 18577574

59. Waltner M, Hammen PK, Weiner H. Influence of the mature portion of a precursor protein on the mitochondrial signal sequence. Journal of Biological Chemistry. 1996; 271(35):21226–21230. https://doi.org/10.1074/jbc.271.35.21226 PMID: 8702895

60. Zhao T, Chen YM, Li Y, Wang J, Chen S, Gao N, et al. Disome-seq reveals widespread ribosome collisions that promote cotranslational protein folding. Genome Biology. 2021; 22(16). https://doi.org/10.1186/s13059-020-02256-0 PMID: 33402206

61. Deshaies RJ, Koch BD, Werner-Washburne M, Craig EA, Schekman R. A subfamily of stress proteins facilitates translocation of secretory and mitochondrial precursor polypeptides. Nature. 1988; 332 (6167):800–805. https://doi.org/10.1038/332800a0 PMID: 3282178

62. Eliyahu E, Lesnik C, Arava Y. The protein chaperone Ssa1 affects mRNA localization to the mitochondria. FEBS Letters. 2012; 586(1):64–69. https://doi.org/10.1016/j.febslet.2011.11.025 PMID: 22138184

63. Sharma SK, De Los Rios P, Christen P, Lustig A, Goloubinoff P. The kinetic parameters and energy cost of the Hsp70 chaperone as a polypeptide unfoldase. Nature chemical biology. 2010; 6(12):914–920. https://doi.org/10.1038/nchembio.455 PMID: 20953191

64. Banecki B, Zylicz M. Real time kinetics of the DnaK/DnaJ/GrpE molecular chaperone machine action. Journal of Biological Chemistry. 1996; 271(11):6137–6143. https://doi.org/10.1074/jbc.271.11.6137 PMID: 8626401

65. Wu S, Hong L, Wang Y, Yu J, Yang J, Yang J, et al. Kinetics of the conformational cycle of Hsp70 reveals the importance of the dynamic and heterogeneous nature of Hsp70 for its function. Proceedings of the National Academy of Sciences. 2020; 117(14):7814–7823. https://doi.org/10.1073/pnas.1914376117 PMID: 32198203

66. Gnesotto FS, Mura F, Gladrow J, Broedersz CP. Broken detailed balance and non-equilibrium dynamics in living systems: a review. Reports on Progress in Physics. 2018; 81(6):066601. https://doi.org/10.1088/1361-6633/aab3ed PMID: 29504517

67. Chia LL, McLaughlin C. The half-life of mRNA in Saccharomyces cerevisiae. Molecular and General Genetics MGG. 1979; 170(2):137–144. https://doi.org/10.1007/BF00337788 PMID: 372758

68. Chan LY, Mugler CF, Heinrich S, Vallotton P, Weis K. Non-invasive measurement of mRNA decay reveals translation initiation as the major determinant of mRNA stability. Elife. 2018; 7:e32536. https://doi.org/10.7554/eLife.32536 PMID: 30192227

69. Mishima Y, Han P, Ishibashi K, Kimura S, Iwasaki S. Ribosome slowdown triggers codon-mediated mRNA decay independently of ribosome quality control. The EMBO Journal. 2022; p. e109256. https://doi.org/10.15252/embj.2021109256 PMID: 35040509

70. MacDonald CT, Gibbs JH, Pipkin AC. Kinetics of biopolymerization on nucleic acid templates. Biopolymers: Original Research on Biomolecules. 1968; 6(1):1–25. https://doi.org/10.1002/bip.1968.360060102 PMID: 5641411

71. Duc KD, Saleem ZH, Song YS. Theoretical analysis of the distribution of isolated particles in totally asymmetric exclusion processes: Application to mRNA translation rate estimation. Physical Review E. 2018; 97(1):012106. https://doi.org/10.1103/PhysRevE.97.012106

72. Varenne S, Buc J, Lloubes R, Lazdunski C. Translation is a non-uniform process: effect of tRNA availability on the rate of elongation of nascent polypeptide chains. Journal of molecular biology. 1984; 180(3):549–576. https://doi.org/10.1016/0022-2836(84)90027-5 PMID: 6084718

73. Thanaraj T, Argos P. Ribosome-mediated translational pause and protein domain organization. Protein Science. 1996; 5(8):1594–1612. https://doi.org/10.1002/pro.5560050814 PMID: 8844849

74. Charneski CA, Hurst LD. Positively charged residues are the major determinants of ribosomal velocity. PLoS biology. 2013; 11(3):e1001508. https://doi.org/10.1371/journal.pbio.1001508 PMID: 23554576

75. Sabi R, Tuller T. Computational analysis of nascent peptides that induce ribosome stalling and their proteomic distribution in Saccharomyces cerevisiae. Rna. 2017; 23(7):983–994. https://doi.org/10.1261/rna.059188.116 PMID: 28363900

76. Elstner M, Andreoli C, Klopstock T, Meitinger T, Prokisch H. The mitochondrial proteome database: MitoP2. Methods in enzymology. 2009; 457:3–20. https://doi.org/10.1016/S0076-6879(09)05001-0 PMID: 19426859

77. Rühle T, Leister D. Assembly of F1F0-ATP synthases. Biochimica et Biophysica Acta (BBA)-Bioenergetics. 2015; 1847(9):849–860. https://doi.org/10.1016/j.bbabio.2015.02.005 PMID: 25667968

78. Gehrke S, Wu Z, Klinkenberg M, Sun Y, Auburger G, Guo S, et al. PINK1 and Parkin Control Localized Translation of Respiratory Chain Component mRNAs on Mitochondria Outer Membrane. Cell Metabolism. 2015; 21(1):95–108. https://doi.org/10.1016/j.cmet.2014.12.007 PMID: 25565208

79. Fazal FM, Han S, Parker KR, Kaewsapsak P, Xu J, Boettiger AN, et al. Atlas of Subcellular RNA Localization Revealed by APEX-Seq. Cell. 2019; 178(2):473–490.e26. https://doi.org/10.1016/j.cell.2019.05.027 PMID: 31230715

80. Zhang D, Shan So. Translation elongation regulates substrate selection by the signal recognition particle. Journal of Biological Chemistry. 2012; 287(10):7652–7660. https://doi.org/10.1074/jbc.M111.325001 PMID: 22228766

81. Zhao L, Cui Y, Fu G, Xu Z, Liao X, Zhang D. Signal Recognition Particle Suppressor Screening Reveals the Regulation of Membrane Protein Targeting by the Translation Rate. mBio. 2021; 12(1):e02373–20. https://doi.org/10.1128/mBio.02373-20 PMID: 33436432

82. Gillespie DT. Exact stochastic simulation of coupled chemical reactions. The journal of physical chemistry. 1977; 81(25):2340–2361. https://doi.org/10.1021/j100540a008

83. Gillespie DT. Stochastic simulation of chemical kinetics. Annu Rev Phys Chem. 2007; 58:35–55. https://doi.org/10.1146/annurev.physchem.58.032806.104637 PMID: 17037977

84. Mogre SS, Koslover EF. Multimodal transport and dispersion of organelles in narrow tubular cells. Physical Review E. 2018; 97(4):042402. https://doi.org/10.1103/PhysRevE.97.042402 PMID: 29758750

85. Verschoor A, Warner JR, Srivastava S, Grassucci RA, Frank J. Three-dimensional structure of the yeast ribosome. Nucleic acids research. 1998; 26(2):655–661. https://doi.org/10.1093/nar/26.2.655 PMID: 9421530

86. Dong C, Shi Z, Huang L, Zhao H, Xu Z, Lian J. Cloning and characterization of a panel of mitochondrial targeting sequences for compartmentalization engineering in Saccharomyces cerevisiae. Biotechnology and Bioengineering. 2021; 118(11):4269–4277. https://doi.org/10.1002/bit.27896 PMID: 34273106

87. Georgiades P, Allan VJ, Dickinson M, Waigh TA. Reduction of coherent artefacts in super-resolution fluorescence localisation microscopy. Journal of Microscopy. 2016; 264(3):375–383. https://doi.org/10.1111/jmi.12453 PMID: 27541861

88. Özisik MN. Heat conduction. John Wiley & Sons; 1993.

89. Calderwood A, Kopriva S, Morris RJ. Transcript abundance explains mRNA mobility data in Arabidopsis thaliana. The Plant Cell. 2016; 28(3):610–615. https://doi.org/10.1105/tpc.15.00956 PMID: 26952566

Chapter 4

Biophysical mechanism of MTS-mediated mRNA-mitochondria association may be conserved to mammalian cells

Eukaryotic cells coordinate the mitochondrial and nuclear genomes to ensure proper stoichiometry of large key complexes. For example, human ATP synthase comprises 25 subunits of nuclear origin and 2 subunits of mitochondrial origin [20]. Similarly, *S. cerevisiae* ATP synthase comprises 17 subunits and requires the coordination of nuclear and mitochondrial gene expression [21]. Given the degree of conservation between *S. cerevisiae* and mammalian mitochondrial proteins, brewer's yeast has long been a model organism for elucidating the key molecular players in metabolic switching, mitochondrial biogenesis, and the coordination of the nuclear and mitochondrial genomes.

mRNA localization is a post transcriptional method for regulating gene expression in parallel with transcriptional methods. The regulation of subcellular mRNA localization has been studied in Drosophila melanogaster embryos [10], neurons [11], Xenopus laevis oocytes [12], and other eukaryotes [13] with a particular focus on the mechanisms of recognition and transport by cytoskeleton-associated motor proteins. The current view of mRNA sequences as subcellular "zipcodes" or localization elements (LEs) [13, 14, 15] that function as recognition sites for RNA-binding proteins positions the RNA-protein complex, or RNA granule, as the foundation of mRNA localization regulation more generally.

Similar work has been carried out in *S. cerevisiae*, identifying RNA-binding proteins (RBPs) and mRNAs that are transported by cytoskeleton-associated motor proteins [citations] and studying mRNA sequences through the lens of RBP recognition motifs [citation] or secondary structures [citation]. Specific sequences and motifs, e.g. hydrophobic

41

regions, in ORFs and untranslated regions have been identified as necessary for proper localization of transcripts to the endoplasmic reticulum [18] and mitochondria [32, 33]. More recent work has elucidated the kinetics of mRNA complexation and mitochondrial localization in *S. cerevisiae* [34, 35, 7] but not in other eukaryotes. While numerous localization modalities have been posited and studied for decades in mammalian systems, pointing to RBPs for some transcripts and ribosome-nascent peptide complexes for others [1], diffusion has been largely dismissed as a potentially important component of mRNA localization after research on inert tracers in the cytoplasm of mouse cells [36, 37].

Following my research into the kinetics of translation, diffusion, and mRNA localization in *S. cerevisiae*, I applied the same mathematical modelling to the translation kinetics of nuclear-encoded mitochondrial mRNAs from mammalian systems and to diffusion search times of mitochondrial networks in mammalian cells. My calculations of translation rates of transcripts coding for mitochondrial proteins uncovered the same trends we observed in brewer's yeast for nuclear-encoded mitochondrial genes. Furthermore, the diffusion search times of mRNAs in mammalian cells were longer than in brewer's yeast, but were still close to the translation durations of mRNAs in mammalian cells. The relative values of diffusive kinetics and translation kinetics are more important for the mechanism of nascent-peptide-mediated mRNA localization. Given that these trends in translation and diffusion are consistent with what I observed in S. cerevisiae, we posited that condition-dependent mRNA localization is a conserved post-transcriptional mechanism for responding to fluctuating metabolic needs of eukaryotic cells.

4.0.1 Translation kinetics of mammalian cells

I analyzed the mitochondrial localization of nuclear-encoded mitochondrial mRNAs reported in HEK293T cells, and found that the mRNA localization behavior of many genes is conserved from yeast to mammalian cells. Gene ontology term analysis revealed that in addition to nuclear-encoded mitochondrial genes being largely conserved from *S. cerevisiae* to mammalian species, the biological processes are conserved for conditional and constitutive groups. Calculations found that, like *S. cerevisiae*, conditionally localized mRNAs tend to have faster translation kinetics than consitutively localized mRNAs If genes and translation kinetics are conserved, it is plausible that the biophysical mechanism of localization may be conserved as well. Lastly, I applied the stochastic simulation described in Chapter 2 to mammalian genes in mammalian cells and recapitulated empirical trends in localization for conditionally localized mRNAs and constitutively localized mRNAs.

I determined the translation initiation rate and elongation rate of my genes of interest by using a published dataset [31] of translation in U2OS cells. This dataset published relative translation elongation rates that I then standardized with the globally measured average of 5.6 aa/s [38]. Translation initiation rates were standardized and converted to units of s^{-1} with the absolute initiation rate 2.5/min, which is the middle of the range the authors reported for their well-characterized reporter gene kif18b [31]. After determining the initiation and elongation rates in absolute units, I

analyzed a dataset on mRNA subcellular spatial heterogeneity in mammalian cell lines to identify possible trends in translation speeds and mRNA localization.

Similar to findings in yeast, fast translation is a hallmark of conditional mRNA localization HeLa and A549 mammalian cell lines (Figs 4.1, 4.2, and 4.3). Translation data was found for 256 conditional genes (Table 4.1), and 249 of those had ORF lengths greater than the minimal length of 100 aa. (The MTS length is 100 aa in the stochastic simulation and any gene shorter than that is presumed to use a different MTS-driven import mechanism or none at all.) Additionally, translation data was found for 126 constitutive genes (Table 4.2), all of which had ORF lengths greater than the minimal length of 100 aa. Simulations were carried out on all 375 genes after the k_{MTS} value was determined.

Table 4.1: Translation kinetics were calculated for 249 conditional genes. Their mitochondrial enrichment is reported in units of log2fold in the absence ("CHXminus") and presence ("CHXplus") of CHX.

Gene Name	ORF (aa)	Elongation (aa/s)	Initiation (1/s)	CHXminus	CHXplus
SLC5A3	719	3.21	0.0114	1.49	1.88
SIGMAR1	224	8.3	1.28	1.49	2.06
UXS1	421	4.47	0.0299	1.48	2.14
GALNS	523	2.84	0.0225	1.48	2.27
SERINC2	456	5.25	0.107	1.48	1.82
NPTN	399	5.32	0.12	1.48	1.86
LTBP3	1304	2.12	0.0317	1.48	1.92
MXRA7	205	6.9	0.213	1.47	2.03
SLC39A1	325	6.39	0.711	1.47	2.31
TTC13	861	4.83	0.0839	1.47	2.26
POLG	1240	4.35	0.106	1.47	3.9
ESYT1	1105	3.01	0.124	1.47	1.85
SMPD1	631	3.8	0.107	1.46	2.31
MARS2	594	6.31	0.0642	1.45	3.99
IFNGR1	490	5.47	0.114	1.45	1.82
GRN	594	2	0.0647	1.45	3.02
GGCX	759	2.19	0.0295	1.44	1.96
M6PR	278	6.42	0.379	1.44	2.19
SELO	670	2.92	0.0453	1.44	3.79
TYRO3	891	5.18	0.161	1.44	1.8
TSPAN6	246	7.69	0.23	1.44	2.08

TEX261	197	6.6	0.197	1.42	1.99
RPN2	632	3.79	0.127	1.42	2.2
SLC29A1	457	4.55	0.0718	1.42	2
SEZ6L2	854	1.77	0.026	1.42	1.95
DEGS1	324	3.9	0.14	1.41	2.05
RFT1	542	5.64	0.0297	1.41	2
TCTN3	608	8.2	0.0487	1.41	1.91
SRPR	639	4.94	0.16	1.4	2.27
CHST11	353	4.65	0.0159	1.4	1.82
GBA	537	2.59	0.157	1.4	2.58
ALG1	465	5.71	0.00402	1.4	2.47
DPAGT1	409	4.46	0.194	1.4	1.86
ERP29	262	4.39	0.0968	1.39	2.13
EPHA2	977	5.16	0.0933	1.38	1.86
TOR1A	333	6.78	0.231	1.38	2
HMGCR	889	3.26	0.0364	1.38	1.8
NAGLU	744	4.02	0.0177	1.38	1.92
SRPRB	272	8.85	0.601	1.38	2.23
SLC19A1	592	7.2	0.0117	1.38	2.1
SLC2A8	478	8.52	0.0888	1.37	1.97
PLTP	494	3.49	0.0369	1.37	2.16
SSR2	184	7.52	0.326	1.37	2.34
IGSF8	614	5.35	0.002	1.36	2.48
ATP1A1	1024	2.49	0.0781	1.36	1.91
HYAL2	474	8.97	0.302	1.36	2.81
ABCB7	754	2.98	0.0182	1.36	4.25
IGFBP2	326	7.34	0.036	1.36	2.82
SCARB1	510	3.68	0.237	1.36	2.15
POMT1	726	2.86	0.0176	1.35	2.08
NCLN	564	6.69	0.268	1.35	2.06
TARS2	719	3.7	0.0912	1.35	4.12
HSPA5	655	4.25	0.101	1.35	2.33

SLC20A1	680	4.32	0.199	1.35	2.14
DERL2	240	6.74	0.212	1.35	1.93
FAM73A	633	2.33	0.0155	1.34	2.2
PPT2	309	5.52	0.258	1.33	2.38
SIL1	462	4.71	0.0317	1.33	2.04
RHBDD2	365	7.2	0.923	1.33	2.35
TOP3A	1002	3.17	0.0394	1.32	2.82
NAGA	412	6.25	0.118	1.32	2.1
PITRM1	1039	4.23	0.0786	1.32	3.63
CLPTM1	670	4.9	0.158	1.32	2.64
BCAP31	247	6.01	0.152	1.32	2.58
EMC10	263	5.34	0.124	1.32	2.6
DHRS7B	326	5.5	0.0791	1.31	2.06
ATRAID	285	9.63	0.556	1.31	2.41
PDIA4	646	4.14	0.0318	1.31	2.32
PC	1179	2.28	0.00647	1.3	4.48
PCOLCE2	416	4.52	0.00449	1.3	2.24
LSR	650	12.8	0.00261	1.29	2.97
SURF1	301	6.76	0.0914	1.28	2.3
SLC12A9	915	3.04	0.00324	1.28	1.84
TMED9	236	7.41	0.14	1.27	2.29
NDUFB9	180	7.85	0.215	1.26	2.58
LRP5	1616	3.94	0.136	1.26	1.92
CD9	229	4.45	0.0539	1.26	2.26
LMAN2	357	5.84	0.0987	1.25	2.55
SLC2A6	508	2.77	0.0252	1.23	2.13
BTD	544	3.6	0.0333	1.23	2.2
HLA-A	366	6.25	0.544	1.23	2.89
CLPB	708	6.17	0.179	1.22	4.18
CTSA	499	2.77	0.231	1.22	2.68
CHID1	394	6.41	0.0481	1.22	2.25
PNPT1	784	4.21	0.00537	1.21	4.28

TMEM104	497	4.13	0.0867	1.2	2.01
ACP2	424	5.62	0.365	1.2	2.09
PERP	194	4.4	0.398	1.2	1.88
R3HDM4	269	7.14	0.355	1.19	2.14
ILVBL	633	6.25	0.209	1.19	2.53
XXYLT1	394	7.37	0.235	1.19	1.93
GPAA1	622	6.05	0.358	1.18	2
LAPTM4A	234	5.43	0.154	1.18	2.3
LRPAP1	358	4.28	0.036	1.18	2.86
ST3GAL4	330	7.52	0.307	1.17	2.29
LMF2	708	3.2	0.122	1.17	2.16
SDF4	349	5.31	0.256	1.16	2.3
SELM	146	6.86	0.306	1.15	2.36
HADHB	475	4.2	0.0238	1.15	4.53
CHPF	776	5.35	0.18	1.15	2.22
SCPEP1	453	3.15	0.0444	1.15	2.34
ASAH1	396	4.73	0.0531	1.14	1.86
PLD3	491	3.74	0.153	1.13	2.21
CD81	237	5.92	0.278	1.13	2.17
B3GAT3	336	7.03	0.431	1.13	2.44
FASTKD2	711	4.91	0.0395	1.12	4.04
AUP1	411	9.55	1.64	1.11	2.34
VIMP	190	7.7	0.112	1.1	1.98
OAF	274	7.5	0.0987	1.1	1.9
COX6A1	110	7.48	0.44	1.1	2.89
LMBRD1	541	4.43	0.0567	1.1	1.81
PON2	355	6.27	0.165	1.09	2
ELOVL1	280	6.93	0.332	1.08	1.87
PIGG	976	3.09	0.00511	1.08	2.17
ALG6	508	5.02	0.0248	1.06	2.02
MPDU1	248	10.4	1.93	1.05	2.57
MTIF2	728	6.5	0.148	1.04	3.6

SLC3A2	569	3.46	0.144	1.04	1.95
CMC1	107	7.81	0.0801	1.03	1.66
PCDH7	1070	5.49	0.0239	1.03	1.95
KIAA2013	635	7.64	0.434	1.02	1.92
GLS	670	2.64	0.0193	1.02	4.01
ALDH4A1	564	5.35	0.0306	1.01	5.14
SUCLG2	433	6.9	0.144	1	3.13
CLPTM1L	539	8.3	1.66	1	1.93
SYNGR2	225	8.69	0.381	0.991	2.17
BCOR	1722	3.11	0.0278	0.99	1.95
SPINT2	253	8.41	0.0158	0.99	2.05
POR	681	2.83	0.0299	0.99	2.35
DLD	510	4.72	0.0789	0.981	4.77
SLC27A4	644	6.67	0.219	0.975	1.99
DOLK	539	6.68	0.134	0.971	1.93
TMED1	228	8.34	0.187	0.969	2.37
SUPV3L1	787	6.09	0.0462	0.968	2.17
DNAJB11	359	6.67	0.0721	0.958	1.8
POMGNT1	661	8.54	0.309	0.957	1.86
PNPLA8	783	5.22	0.0568	0.955	2.11
MFSD10	456	4.18	0.0817	0.955	1.91
PMP22	161	7.17	0.249	0.954	1.82
ORMDL2	154	8.15	0.223	0.947	1.91
MOGS	838	2.74	0.0357	0.94	1.82
MGST3	153	6.04	0.0419	0.933	2.18
METTL17	457	3.5	0.125	0.916	4.1
CHST12	415	4.94	0.0516	0.915	1.82
MINPP1	488	6.32	0.0536	0.914	1.97
AIFM1	614	3.86	0.0912	0.907	4.66
TSPO	170	7.36	0.402	0.901	2.09
NAGPA	516	4.83	0.00221	0.892	1.89
PMPCB	490	4.04	0.0265	0.879	3.99

SPG7	796	1.74	0.00643	0.871	2.95
STARD3	446	5.76	0.184	0.869	2.24
PSEN2	449	5.38	0.0422	0.861	1.82
SLC26A6	760	2.39	0.0225	0.857	1.91
TTLL4	1200	4.96	0.00694	0.853	2.47
CPT2	659	4.51	0.0344	0.851	3.73
AGTRAP	160	7.67	0.165	0.847	1.92
RPS2	294	6.75	2.35	0.802	1.85
CLN3	439	5.25	0.186	0.8	2.14
ACAT1	428	4.33	0.0506	0.8	3.34
CD320	283	6.98	0.476	0.788	2
COMT	272	6.11	0.3	0.784	1.97
HIST3H2A	131	4.5	0.0159	0.761	1.98
FH	511	5.97	0.0958	0.739	3.59
EPHX1	456	4.2	0.0373	0.725	1.97
ACADVL	656	3.51	0.189	0.696	3.52
XKR8	396	7.31	0.0584	0.694	1.91
PPIB	217	6.33	0.173	0.692	2.13
NENF	173	7.84	0.321	0.671	2.41
IMMT	759	4.02	0.196	0.663	3.35
AFG3L2	798	6.4	0.14	0.661	2.66
TMEM147	225	8.71	0.139	0.649	1.96
PCCB	540	4.98	0.123	0.646	4.13
OGDH	1024	2.68	0.118	0.63	3.99
EBP	231	4.01	0.238	0.61	2.08
NDUFC2	120	7.88	0.31	0.57	1.62
COX5B	130	7.66	0.17	0.558	1.56
RSPRY1	577	8.29	0.179	0.543	2.46
IDH2	453	6.76	0.0752	0.533	2.74
FPGS	588	6.14	0.302	0.529	2.92
KIAA0141	516	4.1	0.122	0.525	2.17
RPL18	189	9.32	2.66	0.513	1.92

LETM1	740	4.16	0.133	0.497	3.68
RNF181	154	7.15	0.226	0.481	2.13
NLN	705	6.44	0.085	0.458	2.94
PDK1	437	9.83	0.18	0.446	2.18
MRPS22	361	7.32	0.0134	0.408	1.86
TFB2M	397	6.18	0.0155	0.404	2.13
SUCLA2	464	5.89	0.0411	0.346	1.91
ADCK1	524	6.23	0.00917	0.331	3.19
MTPAP	583	4.1	0.0976	0.321	2.45
MRPS5	431	5.72	0.144	0.312	2.11
ATP5A1	554	5.14	0.0783	0.305	2.74
MRPL37	424	8.19	2.51	0.291	2.11
FAM73B	594	3.51	0.0213	0.288	1.83
ME2	585	5.52	0.0625	0.287	3.28
AGK	423	4.87	0.0273	0.283	3.36
TXNRD2	525	4.94	0.066	0.277	3.98
UQCRC1	481	4.67	0.161	0.272	5.08
TOP1MT	602	5.36	0.0499	0.221	2.56
ALDH2	518	3.61	0.041	0.215	4.04
MIF	116	8.89	0.347	0.204	2.01
SDF2L1	222	9.36	0.178	0.202	1.94
CRAT	627	5.2	0.00745	0.192	2.8
SHMT2	505	5.22	0.265	0.191	2.34
PISD	376	4.42	0.092	0.188	2.68
ALDH7A1	540	3.99	0.0195	0.185	2.9
CECR5	394	6.31	0.226	0.171	2.7
YARS2	478	4.41	0.121	0.171	3.62
FASTKD1	848	4.94	0.0172	0.158	2.11
VKORC1	164	8.6	1.89	0.129	1.87
ERAL1	438	6.66	0.251	0.126	3.58
ATP5B	530	5.97	0.335	0.122	3.78
C1QBP	283	8.74	0.443	0.121	1.78

ATP5G1	137	9.31	0.616	0.106	1.89
LONP1	960	4.29	0.467	0.0889	2.46
PPOX	478	3.27	0.00816	0.0715	2.43
PTCD3	690	4.7	0.0643	0.0596	3.63
FDXR	498	5.1	0.0279	0.0538	1.51
HADHA	764	3.61	0.19	0.0529	3.25
NDUFS2	464	4.42	0.127	0.0526	3.23
NDUFA9	378	6.47	0.156	0.051	2.41
MRPS30	440	7.54	0.257	0.00357	2.89
SIGIRR	411	7.4	0.0512	-8.06E-05	2.24
CS	467	5.63	0.875	-0.00614	3.20E+00
BCKDK	413	7.38	0.527	-0.0067	2.31
HSPD1	574	6.65	0.163	-0.055	2.23
L2HGDH	464	2.72	0.0448	-0.0669	2.26
NARS2	478	7.45	0.0141	-0.0727	2.21
CHDH	595	2.56	0.0021	-0.102	2.22
RABAC1	186	7.76	0.328	-0.135	2.2
UQCRC2	454	6.06	0.208	-0.14	2.61
GPT2	524	6.57	0.097	-0.146	2.16
COQ3	370	10.6	0.113	-0.151	1.95
ADCK3	648	3.06	0.057	-0.162	2.19
ALDH9A1	519	5.88	0.253	-0.192	2.49
NDUFV1	465	5.32	0.12	-0.194	1.96
HSPA9	680	4.92	0.159	-0.204	2.91
MTO1	693	5.47	0.193	-0.241	2.56
PDP2	530	2.96	0.0189	-0.247	1.89
CLPX	634	5.91	0.17	-0.295	2.49
RNMTL1	421	6.25	0.0261	-0.32	2.44
NDUFA10	356	5.02	0.0557	-0.336	2.28
TIMM44	453	6.03	0.326	-0.397	2.56
CKMT1A	418	3.67	0.005	-0.426	1.88
SARS2	519	5.34	0.12	-0.454	2.75

PDHA1	391	5.5	0.0756	-0.474	2.24
GOT2	431	5.74	0.438	-0.523	2.38
NDUFS6	125	7.9	0.0627	-0.529	1.54
DDX28	541	6.18	0.0301	-1.17	1.87

Table 4.2: Translation kinetics were calculated for 126 constitutive genes. Their mitochondrial enrichment is reported in units of log2fold in the absence ("CHXminus") and presence ("CHXplus") of CHX.

Gene Name	ORF (aa)	Elongation (aa/s)	Initiation (1/s)	CHXminus	CHXplus
PDPR	880	2.24	0.013	4.07	4.61
ALDH18A1	796	4.91	0.113	3.81	5.73
IARS2	1013	4.15	0.134	3.8	5.19
ACAD10	1060	2.38	0.0119	3.25	4.27
MUT	751	3.5	0.0144	3.11	4.97
AARS2	986	2.69	0.0105	3	4.45
LARS2	904	5.53	0.139	2.91	4.96
SIAE	524	4.11	0.00168	2.77	2.9
PCK2	641	2.78	0.0528	2.7	4.35
ACO2	781	4.79	0.191	2.69	4.88
GFM1	752	4.61	0.0615	2.64	4.72
GFM2	780	5.35	0.111	2.64	4.29
MCCC1	726	3.02	0.0359	2.63	4.59
PCCA	729	3.17	0.0189	2.6	4.44
P4HA1	535	5.15	0.0485	2.59	2.29
ACSF2	616	2.26	0.00247	2.56	4.56
CREG1	221	7.54	0.254	2.53	2.76
VWA8	1040	3.43	0.0243	2.53	3.26
GUF1	670	6.27	0.0754	2.5	4.06
AKAP1	904	4.09	0.0964	2.49	4
GNS	553	3.22	0.106	2.47	2.58
ANGEL1	671	4.98	0.0311	2.47	3.06
CTSD	413	2.57	0.111	2.4	3.76
LIPA	400	2.84	0.0464	2.37	2.97

ELAC2	827	4.1	0.27	2.36	4.68
GPD2	728	5.33	0.152	2.36	4.36
CPT1A	774	4.63	0.14	2.36	3.35
ERLIN2	340	5.95	0.0686	2.33	2.23
CPD	1381	3.18	0.0252	2.3	2.53
ABCB10	739	5.43	0.0359	2.3	3.73
MRC2	1480	2.11	0.00389	2.28	2.68
TFRC	761	2.99	0.0397	2.27	2.24
LMAN1	511	5.16	0.172	2.27	2.42
VARS2	1064	2.15	0.0194	2.26	3.84
FN1	2478	0.494	0.00289	2.22	1.96
NNT	1087	3.28	0.0989	2.22	4.32
PPT1	307	6.21	0.97	2.21	2.95
PSAP	525	2	0.036	2.19	2.9
GANAB	945	2.82	0.125	2.19	3.11
LGALS3BP	586	2.87	0.257	2.18	2.26
F11R	300	4.31	0.057	2.18	2.31
RETSAT	611	4.26	0.14	2.15	2.24
P4HA2	536	2.88	0.0197	2.15	2.41
NLRX1	976	5.63	0.0405	2.13	3.82
FKBP9	571	3.52	0.113	2.13	1.92
OMA1	525	3.94	0.0246	2.13	3.88
CALU	316	4.25	0.0518	2.12	2.35
PLOD2	759	4.12	0.0641	2.11	2.12
QPCTL	383	4.95	0.176	2.11	2.99
PIGK	396	5.21	0.154	2.11	2.26
EMC1	994	2.46	0.0593	2.1	2.68
GALNT7	658	4.67	0.14	2.1	2.14
EXT2	719	3.01	0.054	2.1	2.94
SERPINH1	419	5.48	0.704	2.09	3.26
COL18A1	1755	1.31	0.00041	2.08	3.21
QSOX1	748	2.92	0.0314	2.07	2.75

ARSK	537	3.42	0.0307	2.07	1.85
SUMF2	321	5.99	0.481	2.07	2.43
PCYOX1L	495	2.06	0.00527	2.05	2
MAN2B2	1010	3.48	0.00551	2.05	2.82
HTRA1	481	3.48	0.115	2.04	2.31
GALNT2	572	4.72	0.277	2.03	2.31
LAMC1	1610	1.82	0.0197	2.02	2.13
CLN5	408	7.09	0.0111	2	2.46
CD46	400	4.19	0.287	1.99	2.21
DSC2	902	3.55	0.0117	1.99	1.96
CCDC47	484	4.44	0.0823	1.98	2.17
SCARB2	479	3.83	0.0402	1.97	1.96
CTSB	340	5.73	0.0698	1.97	2.15
PIGO	1090	3.44	0.166	1.97	2.52
PLXNB2	1839	2.75	0.103	1.97	1.81
ABCB8	719	4.01	0.114	1.97	3.83
MIPEP	714	4.36	0.0143	1.96	4.4
PTK7	1071	3.06	0.00345	1.96	2.4
APP	771	2.11	0.0587	1.95	2.65
ITGB1	799	3.06	0.0587	1.95	1.82
IGF2R	2492	0.98	0.00514	1.95	2.05
ECE1	771	2.23	0.0983	1.95	2.3
DAG1	896	3.33	0.0564	1.94	2.34
TMEM87A	556	4.9	0.0562	1.93	2.36
FBLN1	704	3.14	0.0965	1.93	2.31
GAA	953	2.4	0.00635	1.93	2.58
ATP6AP2	351	3.65	0.0486	1.93	2.6
SORL1	2215	3.25	0.00282	1.92	2.12
LAMP2	412	2.71	0.0197	1.92	2.28
PLBD2	590	2.69	0.0319	1.91	2.2
TMEM30A	362	5.2	0.0563	1.91	1.84
CNNM3	708	3.66	0.00359	1.91	2.3

UBE4A	1074	4	0.0703	1.9	2.12
ELOVL5	300	5.19	0.193	1.9	2.36
DSG2	1119	3.07	0.0368	1.89	1.84
FSTL1	309	4.86	0.209	1.89	2.07
NUP210	1888	1.87	0.0733	1.88	2.2
PTPRF	1899	3	0.00241	1.88	2.36
SPCS3	181	6.2	0.175	1.88	1.85
WLS	542	3.38	0.0991	1.87	2.13
PTDSS1	474	7.42	0.782	1.87	2.02
HSPA13	472	6.24	0.158	1.86	2
ADCK4	545	5.18	0.0286	1.86	3.68
NUCB1	462	3.57	0.0943	1.86	2.89
TMX3	455	3.36	0.0237	1.86	2.06
PROS1	677	6.22	0.0267	1.84	2.05
SLC39A14	493	4.42	0.194	1.83	1.85
ALCAM	584	2.42	0.0189	1.83	1.88
KDELC2	508	4.17	0.01	1.82	1.87
TMEM131	1884	2.45	0.00609	1.82	1.96
NCSTN	710	3.8	0.153	1.81	2.03
NOMO3	1223	2.35	0.0739	1.81	2.2
TAP1	809	7.92	0.0412	1.81	2.4
FITM2	263	7.02	0.00777	1.8	1.92
SEMA3C	752	2.81	0.0478	1.8	1.81
OS9	668	2.58	0.0421	1.8	2.75
PRCP	497	4.25	0.0961	1.8	2.5
KIAA0319L	1050	4.27	0.223	1.79	1.8
ITGAV	1049	2.17	0.0215	1.79	1.88
MFGE8	388	3.34	0.0163	1.78	2.71
AGRN	2046	1.25	0.00559	1.78	2.21
TMEM132A	1025	3.31	0.215	1.78	2.5
PIGT	579	4.86	0.39	1.78	2.64
ITGA6	1074	6.67	0.11	1.76	1.81

APLP2	764	2.43	0.0247	1.76	2.51
MAN2B1	1012	3.5	0.0192	1.76	2.23
TMBIM6	238	6.91	0.193	1.76	2.22
PVR	418	5.27	0.103	1.76	2.05
POLRMT	1231	3.49	0.079	1.76	4.69
LAMA5	3696	1.13	0.0101	1.75	1.95

Mitochondrial localization was measured in [1] by using direct proximity labelling of mRNA transcripts by the enzyme APEX2 tethered to the outer mitochondrial membrane (OMM). All RNA transcripts were sequenced and the authors reported the enrichment of tagged transcripts for individual genes, i.e. an enriched gene has a relatively high ratio of tagged transcripts versus nontagged transcripts, in units of $\log_2$ fold enrichment. Transcripts of known mitochondrial genes displayed higher enrichment to the OMM than the genome as a whole Fig. 4.4. Within this group, I further separated genes that had especially high enrichment or changes in enrichment following cycloheximide (CHX) addition. Translation elongation inhibition by the small drug molecule CHX selectively promotes the mRNA localization of some genes but not others. This phenomenon was observed by [18] in *S. cerevisiae* and formed the basis of my stochastic simulation. I was able to identify subpopulations of CHX-sensitive and CHX-insensitive mRNAs based on their localization ratios in basal conditions and after CHX addition Fig 4.5.

Consistent with the definitions applied by others [18] in *S. cerevisiae*, we define conditional localization as $\log_2$fold enrichment < 1.75 in basal i.e. CHX^- conditions and $\log_2$ fold enrichment >1.75 after CHX addition; constitutive localization is $\log_2$fold enrichment >1.75 in both CHX^- and CHX^+ conditions Fig.4.6. 126 mitochondrial genes satisfied the constitutive localization thresholds and 256 mitochondrial genes satisfied the conditional localization thresholds.

4.0.2 Gene Ontology Term Analysis

I conducted gene ontology (GO) term analysis of the conditional and constitutive groups from both mammalian cells and *S. cerevisiae* using the Database for Annotation, Visualization and Integrated Discovery (DAVID) [39]. I downloaded the Biological Processes GO terms for both groups of both species for further analysis. After discarding duplicates and terms with a false discovery rate (FDR) $< 10^{-10}$, I compared and contrasted the terms in the conditional and constitutive groups of both species. Trends in GO terms are conserved from yeast to mammalian cells, which supports our hypothesis that the biophysical mechanism of mRNA localization kinetics is conserved from yeast to mammalian cells.

Genes involved in one or more foundational mitochondrial processes, like mitochondrion organization, mitochondrial translation, or mitochondrial transport, are found in both groups in both species. Specifically in mammalian cells,
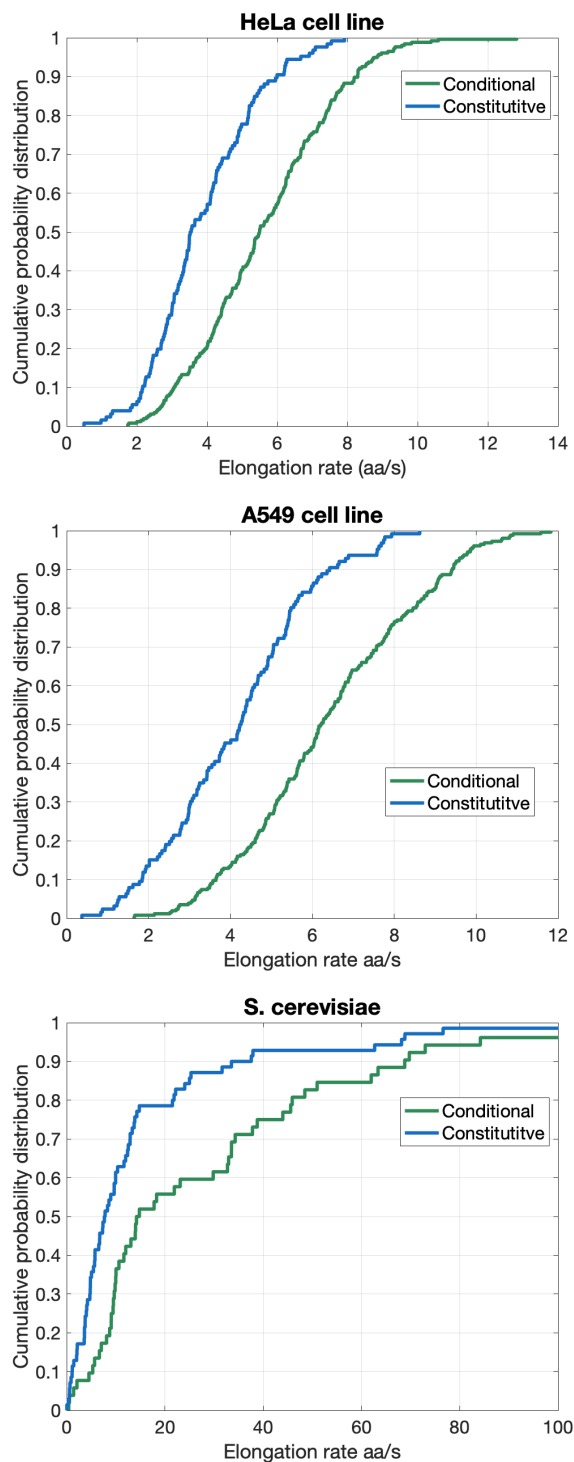
Figure 4.1: Conditional mRNAs (green) typically have faster elongation rates than constitutive mRNAs (blue) in the immortal HeLa cell line, the A549 cancer cell line, and brewer's yeast.
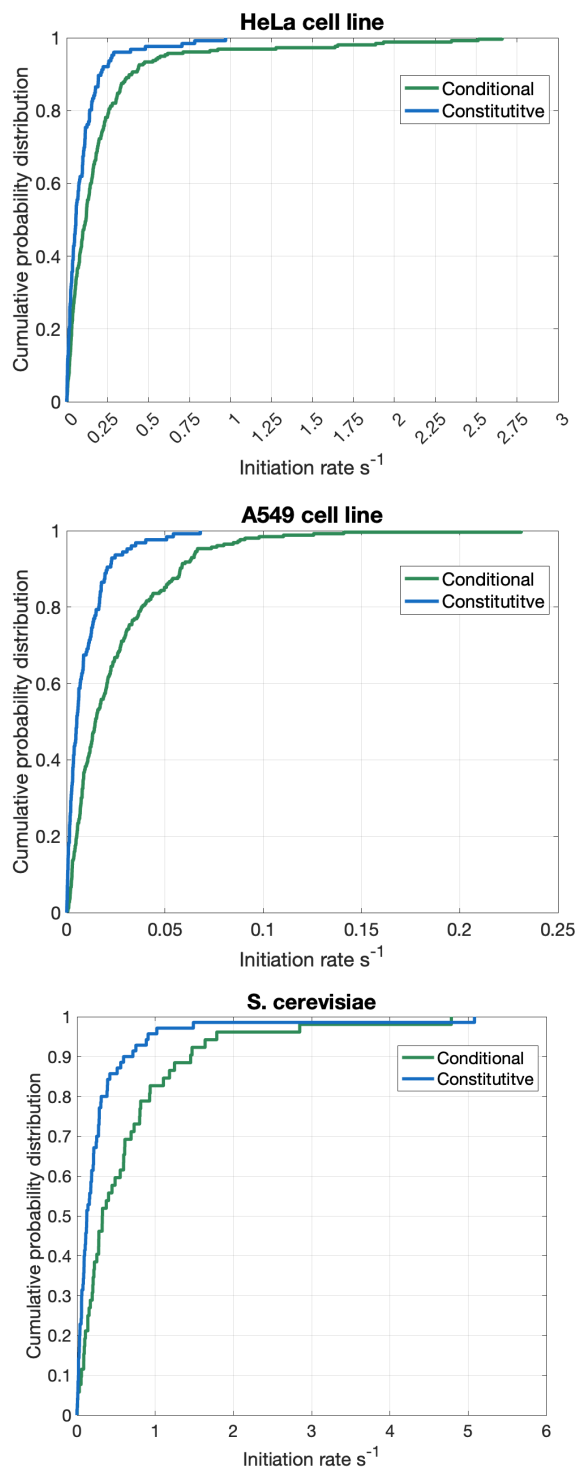
Figure 4.2: Conditional mRNAs (green) typically have faster initiation rates than constitutive mRNAs (blue) in the immortal HeLa cell line, the A549 cancer cell line, and brewer's yeast.
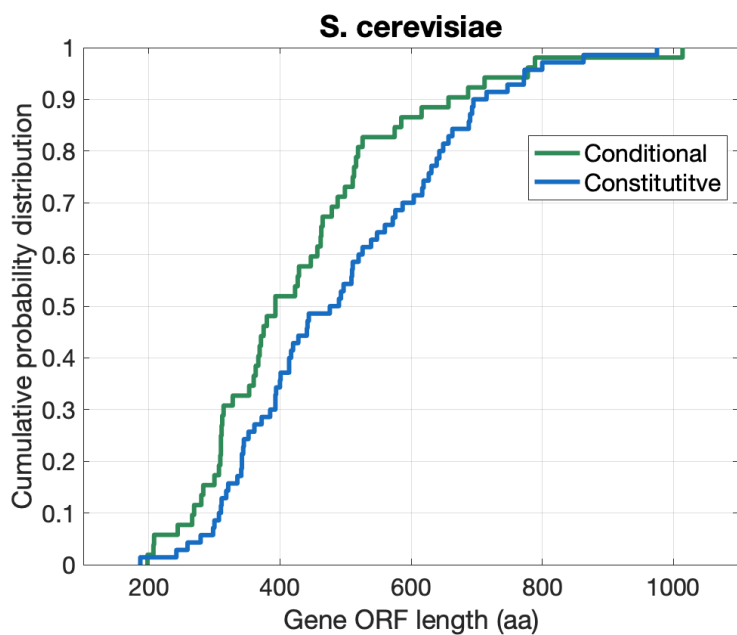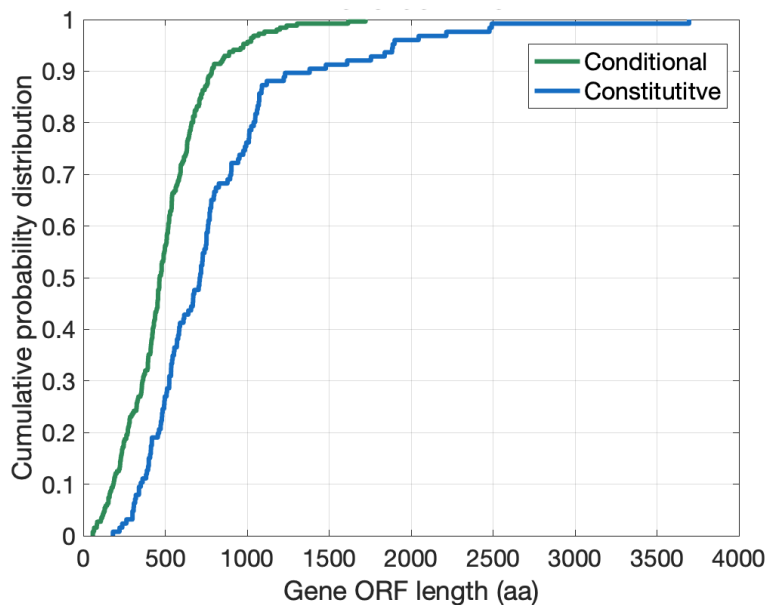
Figure 4.3: Conditional mRNAs (green) typically have shorter open reading frames than constitutive mRNAs (blue) in humans and brewer's yeast.
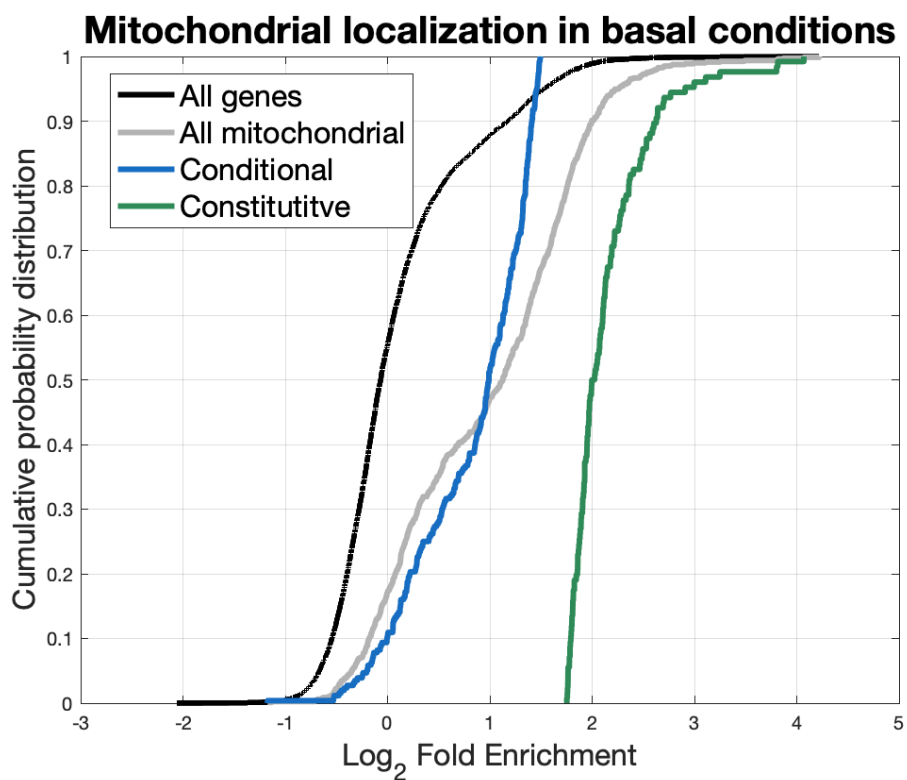
Figure 4.4: Nuclear-encoded mitochondrial mRNAs (gray) were enriched at the mitochondrial surface compared to all mRNAs (black) as a whole. Within the set of mitochondrial mRNAs, subsets of mRNAs with conditional (blue) and constitutive (green) enrichment were identified. Data was replotted from [1].
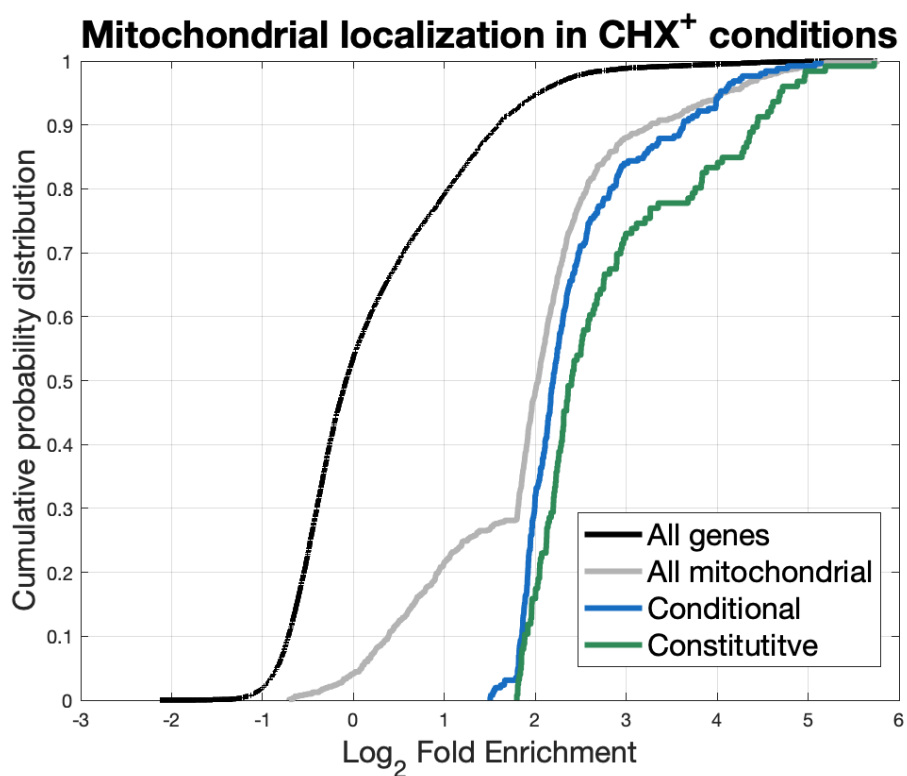
Figure 4.5: Addition of the translation elongation inhibitor CHX increased the relative enrichment of all mitochondrial mRNAs (gray). By definition, mitochondrial mRNAs whose enrichment increased after CHX addition were classified as conditional (blue) whereas mRNAs with consistently high enrichment were classified as constitutive (green). Data was replotted from [1].
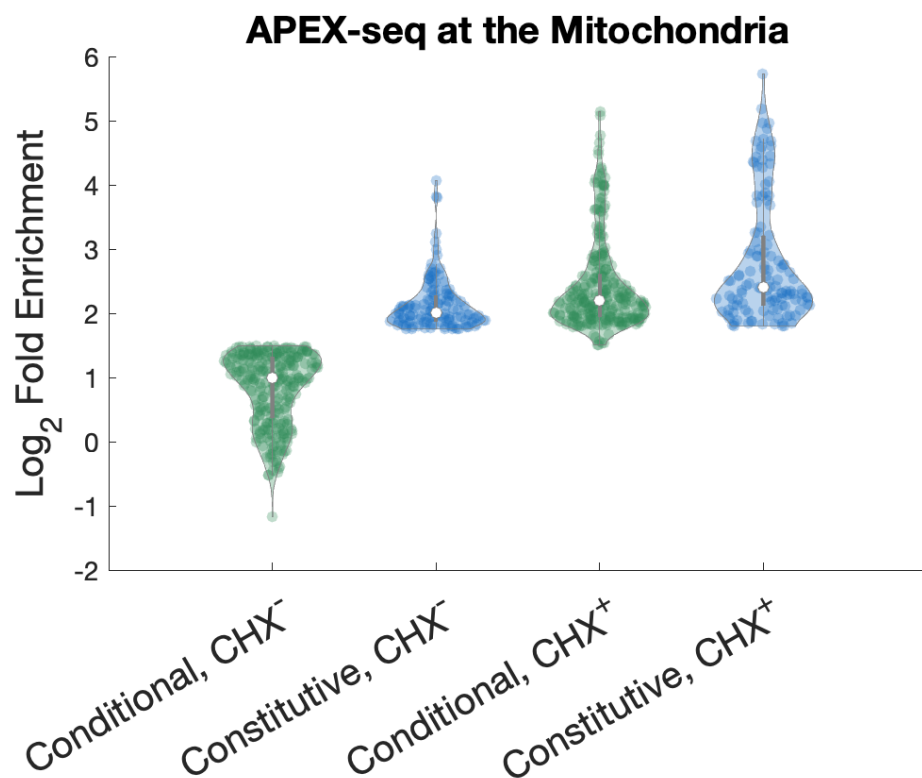
Figure 4.6: Enrichment of a subset of mitochondrial genes at the OMM in units of $\log_2$ fold enrichment. 256 mitochondrial genes meet the conditional localization thresholds (green) and 126 mitochondrial genes meet the constitutive localization thresholds (blue).

Table 4.3: Gene ontology term analysis of the biological process of the 256 conditional genes and 126 constitutive genes in HEK293T cells. Duplicates and terms with a false discover rate (FDR) < 10E-10 were discarded.

Biological Processes (Conditional genes)	Count	FDR
mitochondrion organization	76	1.29E-51
oxidation-reduction process	60	1.30E-36
mitochondrial transport	48	1.17E-34
generation of precursor metabolites and energy	55	1.35E-33
cellular respiration	40	2.14E-32
energy derivation by oxidation of organic compounds	41	3.54E-27
nucleotide metabolic process	55	7.07E-26
ATP metabolic process	38	1.47E-23
electron transport chain	31	5.60E-23
ribose phosphate metabolic process	46	1.16E-21
oxidative phosphorylation	26	1.59E-21
organophosphate metabolic process	60	6.65E-19
mitochondrial translation	24	2.01E-18
protein localization to mitochondrion	20	2.57E-13
cofactor metabolic process	33	4.00E-13
coenzyme metabolic process	29	8.94E-13
mitochondrial RNA metabolic process	14	1.78E-12
carbohydrate derivative metabolic process	52	2.56E-12
cellular amino acid metabolic process	27	3.72E-12
Biological Processes (Constitutive genes)	**Count**	**FDR**
mitochondrial translation	21	3.81E-19
mitochondrion organization	31	4.21E-16
organonitrogen compound biosynthetic process	51	1.84E-15
mitochondrial transport	23	1.79E-14
cellular amide metabolic process	41	5.89E-11
mitochondrial RNA metabolic process	11	2.43E-10

conditional and constitutive groups each contain mitochondrial translation and mitochondrial transport GO terms (Table 4.3); in S. cerevisiae, conditional and constitutive groups each contain mitochondrial translation and mitochondrion organization (Table 4.4). In both species, the conditional group is involved in more metabolic processes than the constitutive group. Crucially, the conditional group is involved in oxidation-reduction, aerobic respiration, and cellular respiration biological processes while the constitutive group is not. Condition-dependent localization is responsive to changing metabolic needs. Slowing down translation elongation boosts localization of mRNAs that code for proteins in the electron transport chain, thus promoting localized expression of these genes in parallel with other methods of transcription regulation.

4.0.3   Computationally determining MTS maturation time for HeLa cells

A parameter sweep was conducted to determine the global value of the free parameter k_{MTS}. A representative conditional gene and a representative constitutive gene were created from the median values of the ORF length (aa), elongation rate (aa/s) and initiation rate (s^{-1}) in the conditional and constitutive cohort, respectively (Table 4.5).

Table 4.4: Gene ontology term analysis of the biological process of the 182 conditional genes and 208 constitutive genes in brewer's yeast. Duplicates and terms with a false discover rate (FDR) < 10E-10 were discarded.

Biological Processes (Conditional genes)	Count	FDR
cellular respiration	31	7.89E-18
aerobic respiration	24	9.93E-15
mitochondrial translation	31	9.93E-15
energy derivation by oxidation of organic compounds	32	9.93E-15
oxidation-reduction process	35	9.93E-15
generation of precursor metabolites and energy	35	1.80E-14
mitochondrion organization	42	2.66E-14
carboxylic acid metabolic process	44	1.14E-10
citrate metabolic process	14	1.47E-10
Biological Processes (Constitutive genes)	Count	FDR
mitochondrion organization	62	9.98E-29
mitochondrial translation	36	7.92E-18
mitochondrial RNA metabolic process	22	2.72E-17
mitochondrial transmembrane transport	25	1.26E-14

Table 4.5: Representative conditional and constitutive mRNAs were created using the median translation parameters of the conditional group and the constitutive group, respectively.

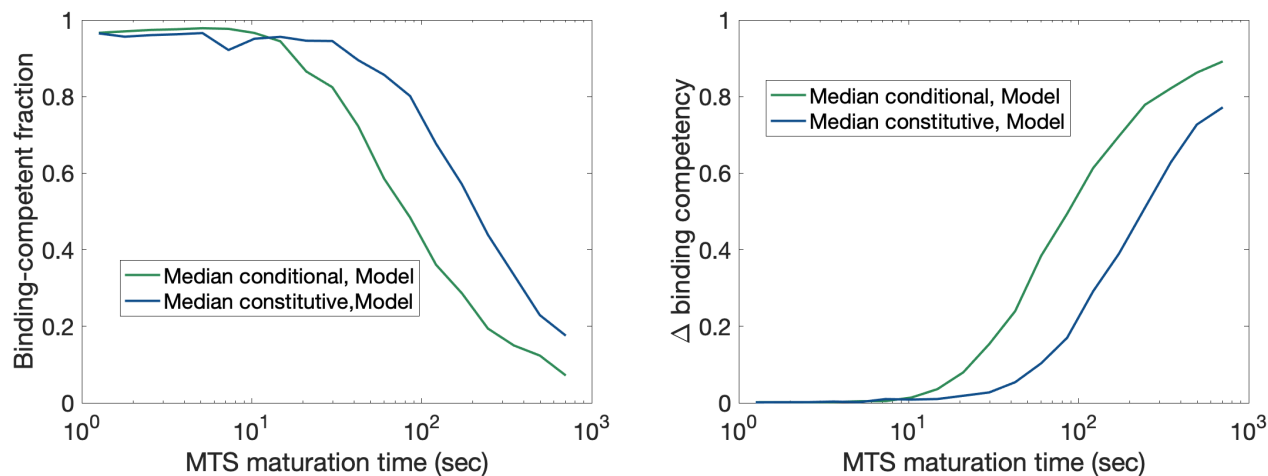| Median gene	ORF length (aa)	Elongation rate (aa/s)	Initiation rate (1/s)
Conditional	466	5.49	0.118
Constitutive	712	3.53	0.0563

Figure 4.7: Parameter sweep determined MTS maturation time in mammalian system

(a) Basal binding competency of the median conditional mRNA (green) drops more rapidly with respect to MTS maturation time ($1/k_{MTS}$) than the median constitutive mRNA (blue). (b) For maturation times of ≈ 100 sec, the change in binding competency starts increasing rapidly for the median conditional mRNA (green).]

Stochastic simulations of binding competency were conducted on the pair of representative genes using numerous k_{MTS} values. In general, an appropriate k_{MTS} value should satisfy two related requirements if it is close to the "actual" global value. It would result in higher binding competency for the constitutive representative than for the conditional representative. Given that binding competency generally decreases as k_{MTS} decreases, there should be a regime in which the conditional mRNA sees a relatively larger change in its binding competency whereas the constitutive mRNA does not. Additionally, there should be a large increase for the conditional representative mRNA after CHX addition and a minimal change to the constitutive representative mRNA. Because binding competency depends only on translation kinetics of the MTS sequence and not on MTS maturation after CHX addition, binding in +CHX conditions does not vary with respect to k_{MTS}. However, the change in binding competency relative to -CHX conditions does depend on k_{MTS}. Therefore, the likeliest k_{MTS} value must maximize the binding competency of the constitutive representative mRNA in all conditions while minimizing the binding competency of the conditional mRNA in basal (-CHX) conditions. For k_{MTS} values between 1/200 and 1/100 seconds, the basal binding competency of the constitutive mRNA remains relatively high ($\approx 60\%$) while the CHX-induced change in binding competency of the median conditional mRNA is also high (Fig 4.8a).

4.0.4 Stochastic simulation recapitulates experimental observations of conditional and constitutive enrichment at the mitochondria

Conditional genes display a wide range of localization ratios in basal (-CHX) conditions compared to constitutive genes in basal (-CHX) conditions and compared to the same genes in +CHX conditions (Fig 4.9). Two-sample Kolomogorov-Smirnov tests were conducted using MATLAB to compare the continuous distributions of localization ratios across conditions and gene groups. At a 1% significance level, or better, the Conditional group (far left) is a different continuous distribution compared to the Conditional+CHX condition (second from left). The former is also a different continuous distribution compared to the Constitutive group (second from right). This indicates that despite the range of localization ratios observed for both conditional and constitutive groups in the absence of CHX, their respective distributions are significantly different from each other. These findings support the hypothesis that translation and diffusion kinetics combine to determine mRNA localization to the mitochondria in mammalian cells. This co-translational mechanism of mRNA localization is a potential conserved mechanism from yeast that can regulate gene expression post-transcriptionally in shifting cellular conditions.
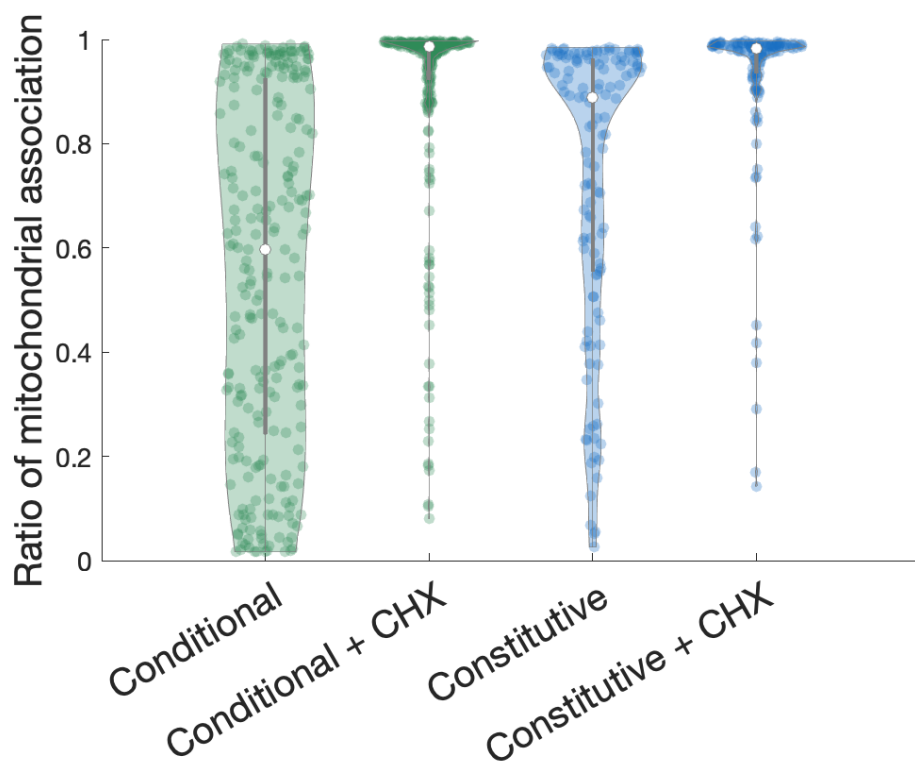
Figure 4.9: Stochastic simulation recapitulates mRNA enrichment observations in mammalian cells
Conditional mRNAs are predicted to have moderate mitochondrial association in basal, fermentative conditions, and become highly associated after cycloheximide treatment. Constitutive mRNAs are predicted to have high mitochondrial association in both conditions.

Chapter 5

Ribosome stalling promotes MTS-mediated mitochondrial association of co-translationally targeted mRNAs

Chapter 5, in part is currently being prepared for submission for publication of the material. The dissertation author was the primary investigator and author of this paper.

Ribosome stalling promotes MTS-mediated mitochondrial association of co-translationally targeted mRNAs

Ximena G. Arceo[1][§]**, Wanfu Hou**[1]**, Cynthia M. Rong**[1]**, Brian M Zid**[1]

[1]UCSD Chemistry Dept

*For correspondence:
zid@ucsd.edu (BZ)

Present address: [§]UCSF

Abstract   For many nuclear-encoded mitochondrial genes, a mitochondrial targeting sequence (MTS) is required but not sufficient for driving localization of mRNA to the mitochondrial surface. During co-translational localization, the MTS on the nascent peptide associates with chaperones from the Hsp70 family and others that mediate interactions with the mitochondrial import complex. A subset of co-translationally localized mRNAs are constitutively highly enriched at the mitochondrial surface while others are conditionally enriched because they exhibit an increase following total translation elongation inhibition. Even though both mRNA types contain an MTS, the constitutively enriched type was more likely to contain ribosomal stalling motifs, which are implicated in chaperone recruitment. While ribosomal stalling slows down overall translation elongation rate, constitutively enriched mRNAs also contain longer ORFs, and both characteristics result in long translation duration and thus long-lived nascent peptides. Insertion of a well-characterized mild ribosomal stalling motif downstream of the MTS promoted mRNA localization whereas the absence of a ribosomal stalling motif led to low localization. Our work indicates that ribosomal stalling promotes mRNA localization more than ORF length. For co-translationally localized mRNAs, translation elongation slowdowns act in coordination with chaperone recruitment to regulate the degree of mitochondrial association.

Introduction

Cells adapt their proteome to changing environmental conditions by controlling protein production at the transcriptional and post-transcriptional level. Similarly, to maintain homeostasis, cells regulate gene expression with transcriptional and post-transcriptional methods. In addition to regulating protein levels and proteome composition, eukaryotic cells also regulate subcellular organization. Proteins can be localized co-translationally, i.e. as part of the mRNA-ribosome complex, or post-translationally, i.e. after the fully-translated sequence has terminated translation and is released from the mRNA-ribosome complex. Proteins with transmembrane domains [CITATIONS], highly structured elements [CITATIONS], and other folding challenges [CITATIONS] rely on co-translational methods of localization, wherein the mRNA-ribosome complex typically associates with a peptide-binding chaperone before completing translation. For co-translationally localized proteins, mRNA localization and chaperone recruitment are essential to maintain subcellular organization in general and safe-guard membrane proteins and aggregation-prone proteins in particular. Nuclear-encoded mitochondrial gene expression is tightly coupled to nutrient conditions and cellular metabolic load and is highly reliant on the post-transcriptional process of mRNA local-

40 ization to ensure mitochondrial proteins are imported into the mitochondria *Saint-Georges et al.*
41 (*2008*); *Young et al.* (*2003*). Co-translational import protects these highly structured and hydropho-
42 bic membrane proteins from misfolding and aggregation in the cytosol *Stein et al.* (*2019*) whereas
43 mRNA localization generally helps coordinate the expression of the nuclear and mitochondrial
44 genomes *Couvillion et al.* (*2016*).
45   In brewer's yeast, hundreds of nuclear-encoded mitochondrial genes are known to contain a
46 mitochondria targeting sequence (MTS) on the 5' end. These mRNAs localize asymmetrically to the
47 mitochondria only after the MTS has been translated and the nascent peptide chain containing the
48 mitochondria-targeting signal has exited the ribosomal tunnel. Translation can be broken down
49 into three sequential steps: initiation, during which ribosomes assemble at the initiation site on an
50 mRNA, elongation, during which ribosomes translocate across the mRNA and build upon a nascent
51 peptide, and termination, during which ribosomes are removed from the mRNA, recycled, and the
52 newly synthesized protein is released.
53   While each step of translation is regulated, initiation has generally been considered the rate-
54 limiting step and thus subject to the tightest regulation. However, recent studies have illuminated
55 the importance of elongation, and elongation rate modulation, in governing proper protein folding
56 *Thanaraj and Argos* (*1996*); *Stein et al.* (*2019*), protein localization *Zhao et al.* (*2021a*), and mRNA
57 localization *Zhang and Shan* (*2012*). For co-translationally imported mitochondrial proteins, the
58 recruitment of chaperones to the nascent peptide is required for the formation of a competent
59 mitochondrial-targeting complex *Hoseini et al.* (*2016*); *Deshaies et al.* (*1988*). More generally, a
60 regime of moderate ribosome collisions has been identified wherein ribosome stalls can be func-
61 tional and important for recruiting peptide-binding chaperones during active translation *Zhao et al.*
62 (*2021b*).
63   When ribosomes encounter certain mRNA sequences, they can pause or stall during translation.
64 This can have a significant impact on the final protein product and interactions with chaperones.
65 Ribosome stalling has been shown to play a role in quality control mechanisms that detect and
66 degrade abnormal mRNAs. In the case of non-aberrant translation, ribosome stalling can also
67 modulate the folding of nascent proteins and recruitment of peptide chaperones, leading to their
68 proper folding or activation as localization signals
69   In this study, we used an *in vivo* quantitative luciferase-based assay to measure elongation time
70 for all mRNAs of interest. We quantified the effects of two ribosomal stalling motifs on elongation
71 duration: non-optimal codons and polyprolines. Codon optimality describes the translational effi-
72 ciency of the 61 codons and accounts for numerous biochemical factors, including tRNA availability
73 and demand *Varenne et al.* (*1984*), frequency of use in the genome, GC content, and interactions
74 with the ribosome exit tunnel *Charneski and Hurst* (*2013*). Intriguingly, our analysis of *Stein et al.*
75 (*2019*) reveals that ribosomal stalls can act as binding sites for Ssb, a member of the Hsp70 family of
76 chaperones. Hsp70 proteins have a central role in co-translational activity given their widespread
77 binding to nascent peptides and their importance to co-translational folding (Doring et al., 2017;
78 Hanebuth et al., 2016; Koplin et al., 2010; Willmund et al., 2013). Hsp70s recognize hydrophobic
79 sequences, which are vulnerable to misfolding but also common in mitochondrial membrane pro-
80 teins. Peptides can have numerous Hsp70 binding sites because their recognition motifs have been
81 found 36 amino acids apart, on average, along the linear peptide sequence (Ru€diger et al., 1997).
82 Loss of Hsp70 proteins leads to aggregation of nascent peptides (Koplin et al., 2010; Willmund
83 et al., 2013), compromising the functional ability of nascent peptides to mediate co-translational
84 association of mRNA-ribosome complexes to the mitochondria.
85   Co-translationally localized mitochondrial mRNAs, also called Class II mRNAs, associate with
86 imort complexes on the outer mitochondrial membrane after translation of the N-terminal mito-
87 chondrial targeting sequence (MTS) (*Garcia et al., 2010*). All Class II mRNAs contain an MTS but
88 some are only asymmetrically localized to the mitochondria under certain conditions. MTS swap-
89 ping experiments demonstrate that the downstream coding sequence (CDS) *Tsuboi et al.* (*2020*);
90 *Garcia et al.* (*2010*) sets the quantitative localization behavior. In summary, the MTS is required

91 but not sufficient for asymmetric localization to the mitochondria. We created constructs using
92 the same MTS (Tim50 aa1-100) and different CDSs to elucidate the mechanism of constitutive lo-
93 calization to the mitochondria. We used the MS2-MCP system to locate individual mRNAs in yeast
94 during live imaging. We found that mRNAs with ribosomal stall motifs were more about twice as
95 likely to be located near the mitochondrial ($\leq 500~\mu m$).

96 **Results**

97 **Stochastic simulations suggest ribosome stalls are central to constitutive mRNA**
98 **localization**

99 Tim50 is co-translationally localized to mitochondria. After subtracting the contributions of tran-
100 scription and translation initiation, the translation elongation duration of Tim50 was measured
101 to be 91 seconds. Given the ORF length of 476 aa, Tim50's average elongation rate is 5.20 aa/s.
102 However, Tim50 contains robust ribosome stalls that contribute disproportionately to ribosome
103 dwell time. Downstream of the MTS there is a polyproline-rich site between aa174 to aa187, which
104 contain 10 prolines total and 7 consecutive prolines at aa181 to aa187. A ribosome dwells for 15
105 seconds on the stretch of 7 consecutive prolines "p7" (aa181-187), resulting in a slow elongation
106 rate measurement of 0.44 aa/s along these 7 amino acids. When a larger sequence of 14 amino
107 acids "p14" (aa174-187), which contained 10 non-consecutive prolines, was deleted, the translation
108 duration difference was 30 seconds. This resulted in a similarly slow elongation rate measurement
109 of 0.44 aa/s along these 14 amino acids. (Fig 2).

110 The polyproline-specific elongation rate was incorporated into simulated constructs with or
111 without p7 and p14 insertions (Fig 2) and compared to Tim50 with a uniform 5.2 aa/s elongation
112 rate and no deletions. All 5 constructs were simulated in the stochastic simulation developed in
113 *Arceo et al.* (*2022*) so we could compare the effects of ribosome stalls on mRNA localization behav-
114 ior across the physiological range of mitochondrial volume fractions. Constructs with p7 and p14
115 ribosome stalls have a locally slower elongation rate of 0.44 aa/s. To keep the gene-wide average
116 elongation rate the same for the explicit p7 and p14 constructs, the elongation rate everywhere
117 else in the mRNA increases to 7.7 aa/s. For constructs with p7 and p14 deletions, the gene-wide
118 elongation rate is consistently 7.7 aa/s, and 7 (p7) or 14 (p14) amino acids are deleted from the
119 simulated mRNA. The initiation rate was set at 0.1264 s^{-1} for all 5 constructs, and was previously
120 calculated in *Arceo et al.* (*2022*).

121 Tim50 mRNAs with p7 and p14 deletions display more dynamic localization behavior compared
122 to the constructs with polyproline ribosome stalls and the construct with a consistent and more
123 moderate elongation rate. Despite the relatively faster elongation rate outside of the p7 and p14
124 motifs, these mRNAs nonetheless display constitutive localization behavior. A ribosome stall of 15
125 (p7) or 30 (p14) seconds downstream of the MTS is sufficient to capture Tim50's observed consti-
126 tutive localization. Deletion of p7 led to lower localization in fermentative (small MVF) conditions,
127 which is consistent with findings from *Tsuboi et al.* (*2020*). Deletion of 7 more amino acids in the
128 p14 construct led to a shorter translation duration and lower mRNA localization but was still on
129 par with the effects of the p7 deletion. Conversely, the explicit inclusion of the p14 ribosome stall
130 motif led to a longer translation duration than the p7 ribosome stall motif but resulted in identical
131 mRNA localization behavior. Altogether, this suggests that the 15 second delay caused by the p7
132 ribosome stall is sufficient to shift the localization of Tim50 from conditional or moderate to con-
133 stitutive or high in the fermentative MVF regime. Given the overall translation duration of 91 sec
134 for the endogenous Tim50 sequence, 15 seconds accounts for only a 16% difference. However,
135 concentrating this 16% delay in a hyperlocal ribosomal slowdown has an outsized effect on mRNA
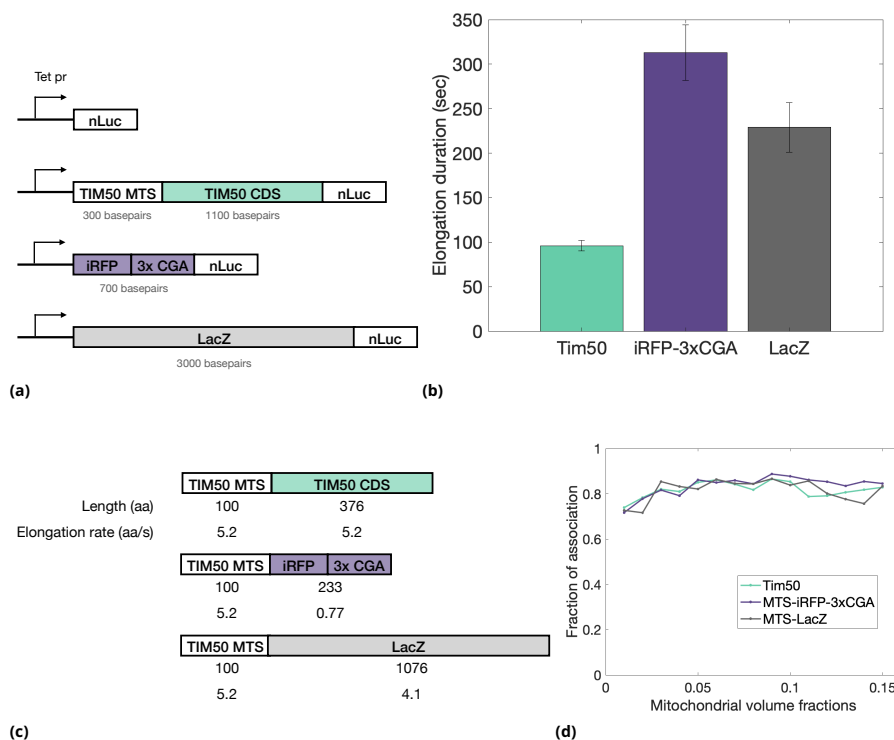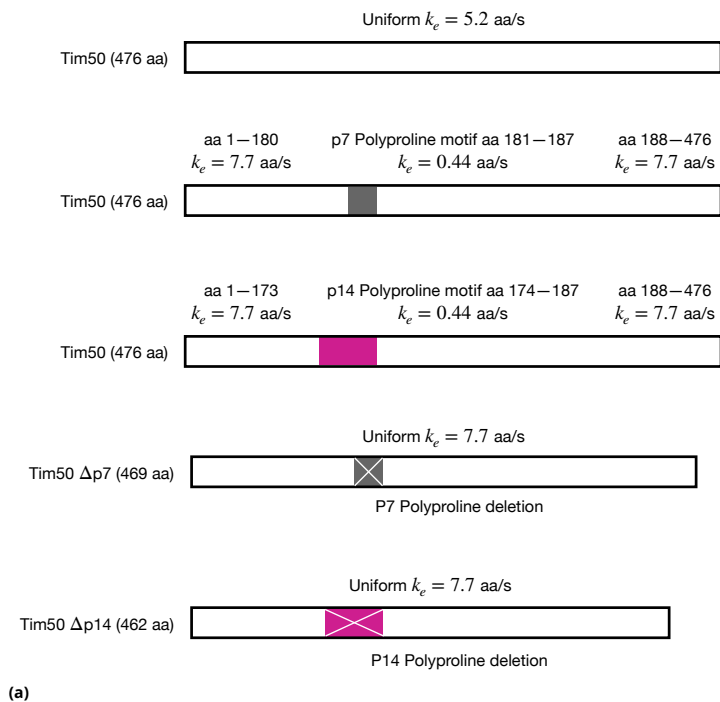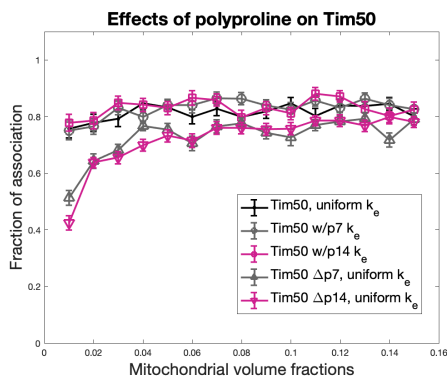136 localization.

Figure 1. (a) Schematic of constructs of various lengths. The endogenous Tim50 sequence, iRFP-3xCGA, or LacZ are set upstream of a nanoluciferase (nLuc) reporter. Constructs are expressed from an inducible Tet07 promoter. (b) Elongation duration of all 3 constructs. (c) Length and elongation rate of the MTS and CDS regions of all 3 constructs. (d) Stochastic simulation of all 3 constructs indicates their localization ratios are equally insensitive to MVF.

Figure 5.1: Sequence-specific elongation rate of 3 chimeric constructs was measured from translation duration measurements.

Figure 2. (a) Elongation rates of simulated constructs. (b) Simulations indicate that ribosome stalls at two overlapping polyproline motifs downstream of the MTS promote mitochondrial association for Tim50 more than uniformly slow elongation.

Figure 5.2: Elongation slowdown at polyproline sites promotes mRNA localization in simulation.

Ribosome stalls promote mRNA localization independently of translation duration

Chimeric reporter genes were created to parse the effects of ribosome stalls on translation duration and mRNA localization. Previously, we had showed that constitutive mRNAs have overall longer translation durations given their combination of longer ORFs and faster elongation rates (*Arceo et al.* (*2022*)). However, constitutive mRNAs are also known to contain ribosome stalls, which can also lead to overall longer translation duration with hyperlocalized ribosome slowdowns. Therefore, it was unclear if translation duration was a confounding variable in the co-translational mechanism of mRNA localization or whether another factor, like ribosome stalls, was needed for constitutive localization. We created chimeric reporter mRNAs with the same MTS and different CDSs to isolate the effect of ribosome stalls and translation duration. These reporter mRNAs contain 12 MS2 stem loops downstream of the ORF that bind to an MS2 coat protein (MCP) and a green fluorescent protein (GFP). The MS2-MCP visualization system was previously described (*Gadir et al.* (*2011*)) and validated as a microscopy method for tracking individual mRNAs *in vivo*.

mRNA localization was quantified and compared for all 3 constructs. The percentage of mRNA foci that were located ≤ 500 *nm* from the nearest mitochondrial surface were reported as the localization ratio. Error bars are given as the standard error between technical replicates containing more than 3 cells each. All microscopy experiments were conducted in fermentative conditions. Localization ratio was not found to correlate with total mitochondrial volume or cell area, supporting our hypothesis that construct-specific differences in mRNA localization are a result of translation kinetics. The LacZ construct (gray) had the lowest localization ratio whereas the shorter constructs with ribosome stalls, iRFP-3xCGA (purple) and endogenous Tim50 CDS (teal), had similarly high localization ratios. According to translation duration measurements (Fig 3b), LacZ had a moderate translation duration (≈ 200 sec), that was shorter than iRFP-3xCGA's translation duration (*approx* 300 sec) and greater than Tim50's translation duration (*approx* 100 sec) despite the fact the latter measurement also contained the MTS. All 3 reporters were simulated (Fig 3c,d) using elongation rates calculated from the translation duration measurements and with the same initiation rate of 0.1264 s^{-1} because they have the same 5' ORF sequence. The stochastic simulation predicted erroneously that MTS+LacZ would have constitutively high localization like MTS+iRFP-3xCGA and Tim50. Given the centrality of ribosome stalls to Tim50's localization behavior (Fig 2), we concluded that ribosome stalls promote MTS-driven mRNA localization independently of translation duration. More quantitative measurements of ribosome stalls in general and of translation duration downstream of the MTS in particular in order to fully elucidate the mechanism and grasp of the kinetic behavior of co-translational mRNA localization.

Discussion

We previously demonstrated that the interplay of diffusion and translation kinetics combine to regulate mRNA localization (*Arceo et al.* (*2022*)). mRNAs with faster translation kinetics display more dynamic localization behavior because they switch between binding competent and incompetent at the same time scale as diffusion, and the kinetics of binding compete with the nonspecific effects of diffusion. While fast translation is a hallmark of conditional mRNAs, translation duration measurements for Tim50 and Atp3 indicate the opposite is true. Intriguingly, Schleif plot results conflict with gene-specific elongation rates we previously calculated using a combination of numerous datasets and techniques. When measured with the Schleif technique, conditional mRNAs had slower elongation rates than constitutive mRNAs. It is unclear if these inconsistencies are limited to the five mRNAs that were studied–OMA1, NDI1, ATP2, ATP3, and TIM50–or if there is systematic issue in the elongation rates published in *Arceo et al.* (*2022*) stemming from assumptions about the underlying physics, the nature of the various techniques in each dataset, or another unanticipated problem. Conversely, it is plausible that the elongation rates are imprecise for a handful of genes while the trends observed for over 100 genes are nonetheless accurate. In other words, it is plausible that the trend of faster elongation that was calculated and observed for the constitutive
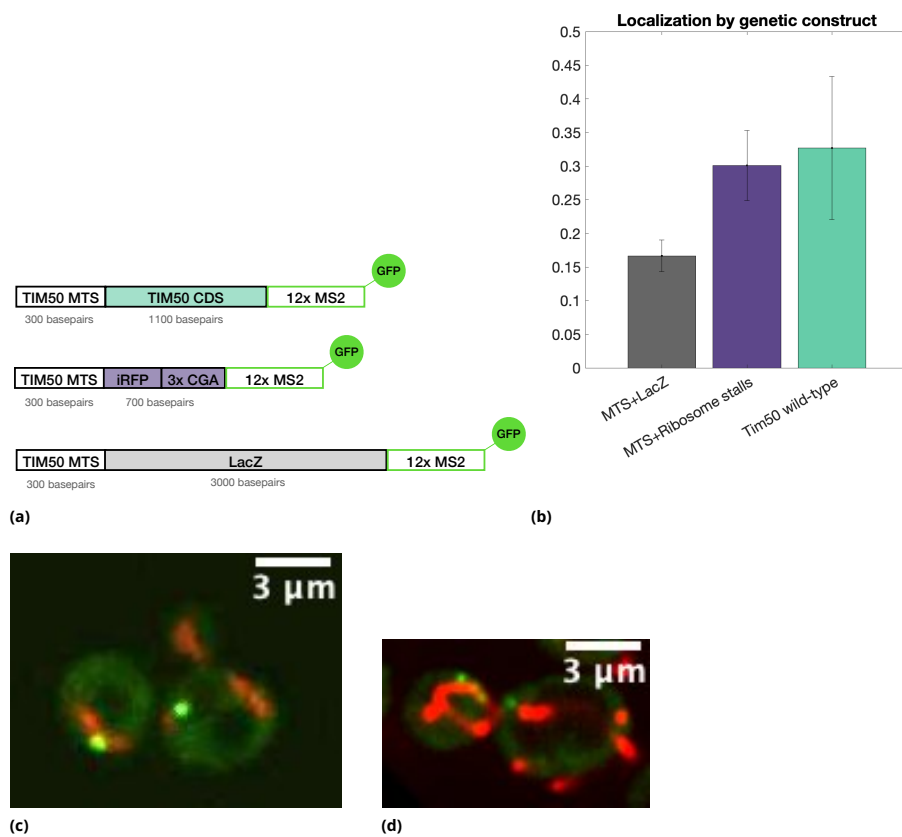
(a)

(b)

(c)

(d)

Figure 3. (a) Schematic of chimeric reporter mRNAs visualized using GFP with an MS2-MCP system. (b) Percentage of mRNAs found $\leq 500\ nm$ from the nearest mitochondrial surface for all 3 constructs. (c) Representative image of live yeast cell with iRFP-3xCGA construct in the mCherry (mitochondrial) and GFP (mRNA) channels. (d) Representative image of live yeast cell with Tim50 construct in the mCherry (mitochondrial) and GFP (mRNA) channels.

Figure 5.3: mRNA localization was quantified for all 3 chimeric MS2-MCP reporters.

186 mRNA subset is accurate despite the calculations being incorrect for all 5 aforementioned mRNAs.
187 The central approach of blending multiple datasets with various techniques into calculations of
188 initiation rates, and then elongation rates, inadvertently propagates or even multiplies the impre-
189 cision in each technique. In conclusion, it is unclear whether the inconsistencies stem simply from
190 noise in the calculations from *Arceo et al.* (*2022*) or if they point to a systematic issue that requires
191 a fundamentally different approach to translation rate calculations and thus a reconsideration of
192 *in silico* results and discussion from *Arceo et al.* (*2022*).
193   The preponderance of ribosome stall motifs in the constitutively-localized group suggests that
194 elongation modulation coordinates with chaperone recruitment to promote mitochondrial localiza-
195 tion. Insertion of polyprolines and non-optimal codon stretches has been found to increase mRNA
196 localization independently of the MTS. In essence, the amphiphalic structure of the MTS nascent
197 peptide is required for association to import machinery at the mitochondrial surface, whereas
198 the CDS appears to determine the dynamics and quantity of localization. This modular composi-
199 tion is ideal for post-transcriptional regulation of metabolic mitochondrial genes whose proteins
200 need to be upregulated in response to metabolic changes, such as the switch from fermentative
201 to respiratory metabolism. mRNA localization behavior is sensitive to the metabolic state along a
202 number of avenues, including the susceptibility of elongation to perturbations in the concentra-
203 tions of GTP, eIF5a, charged tRNAs, and other molecules involved in ribosome translocation. Many
204 ribosomal stall motifs require more translation regulation chaperones during all cellular states.
205 Due to the challenge of forming a peptide bond between sequential prolines, eIF5a is required
206 for the proper expression of genes with polyproline stretches, which are otherwise susceptible to
207 mRNA degradation via the ribosome quality control (RQC) pathway. Conversely, mRNAs devoid
208 of ribosomal stall motifs and with relatively fast elongation rates experience slowdowns during
209 certain conditions, like low ATP production, that may indicate a large metabolic shift is underway.
210 We postulate that conditional mRNAs, which are generally devoid of the ribosomal stall motifs ob-
211 served in constitutive mRNAs, undergo a relatively larger decrease in elongation in conjunction
212 with a decrease in the cell's growth rate. For conditional mRNAs, these stochastic slowdowns pro-
213 mote chaperone recruitment in a manner similar to ribosomal stall motifs in constitutive mRNAs.
214 Thus, the decrease in growth rate and ribosome translocation combine to increase the binding-
215 competency of conditional mRNAs, drive conditional mRNA localization to the mitochondria, and
216 promote the expression of this gene group. Indeed, tethering experiments have demonstrated the
217 mitochondrial milieu increases protein levels even for non-mitochondrial genes like GFP. Given the
218 prevalence of Krebs cycle proteins in the conditional gene group, their responsive localization dur-
219 ing metabolic switches or perturbations points to co-translational mRNA localization as a potential
220 post-transcriptional mechanism of gene expression.

221 ## Methods and Materials

222 ### Luciferase assay

223 We previously developed and validated a quantitative elongation duration reporter assay utilizing
224 a tetracycline-inducible promoter to control mRNA induction of a bioluminescent nanoluciferase
225 (nLuc) reporter downstream of open reading frames (ORFs) of interest *Hou et al.* (*2023*). All mR-
226 NAs of interest contained the same first 100 amino acids (AAs), aa(1-100) of the Tim50 ORF. We
227 developed a series of chimeric sequences in which we varied the translation duration of the down-
228 stream coding sequence (CDS) by insertion of a long sequence (LacZ) or non-optimal codons. The
229 third ORF of interest was the endogenous Tim50 sequence, which includes ribosomal stalling mo-
230 tifs: 7 sequential prolines at aa, and 10 prolines at aa . Elongation time was calculated using a
231 Schleif plot *Schleif et al.* (*1973*) and adjusted based on an average mRNA transcription time of
232 1500 nucleotides per minute *Mason and Struhl* (*2005*); *Edwards et al.* (*1991*). We find a delay in the
233 first appearance of nLuc upon the addition of Tim50, LacZ and iRFP-3xCGA upstream of nLuc. We
234 then used these measured delays to calculate the translation elongation rate of Tim50, LacZ and

235 iRFP-3xCGA as 5 aa/s, 7 aa/s, or 0.077 aa/s, respectively, which is consistent with the maximum

236 observed elongation rate measurement of 10 aa/s (Fig 1). *Riba et al.* (*2019*); *Karpinets et al.* (*2006*).

Microscopy

238 Single molecule mRNA visualization with mitochondria was performed as follows: Yeast cells were

239 grown in YPA medium containing 2% glucose (fermentative) or 3% glycerol + 2% ethanol (respira-

240 tory) with 15 mL glass tube at 30 C with rotator speeds of 60 rpm. Mid-log phase wild-type yeast

241 cells (OD600 of 0.4 to 0.7) were grown in appropriate medium and 20 μ L were placed into a 96-well

242 Glass Bottom Plate (Cellvis LLC). Cells were imaged by an Eclipse Ti2-E Spinning Disk Confocal with

243 Yokogawa CSU-X1 (Yokogawa) with 50 mm pinholes, located at the Nikon Imaging Center UCSD.

244 Imaging was performed using SR HP APO TIRF 100 × 1.49 NA oil objective with the correction collar

245 set manually for each experiment (pixel size 0.090 mm). Z-stacks (200 nm steps) were acquired by

246 a Prime 95B sCMOS camera (Photometrics). Imaging was controlled using NIS-Elements software

247 (Nikon).

Segmentation of cell boundaries and 3D mitochondrial architecture

249 We segmented cell boundaries from the GFP channel of images, using the DIC channel as reference.

250 The ROIs were saved in the FIJI ROI GUI and then applied to the GFP channel and for all of the

251 z-planes in the mCherry channel. For the GFP channel, a single z-plane was exported in the text-

252 image format for further analysis. For the mCherry channel, a z-stack was generated containing all

253 the z-planes for a single cell. This z-stack was exported in a tif format for processing in MitoGraph

254 *Harwig et al.* (*2018*). MitoGraph is available from https://github.com/vianamp/MitoGraph. MitoGraph

255 required two inputs regarding the precision in 2D (0.090 nm/pixel) and in z (0.200 nm/step).

Quantification of mRNA localization

257 MitoGraph analyzes microscopy images of mitochondria and generates high-resolution, cell-specific

258 data about mitochondrial network architecture. This information was used to reconstruct the 3D

259 surface of mitochonddria and determine the 3D coordinates of the mitochondrial network inside

260 an individual cell. To determine the 3D coordinate of the foci(s) in the individual cell, the text-

261 image of the GFP channel was processed in a script available from the authors. The script defines

262 an mRNA molecule as the brightest pixel above a threshold. The threshold of minimum mRNA

263 foci brightness is determined for each experimental condition because it varies with laser power.

264 The threshold was kept constant for all images collected with a particular experimental condition

265 regardless of the mRNA construct. We defined a localized mRNA as a foci located 0.500 μm or less

266 from a mitochondrial surface. For LacZ and iRFP-3xCGA constructs, there was typically one foci per

267 cell, rarely two. For the Tim50 construct, which has an endogenous promoter, there was typically

268 more than one foci per cell. For all constructs, the number of localized mRNA molecules was di-

269 vided by the total number of mRNA molecules and the mean is reported as the localization ratio

270 of every construct. We calculated the standard deviation of the mean localization ratio in every

271 field-of-view ($n \geq 20$) and reported this as the error in localization ratio of a given construct.

References

273 **Arceo XG**, Koslover EF, Zid BM, Brown AI. Mitochondrial mRNA localization is governed by translation kinetics

274 and spatial transport. PLOS Computational Biology. 2022 08; 18(8):1–28. https://doi.org/10.1371/journal.pcbi.

275 1010413, doi: 10.1371/journal.pcbi.1010413.

276 **Charneski CA**, Hurst LD. Positively charged residues are the major determinants of ribosomal velocity. PLoS

277 biology. 2013; 11(3):e1001508.

278 **Couvillion MT**, Soto IC, Shipkovenska LS Gergana & Churchman. Synchronized mitochondrial and cytosolic

279 translation programs. Nature. 2016; 533:499–503.

280 **Deshaies RJ**, Koch BD, Werner-Washburne M, Craig EA, Schekman R. A subfamily of stress proteins facilitates

281 translocation of secretory and mitochondrial precursor polypeptides. Nature. 1988; 332(6167):800–805.

Edwards AM, Kane CM, Young RA, Kornberg RD. Two dissociable subunits of yeast RNA polymerase II stimulate the initiation of transcription at a promoter in vitro. Journal of Biological Chemistry. 1991; 266(1):71–75.

Gadir N, Haim-Vilmovsky L, Kraut-Cohen J, Gerst JE. Localization of mRNAs coding for mitochondrial proteins in the yeast Saccharomyces cerevisiae. RNA. 2011; 17(8):1551–1565.

Garcia M, Delaveau T, Goussard S, Jacq C. Mitochondrial presequence and open reading frame mediate asymmetric localization of messenger RNA. European Molecular Biology Organization Reports. 2010; 11(4):285–291.

Harwig MC, Viana MP, Egner JM, Harwig JJ, Widlansky ME, Rafelski SM, Hill RB. Methods for imaging mammalian mitochondrial morphology: A prospective on MitoGraph. Analytical Biochemistry. 2018; 552:81–99. https://www.sciencedirect.com/science/article/pii/S0003269718301921, doi: https://doi.org/10.1016/j.ab.2018.02.022, mitochondrial Biochemistry and Bioenergetics.

Hoseini H, Pandey S, Jores T, Schmitt A, Franz-Wachtel M, Macek B, Buchner J, Dimmer KS, Rapaport D. The cytosolic cochaperone Sti1 is relevant for mitochondrial biogenesis and morphology. The FEBS Journal. 2016; 283(18):3338–3352.

Hou W, Harjono V, Harvey AT, Subramaniam AR, Zid BM. Quantification of elongation stalls and impact on gene expression in yeast. bioRxiv. 2023; doi: 10.1101/2023.03.19.533377.

Karpinets TV, Greenwood DJ, Sams CE, Ammons JT. RNA:protein ratio of the unicellular organism as a characteristic of phosphorous and nitrogen stoichiometry and of the cellular requirement of ribosomes for protein synthesis. BioMed Central Biology. 2006; 4(30).

Mason PB, Struhl K. Distinction and Relationship between Elongation Rate and Processivity of RNA Polymerase II In Vivo. Molecular Cell. 2005; 17(6):831–840. doi: https://doi.org/10.1016/j.molcel.2005.02.017.

Riba A, Di Nanni N, Mittal N, Arhné E, Schmidt A, Zavolan M. Protein synthesis rates and ribosome occupancies reveal determinants of translation elongation rates. Proceedings of the National Academy of Sciences. 2019; 116(30):15023–15032.

Saint-Georges Y, Garcia M, Delaveau T, Jourdren L, Le Crom S, Lemoine S, Tanty V, Devaux F, Jacq C. Yeast Mitochondrial Biogenesis: A Role for the PUF RNA-Binding Protein Puf3p in mRNA Localization. PLOS ONE. 2008; 3(6):1–12.

Schleif R, Hess W, Finkelstein S, Ellis D. Induction Kinetics of the L-Arabinose Operon of *Escherichia coli*. Journal of Bacteriology. 1973; 115(1):9–14. doi: 10.1128/jb.115.1.9-14.1973.

Stein KC, Kriel A, Frydman J. Nascent Polypeptide Domain Topology and Elongation Rate Direct the Cotranslational Hierarchy of Hsp70 and TRiC/CCT. Molecular Cell. 2019; 75(6):1117–1130.e5.

Thanaraj T, Argos P. Ribosome-mediated translational pause and protein domain organization. Protein Science. 1996; 5(8):1594–1612.

Tsuboi T, Viana MP, Xu F, Yu J, Chanchani R, Arceo XG, Tutucci E, Choi J, Chen YS, Singer RH, Rafelski SM, Zid BM. Mitochondrial volume fraction and translation duration impact mitochondrial mRNA localization and protein synthesis. eLife. 2020; 9:e57814.

Varenne S, Buc J, Lloubes R, Lazdunski C. Translation is a non-uniform process: effect of tRNA availability on the rate of elongation of nascent polypeptide chains. Journal of molecular biology. 1984; 180(3):549–576.

Young JC, Hoogenraad NJ, Hartl FU. Molecular Chaperones Hsp90 and Hsp70 Deliver Preproteins to the Mitochondrial Import Receptor Tom70. Cell. 2003; 112(1):41–50.

Zhang D, Shan So. Translation elongation regulates substrate selection by the signal recognition particle. Journal of Biological Chemistry. 2012; 287(10):7652–7660.

Zhao L, Cui Y, Fu G, Xu Z, Liao X, Zhang D. Signal Recognition Particle Suppressor Screening Reveals the Regulation of Membrane Protein Targeting by the Translation Rate. mBio. 2021; 12(1):e02373–20.

Zhao T, Chen YM, Li Y, Wang J, Chen S, Gao N, Qian W. Disome-seq reveals widespread ribosome collisions that promote cotranslational protein folding. Genome Biology. 2021; 22(16).

Chapter 6

Discussion

The shifting competition between diffusion and MTS association to the mitochondrial surface is a potential design principle for responsive mRNA localization conserved between eukaryotes. The key takeaway is that mitochondria require more metabolic proteins in non-fermentable carbon sources, and that is precisely when metabolic mRNAs localize more. I postulate that translation speeds decrease when fermentable carbon sources start running low, when media is switched altogether for one with non-fermentable carbon sources, or when the cell is otherwise unable to derive ATP from glycolysis. As translation speeds decrease, the translation of the MTS will slow as well, and ribosomes downstream of the MTS will take longer to complete translation. Scarcity of ATP, and of its downstream product GTP, lead to longer MTS exposure times and thus higher mRNA localization for MTS-mediated mRNAs. Whereas the switch from glycolytic to respiratory metabolism is accompanied by many well-studied transcriptional and post-transcriptional changes, this scheme is a potential post-transcriptional method of sensing and responding to metabolic needs on relatively short timescales (mRNA half-lives are around 10 minutes), and promotes protein production in parallel with other transcriptional and post-transcriptional changes.

The link between mRNA localization and protein production has been well-established for numerous nuclear-encoded mitochondrial mRNAs and for non-mitochondrial mRNAs tethered to the mitochondria. Translation elongation inhibition and larger mitochondrial volume fraction promote localization for certain nuclear-encoded mitochondrial mRNAs, which are defined as conditional or conditionally-localized mRNAs. Given that localization decreases when translation elongation slow down, mRNA localization can serve as an indirect measurement of the availability of energetic molecules like GTP, that are necessary for translation elongation as well as many other essential cellular processes. Paradoxically, as slower translation promotes mRNA localization, the localization to the mitochondria promotes protein production. This is potentially because of the density of ribosomes around the mitochondria, as observed by electron microscopy. I propose that the increase in mitochondrial association observed for conditional

mRNAs, which are enriched for Krebs cycle and other metabolic mitochondrial proteins, promotes mitochondrial biogenesis.

While there is a lot of interest in ATP generation, the ratio of NADH and NAD+ levels has been proposed as a crucial metric for setting the oxygen intake rate, respiratory efficiency, and growth rate. Glucose uptake rate determines glycolytic flux rate and is anti-correlated with mitochondrial activity; cell media with less preferable sugars, e.g. galactose or raffinose, resulted in slightly slower growth and more mitochondrial activity. At the other end of the spectrum, growth in ethanol media resulted in the slowest growth rate, the most mitochondrial activity i.e. the highest oxygen intake rate, and similar ATP levels [40]. Knockout experiments elucidated the underlying mechanism of regulating mitochondrial activity and efficiency: the precursors and products of most OXPHOS proteins are at equilibrium. Deleting or overexpressing mitochondrial NAD+ carriers NDT1 and NDT2 perturbed this equilibrium, driving mitochondria into inefficient regimes and lowering ATP production. By operating at near-equilibrium, mitochondrial proteins sense and respond to metabolic needs in real time and independently of the activity of other metabolism processes such as, hexose transporters and glycolytic enzymes [41].

Our understanding of metabolic switching at the molecular and cellular levels are key to untangling mitochondrial loss of function observed in diseased states and senescence. Metabolic engineering of brewer's yeast has also contributed to cancer research given that both cell types preferentially use glycolysis to consume nutrients and proliferate rapidly. Analogously, research into the Crabtree effect has contributed to our understanding of the Warburg effect. It has been long postulated that glycolytic flux and respiratory flux are governed by distinct biochemical principles despite using the same precursors to create the same end product ATP. The cytosolic concentration of a biochemical intermediate–the likeliest candidate is fructose-1,6-bisphosphate–determines the amount of carbon source that is routed into each pathway [42]. From there, glycolytic flux is determined by glucose uptake rates whereas respiratory flux is determined by enzyme levels, particularly TCA enzymes. In other words, under glycolysis, the rate of ATP production is set by the rate at which the cell takes in raw material whereas, under respiration, the rate of ATP production is set by the amount of available enzymes, not the rate of raw material. Levels of TCA cycle enzymes increase drastically after a shift to non-fermentable media, possibly to generate sufficient NADH to drive respiration in a less nutrient-rich environment [43]. Crucially, upregulation of TCA cycle enzyme levels is concentrated in cytosol-localized TCA cycle enzymes whereas mitochondria-localized TCA cycle enzymes remain at the same level or drop in abundance [43]. TCA cycle proteins are mostly encoded by conditional mRNAs; a few are encoded by diffuse mRNAs. I propose that increased localization to the mitochondria contributes to the increase in TCA protein levels that accompanies gluconeogenesis and the switch to respiration.

Bibliography

[1] Furqan M. Fazal, Shuo Han, Kevin R. Parker, Pornchai Kaewsapsak, Jin Xu, Alistair N. Boettiger, Howard Y. Chang, and Alice Y. Ting. Atlas of subcellular rna localization revealed by apex-seq. *Cell*, 178(2):473–490.e26, 2019.

[2] Michael R. Duchen. Roles of Mitochondria in Health and Disease. *Diabetes*, 53(suppl$_1$) : $S96 - -S102, 022004$.

[3] Peter Dromparis and Evangelos D. Michelakis. Mitochondria in vascular health and disease. *Annual Review of Physiology*, 75(1):95–126, 2013.

[4] Martin Picard, Tanja Taivassalo, Gilles Gouspillou, and Russell T. Hepple. Mitochondria: isolation, structure and function. *The Journal of Physiology*, 589(18):4413–4421, 2011.

[5] JW Posakony, JM England, and G Attardi. Mitochondrial growth and division during the cell cycle in HeLa cells . *Journal of Cell Biology*, 74(2):468–491, 08 1977.

[6] Tatsuhisa Tsuboi, Matheus P Viana, Fan Xu, Jingwen Yu, Raghav Chanchani, Ximena G Arceo, Evelina Tutucci, Joonhyuk Choi, Yang S Chen, Robert H Singer, Susanne M Rafelski, and Brian M Zid. Mitochondrial volume fraction and translation duration impact mitochondrial mrna localization and protein synthesis. *eLife*, 9:e57814, 2020.

[7] Ximena G. Arceo, Elena F. Koslover, Brian M. Zid, and Aidan I. Brown. Mitochondrial mrna localization is governed by translation kinetics and spatial transport. *PLOS Computational Biology*, 18(8):1–28, 08 2022.

[8] Wesley R. Legant Justin Melunis Uri Hershberg Eric Wait Andrew R. Cohen Michael W. Davidson Eric Betzig Jennifer Lippincott-Schwartz Alex M. Valm, Sarah Cohen. Applying systems-level spectral imaging and analysis to reveal the organelle interactome. *Nature*, 546:162–167, 2017.

[9] Thomas Misgeld and Thomas L. Schwarz. Mitostasis in neurons: Maintaining mitochondria in an extended cellular architecture. *Neuron*, 96(3):651–666, 2017.

[10] Daniel St. Johnston. Moving messages: the intracellular localization of mrnas. *Nature Reviews Molecular Cell Biology*, 6(5):363–375, 2005.

[11] Isabel M. Palacios and Daniel St. Johnston. Getting the message across: The intracellular localization of mrnas in higher eukaryotes. *Annual Review of Cell and Developmental Biology*, 17(1):569–614, 2001. PMID: 11687499.

[12] Mary Lou King, Timothy J. Messitt, and Kimberly L. Mowry. Putting rnas in the right place at the right time: Rna localization in the frog oocyte. *Biology of the Cell*, 97(1):19–33, 2005.

[13] Kevin Czaplinski and Robert H. Singer. Pathways for mrna localization in the cytoplasm. *Trends in Biochemical Sciences*, 31(12):687–693, 2006.

[14] Kelsey C. Martin and Anne Ephrussi. mrna localization: Gene expression in the spatial dimension. *Cell*, 136(4):719–730, 2009.

[15] Yuliang Ma and Susan S. Taylor. A molecular switch for targeting between endoplasmic reticulum (er) and mitochondria. *Journal of Molecular Biochemistry*, 283(17):11743 – 11751, 2008.

[16] Susanne M. Rafelski. Mitochondrial network morphology: building an integrative, geometrical view. *BioMed Central Biology*, 11(71), 2013.

[17] Melanie A. Miller, Joseph Russo, Anthony D. Fischer, Florencia A. Lopez Leban, and Wendy M. Olivas. Carbon source-dependent alteration of Puf3p activity mediates rapid changes in the stabilities of mRNAs involved in mitochondrial function. *Nucleic Acids Research*, 42(6):3954–3970, 12 2013.

[18] Christopher C. Williams, Calvin H. Jan, and Jonathan S. Weissman. Targeting and plasticity of mitochondrial proteins revealed by proximity-specific ribosome profiling. *Science*, 346(6210):748–751, 2014.

[19] Yann Saint-Georges, Mathilde Garcia, Thierry Delaveau, Laurent Jourdren, Stephane Le Crom, Sophie Lemoine, Veronique Tanty, Frederic Devaux, and Claude Jacq. Yeast mitochondrial biogenesis: A role for the puf rna-binding protein puf3p in mrna localization. *PLOS ONE*, 3(6):1–12, 2008.

[20] Jiuya He, Holly C. Ford, Joe Carroll, Corsten Douglas, Evvia Gonzales, Shujing Ding, Ian M. Fearnley, and John E. Walker. Assembly of the membrane domain of atp synthase in human mitochondria. *Proceedings of the National Academy of Sciences*, 115(12):2988–2993, 2018.

[21] Jiyao Song, Nikolaus Pfanner, and Thomas Becker. Assembling the mitochondrial atp synthase. *Proceedings of the National Academy of Sciences*, 115(12):2850–2852, 2018.

[22] Mary T. Couvillion, Iliana C. Soto, and L. Stirling Shipkovenska, Gergana & Churchman. Synchronized mitochondrial and cytosolic translation programs. *Nature*, 533:499–503, 2016.

[23] Yulia Gonskikh and Norbert Polacek. Alterations of the translation apparatus during aging and stress response. *Mechanisms of Ageing and Development*, 168:30–36, 2017.

[24] Raymond J Deshaies, Bruce D Koch, Margaret Werner-Washburne, Elizabeth A Craig, and Randy Schekman. A subfamily of stress proteins facilitates translocation of secretory and mitochondrial precursor polypeptides. *Nature*, 332(6167):800–805, 1988.

[25] Jason C. Young, Nicholas J. Hoogenraad, and F.Ulrich Hartl. Molecular chaperones hsp90 and hsp70 deliver preproteins to the mitochondrial import receptor tom70. *Cell*, 112(1):41–50, 2003.

[26] Sandra Backes, Steffen Hess, Felix Boos, Michael W Woellhaf, Sabrina Gödel, Martin Jung, Timo Mühlhaus, and Johannes M Herrmann. Tom70 enhances mitochondrial preprotein import efficiency by binding to internal targeting sequences. *Journal of Cell Biology*, 217(4):1369–1382, 2018.

[27] Mathilde Garcia, Thierry Delaveau, Sebastien Goussard, and Claude Jacq. Mitochondrial presequence and open reading frame mediate asymmetric localization of messenger rna. *European Molecular Biology Organization Reports*, 11(4):285–291, 2010.

[28] Yoshinori Fukasawa, Junko Tsuji, Szu-Chin Fu, Kentaro Tomii, Paul Horton, and Kenichiro Imai. Mitofates: Improved prediction of mitochondrial targeting sequences and their cleavage sites *[s]. *Molecular and Cellular Proteomics*, 14:1113–1126, 2015.

[29] Michael J. Baker, Ann E. Frazier, Jacqueline M. Gulbis, and Michael T. Ryan. Mitochondrial protein-import machinery: correlating structure with function. *Trends in Cell Biology*, 17(9):456–464, 2007.

[30] D. Roise, F. Theiler, S. J. Horvath, J. M. Tomich, J. H. Richards, D. S. Allison, and G. Schatz. Amphiphilicity is essential for mitochondrial presequence function. *The EMBO Journal*, 7(3):649–653, 1988.

[31] Xiaowei Yan, Tim A. Hoek, Ronald D. Vale, and Marvin E. Tanenbaum. Dynamics of translation of single mrna molecules in vivo. *Cell*, 165(4):976–989, 2016.

[32] Noga Gadir, Liora Haim-Vilmovsky, Judith Kraut-Cohen, and Jeffrey E. Gerst. Localization of mrnas coding for mitochondrial proteins in the yeast saccharomyces cerevisiae. *RNA*, 17(8):1551–1565, 2011.

[33] Benjamin L. Weis, Enrico Schleiff, and William Zerges. Protein targeting to subcellular organelles via mrna localization. *Biochimica et Biophysica Acta (BBA) - Molecular Cell Research*, 1833(2):260–273, 2013. Protein Import and Quality Control in Mitochondria and Plastids.

[34] Taolan Zhao, Yan-Ming Chen, Yu Li, Jia Wang, Siyu Chen, Ning Gao, and Wenfeng Qian. Disome-seq reveals widespread ribosome collisions that promote cotranslational protein folding. *Genome Biology*, 22(16), 2021.

[35] Kevin C. Stein, Allison Kriel, and Judith Frydman. Nascent polypeptide domain topology and elongation rate direct the cotranslational hierarchy of hsp70 and tric/cct. *Molecular Cell*, 75(6):1117–1130.e5, 2019.

[36] K Luby-Phelps, P E Castle, D L Taylor, and F Lanni. Hindered diffusion of inert tracer particles in the cytoplasm of mouse 3t3 cells. *Proceedings of the National Academy of Sciences*, 84(14):4910–4913, 1987.

[37] Dahlene Fusco, Nathalie Accornero, Brigitte Lavoie, Shailesh M. Shenoy, Jean-Marie Blanchard, Robert H. Singer, and Edouard Bertrand. Single mrna molecules demonstrate probabilistic movement in living mammalian cells. *Current Biology*, 13(2):161–167, 2003.

[38] Nicholas T. Ingolia, Jeffrey A. Hussmann, and Johnathan S. Weissman. Ribosome profiling: Global views of translation. *Cold Spring Harbor Perspectives Biology*, 11(5), 2019.

[39] Da Wei Huang, Brad T. Sherman, and Richard A. Lempicki. Systematic and integrative analysis of large gene lists using david bioinformatics resources. *Nature Protocols*, 4:44–57, 2009.

[40] Gennaro Agrimi, Luca Brambilla, Gianni Frascotti, Isabella Pisano, Danilo Porro, Marina Vai, and Luigi Palmieri. Deletion or overexpression of mitochondrial nad¡sup¿+¡/sup¿ carriers in ¡i¿saccharomyces cerevisiae¡/i¿ alters cellular nad and atp contents and affects mitochondrial metabolism and the rate of glycolysis. *Applied and Environmental Microbiology*, 77(7):2239–2246, 2011.

[41] Roslyn M. Bill Eva Albers Jacky L. Snoep Eckhard Boles Stefan Hohmann Lena Gustafsson Karin Elbing, Christer Larsson. Role of hexose transport in control of glycolytic flux in saccharomyces cerevisiae. *Applied and Environment Microbiology*, 70(9):651, 2004.

[42] Daphne H. E. W. Huberts, Bastian Niebel, and Matthias Heinemann. A flux-sensing mechanism could regulate the switch between respiration and fermentation. *FEMS Yeast Research*, 12(2):118–128, 03 2012.

[43] Guillermo G Zampar, Anne Kümmel, Jennifer Ewald, Stefan Jol, Bastian Niebel, Paola Picotti, Ruedi Aebersold, Uwe Sauer, Nicola Zamboni, and Matthias Heinemann. Temporal system-level organization of the switch from glycolytic to gluconeogenic operation in yeast. *Molecular Systems Biology*, 9(1):651, 2013.